U.S.NRC
United States Nuclear Regulatory Commission
Protecting People and the Environment

Technical Letter Report
TLR-RES/DE/MEB-2025-04
PNNL-37055

Alloy 690/152(M)/52(M) SCC Initiation Test 5.7-Year Summary Report

September 2025

Prepared by:

Mychailo B. Toloczko, Ziqing Zhai, Karen Kruska, Ryan A. Bouffioux, and Dexter D. Kling

Pacific Northwest National Laboratory

NRC Project Manager:

Eric M. Focht
Materials Engineering Branch

Division of Engineering
Office of Nuclear Regulatory Research
U.S. Nuclear Regulatory Commission
Rockville, MD 20852

DISCLAIMER

This report was prepared as an account of work sponsored by an agency of the U.S. Government. Neither the U.S. Government nor any agency thereof, nor any employee, makes any warranty, expressed or implied, or assumes any legal liability or responsibility for any third party's use, or the results of such use, of any information, apparatus, product, or process disclosed in this publication, or represents that its use by such third party complies with applicable law

This report does not contain or imply legally binding requirements. Nor does this report establish or modify any regulatory guidance or positions of the U.S. Nuclear Regulatory Commission and is not binding on the Commission.

Pacific Northwest
NATIONAL LABORATORY

PNNL-37055

Alloy 690/152(M)/52(M) SCC Initiation Test 5.7-Year Summary Report

September 2025

Mychailo B. Toloczko
Ziqing Zhai
Karen Kruska
Ryan A. Bouffioux
Dexter D. Kling

U.S. DEPARTMENT OF ENERGY

Prepared for the U.S. Department of Energy
under Contract DE-AC05-76RL01830

DISCLAIMER

This report was prepared as an account of work sponsored by an agency of the United States Government. Neither the United States Government nor any agency thereof, nor Battelle Memorial Institute, nor any of their employees, makes **any warranty, express or implied, or assumes any legal liability or responsibility for the accuracy, completeness, or usefulness of any information, apparatus, product, or process disclosed, or represents that its use would not infringe privately owned rights**. Reference herein to any specific commercial product, process, or service by trade name, trademark, manufacturer, or otherwise does not necessarily constitute or imply its endorsement, recommendation, or favoring by the United States Government or any agency thereof, or Battelle Memorial Institute. The views and opinions of authors expressed herein do not necessarily state or reflect those of the United States Government or any agency thereof.

PACIFIC NORTHWEST NATIONAL LABORATORY
operated by
BATTELLE
for the
UNITED STATES DEPARTMENT OF ENERGY
under Contract DE-AC05-76RL01830

PNNL-37055

Alloy 690/152(M)/52(M) SCC Initiation Test 5.7-Year Summary Report

November 2024

Mychailo B. Toloczko
Ziqing Zhai
Karen Kruska
Ryan A. Bouffioux
Dexter D. Kling

Prepared for by
the U.S. Department of Energy
under Contract DE-AC05-76RL01830, and
the U.S. Nuclear Regulatory Commission under
Contract 31310019N0001 Task Order 31310020F0005

Pacific Northwest National Laboratory
Richland, Washington 99354

Summary

Pacific Northwest National Laboratory (PNNL) conducted long-term stress corrosion crack initiation (SCCI) tests on multiple heats of Alloy 690 and one weld each of Alloys 152, 152M, 52, and 52M (hereafter generally referred to as Alloys 690/152(M)/52(M)) for a cooperative research project being conducted by the U.S. Nuclear Regulatory Commission (NRC) and the Electric Power Research Institute (EPRI) under a memorandum of understanding (MOU). The aim of this work was to determine a potential factor of improvement (FOI) in stress corrosion cracking (SCC) resistance of these materials due to increases in time to SCCI compared to Alloy 600 and its primary weld metal, Alloy 182. The FOI could be determined by the ratio of the time to SCCI of Alloys 690/152(M)/52(M) to the time to SCCI of Alloys 600/182.

This project began in 2014, and an exposure time of 5.7 years was reached on the Alloy 690/152(M)/52(M) specimens in 2022. During this time, test systems were built, specimens were fabricated, and mid-test examinations were conducted on select specimens. Alloy 600/182 specimens were tested during this same timeframe.

The selection of materials and material conditions was an important aspect of this test effort. Not only was it necessary to select representative heats and welds of Alloys 690/152(M)/52(M), but also Alloy 600/182 materials. The Alloy 690/152(M)/52(M) materials were largely sourced from material that PNNL had extensively SCC growth rate (SCCGR) tested, thus providing a strong background on the microstructure and SCCGR behavior of the materials. PNNL had previously conducted only a limited number of SCC tests on Alloys 600/182, so the majority of these materials had to be acquired as part of the SCCI testing program. Some of the materials were obtained from the NRC non-destructive examination program at PNNL, while others were obtained from other organizations.

Because Alloys 690/152(M)/52(M) are known to be very resistant to SCC growth and were likely to be similarly resistant to SCCI, suitable test acceleration approaches were implemented. As a result of numerous discussions with the NRC, EPRI, and other entities in the SCC research community, an accelerated testing environment and an accelerated material condition were selected. The accelerated testing environment consisted of testing at 360°C (compared to the standard outlet temperature of 320°C for a pressurized water reactor (PWR) and a peak pressurizer temperature of 347°C) and setting the corrosion potential to the location of the nickel/nickel oxide stability boundary (compared to PWRs that operate in the nickel-metal stability region). This temperature and dissolved hydrogen concentration was the typical condition used by PNNL for PWR primary water SCCGR testing. SCCGRs were shown to be highest at the nickel/nickel oxide stability boundary and testing at the boundary was postulated to be an accelerating environment for initiation as well. An acceleration of the material SCC susceptibility was also applied in the form of cold work (CW). SCCGR testing of Alloy 690/152(M)/52(M) had revealed that CW increases the susceptibility of these materials with 30% CW producing SCCGRs in Alloy 690 similar to that of non-CW Alloy 600. CW is known to exist in plant structures at various levels. Ground surfaces on welds and neighboring base metals can have CW damage with hardness levels similar to 30% CW. However, the majority of the Ni-base alloy pressure boundary structure is expected to have lower levels of CW. For SCCI testing, 15% CW was selected to balance test acceleration and maintaining a representative material condition.

The tests on Alloy 690/152(M)/52(M) and Alloy 600/182 specimens were conducted at the yield strength of the material. Multi-specimen test systems were utilized for this purpose. A fraction of

the Alloy 690/152(M)/52(M) specimens were monitored for in situ detection of crack initiation by the direct current potential drop (DCPD) method, while the remaining specimens were monitored indirectly by displacement of the pullrod.

The Alloy 690/152(M)/52(M) test was stopped at 2.4, 4.0, and 5.7 years for specimen examinations. The results of this testing effort are described in this report and are summarized as follows:

- None of the Alloy 690/152(M)/52(M) specimens exhibited an indication of SCCI during 5.7 years of testing either by DCPD or by pullrod displacement.
- The creep rate was estimated from the test data and was found to be 0.09–0.35%/yr during the second year of testing and 0.07–0.12%/yr during the fifth year of testing. The presence of creep indicates that diffusion processes occurred on a volumetric scale.
- Mid-test specimen examinations conducted at 2.4 and 4.0 years on a small number of specimens revealed very little evolution in the microstructure towards an initiated condition. The weld metals exhibited preexisting cracks that formed during weld fabrication which had the potential to accelerate the weld metal microstructure towards a state susceptible to SCCI.
- Extensive specimen examinations were conducted on more specimens after 5.7 years. The Alloy 690 specimens exhibited an obvious evolution in grain boundary (GB) microstructure compared to 4.0 years, but the microstructure was still very far from a condition susceptible to SCCI. However, the Alloy 152(M)/52(M) specimens had some surface-breaking cracks with a length on the surface of approximately 100 μm. GB cross-section examinations revealed that some of these appeared to be preexisting cracks that formed during weld fabrication, but a few appeared to be due to GB creep cavity formation that is known to allow SCCI in Alloy 690. Surprisingly, one of the weld metal specimens was observed to have a very large crack with a surface length and depth of approximately 800 μm. This specimen was not monitored for SCCI via DCPD, making it impossible to determine if this was a preexisting weld fabrication crack or if it formed during SCCI testing.
- The microstructure observations suggest that the weld metals may be more susceptible to SCCI than Alloy 690. Further testing is recommended to better understand the behavior of these materials, especially the weld metals.

Acronyms and Abbreviations

Alloy 690/152(M)/52(M)	general term for this class of high-chromium nickel-base alloys
BSE	backscattered electron
CF	cold forged
CRDM	control rod drive mechanism
CW	cold work(ed, ing)
DCPD	direct current potential drop
DOE	U.S. Department of Energy
EPRI	Electric Power Research Institute
FIB	focused ion beam
FOI	factor of improvement
GB	grain boundary
IG	intergranular
K	stress intensity factor
LWR	light water reactor
LWRS	Light Water Reactor Sustainability (Program)
MA	mill annealed
MO	metal oxide (composition)
NRC	Nuclear Regulatory Commission
PNNL	Pacific Northwest National Laboratory
PWR	pressurized water reactor
SCC	stress corrosion crack(ing)
SCCGR	stress corrosion crack growth rate
SCCI	stress corrosion crack initiation
SE	secondary electron
SEM	scanning electron microscopy
SIF	stress intensity factor
TT	thermally treated
YS	yield stress

Contents

Figures

Tables

1.0 Introduction

PNNL conducted long-term stress corrosion crack initiation (SCCI) tests on multiple heats of Alloy 690 and one weld each of Alloys 152, 152M, 52, and 52M (hereafter generally referred to as Alloys 690/152(M)/52(M)) for a cooperative research project being conducted by the U.S. NRC and the EPRI under a MOU. The aim of this work was to determine a potential FOI in SCC resistance of these materials due to increases in time to SCCI compared to Alloy 600 and its primary weld metal, Alloy 182. The FOI could be determined by the ratio of the time to SCCI of Alloys 690/152(M)/52(M) to the time to SCCI of Alloys 600/182.

This work began in 2014, and an exposure time of 5.7 years was reached on the Alloy 690/152(M)/52(M) specimens in 2022. During this time, test systems were built, specimens were fabricated, and mid-test examinations were conducted on select specimens. Alloy 600/182 specimens were tested during this same timeframe.

The selection of materials and material conditions was an important aspect of this test effort such that it was necessary to select representative heats and welds of Alloys 690/152(M)/52(M) and Alloy 690/182 materials. The Alloy 690/152(M)/52(M) materials were largely sourced from material that PNNL had extensively SCC growth rate (SCCGR) tested, thus providing a strong background on the microstructure and SCCGR behavior of the materials. PNNL had previously only conducted a limited number of SCC tests on Alloys 600/182, so most of these materials had to be acquired as part of the SCCI testing program. Some were obtained from the NRC non-destructive examination program at PNNL while the remainder were sourced from other organizations. For example, EPRI provided materials as part of the joint cooperative project conducted under the MOU.

Because Alloys 690/152(M)/52(M) are known to be very resistant to SCC growth and were likely to be similarly resistant to SCCI, suitable test acceleration approaches had to be implemented. As a result of numerous discussions with the NRC, EPRI, and other entities in the SCC research community, an accelerated testing environment and an accelerated testing condition were selected. The accelerated testing environment included testing at 360°C (compared to the standard outlet temperature of 320°C for a pressurized water reactor (PWR) and peak pressurizer temperature of 347°C) and setting the corrosion potential to the location of the nickel/nickel oxide (Ni/NiO) stability boundary (compared to PWRs that operate in the nickel-metal stability region). This was the typical condition used by PNNL for PWR primary water SCCGR testing as well. SCCGRs were shown to be highest at the nickel/nickel oxide stability boundary and testing at the boundary was postulated to be an accelerating environment for initiation as well. An acceleration of the material SCC susceptibility was also applied in the form of CW. SCCGR testing of Alloys 690/152(M)/52(M) had revealed that CW increases, the susceptibility of these materials with 30% CW producing SCCGRs similar to that of non-CW Alloy 600. CW is known to exist in plant structures at various levels. Ground surfaces on welds and neighboring base metals can have CW damage with hardness levels similar to 30% CW [1]. However, the majority of structures are expected to have lower levels of CW. For SCCI testing, 15% CW was selected to balance between test acceleration and maintaining a representative material condition.

Tests on Alloy 690/152(M)/52(M) and Alloy 600/182 specimens were conducted at the yield strength (YS) of the material. Multi-specimen test systems were used for this purpose. The Alloy 690/152(M)/52(M) tests were stopped at 2.4, 4.0, and 5.7 years for specimen examinations. The results of these tests are described in this report.

2.0 Experimental – Material Selection and Properties

2.1 Materials

PNNL began interacting with the NRC and EPRI in September 2014 regarding selection and acquisition of materials and weldments. It was desired for the materials to have well-documented processing histories, bulk compositions, and information about SCC susceptibility. The goal was to obtain four different heats of Alloy 690 and four weldments of Alloys 152(M)/52(M) to provide a multi-heat and multi-weld foundation for measuring and understanding a range of SCCI responses. For the Alloy 690 materials, three heats are in a thermally treated (TT) condition while the fourth is in a mill annealed (MA) condition. One weld metal each of Alloy 152, 152M, 52, and 52M was selected. The materials are summarized in Table 1 while their composition and other information are provided in Tables 2 and 3. Other details of the selected materials are covered below.

Table 1. Materials selected and acquired for this testing effort.

Alloy 690	
Valinox RE243 TT CRDM* Tube 2360 TK-VDM 114092 TT Plate	Valinox WP142 TT CRDM Tube 2541 Allvac B25K-2 MA Bar
Alloy 152(M)/52(M)	
MHI Alloy 152 U-Groove Mockup ENSA DPM** Alloy 52M Butter	MHI Alloy 52 U-Groove Mockup EPRI Alloy 152M U-Groove
* CRDM = control rod drive mechanism ** DPM = divider plate mockup	

Table 2. Heat number, composition, and as-received thermal treatment of the Alloy 690 materials for this project.

Manufacturer, AR Condition and Heat #	Composition, wt%	Heat Treatment and Room Temp. Mechanical Properties
Valinox TT WP142 CRDM Tube 2541	Ni-29.0Cr-10.5Fe-0.02C-0.3Mn-0.35Si-0.47Ti-0.01Nb-0.001S-0.003P	1096°C/~1 min, WQ + 716-722°C/10.2 h, Air cool YS = 269 MPa, HV = 163 kgf/mm^2
Valinox TT RE243 CRDM Tube 2360	Ni-28.9Cr-10.4Fe-0.02C-0.3Mn-0.35Si-0.14Al-0.23Ti-0.024N-0.008P-0.0005S	1122°C/~1 min, WQ + 716-725°C/10.5 h, Air cool YS = 255 MPa, HV = 157 kgf/mm^2
Allvac (GE) MA Plate B25K-2 Bar	Ni-29.3Cr-9.2Fe-0.034C-0.22Mn-0.06Si-0.26Al-0.37Ti-<0.01Cu-0.03N-0.006P-<0.0003S-<0.001B	996°C/20 min/AC YS = 294 MPa, HV = 173 kgf/mm^2
TK-VDM TT Plate 114092	Ni-29.5Cr-9.5Fe-0.020C-0.25Mn-0.26Si-0.32Al-0.36Ti-<0.01Cu-0.003P-<0.002S	1030°C/1 hr/WQ + 715°C/10 hr/AC YS = 285 MPa, HV = 155 kgf/mm^2

Table 3. Heat number, composition, and weldment fabrication information of the Alloy 152(M)/52(M) materials selected for this project.

Material – Source and Name	Mockup Description and Heat Number	Weld Metal Composition, wt%
Alloy 152 – MHI U-Groove Mockup	MHI U-groove mockup joining "304" SS plates, probably 304L. Alloy 152 Heat 307380.	Ni-28.7Cr-9.1Fe-0.03C-3.6Mn-0.33Si-0.15Al-0.12Ti-0.003S (independent analysis)
Alloy 152M - IHI U-Groove	U-Groove Weld in gouged Alloy 600 plate. Alloy 152M heat WC83F8 in lower 25 mm, heat 444537 in upper 25-40 mm.	Heat WC83F8: Ni-30.2Cr-8.7Fe-<0.005C-3.0Mn-0.22Si-<0.01Al-0.03Ti-1.176Nb-<0.001P-0.002S-0.03V (mill test report), Heat 444537: Ni-28.6Cr-8.1Fe-0.022C-3.7Mn-0.47Si-<0.025Al-0.06Ti-1.75Nb-0.007P-0.004S-0.022V (mill test report)
Alloy 52 – MHI U-Groove Mockup	MHI U-groove mockup joining "304" SS plates, probably 304L. Alloy 52 Heat NX2686JK.	Ni-28.8Cr-10.1Fe-0.02C-0.03Mn-0.14Si-0.51Ti-0.68Al-<0.005P-<0.005T (independent analysis)
Alloy 52M - ENSA Divider Plate Mockup	Divider Plate Mockup joining Alloy 690 to LAS. Alloy 52M Butter, heat unknown.	Ni-29.7Cr-8.5Fe-0.02C-0.76Mn-0.12Si-0.21Ti-0.09Al-0.77Nb+Ta-<0.005P-<0.001S (independent analysis)

2.1.1 Alloy 690 Material Selection Approach

Extensive SCC testing and microstructure examinations of the Alloy 690 heats in the as-received and CW conditions have been performed at PNNL [2–4]. As a result, the SCCGR susceptibility of many different Alloy 690 heats is known. Similar to Alloy 600, the goal was to have two Alloy 690 CRDM tube heats and two plate heats in the matrix. For this, PNNL obtained two CRDM heats (Valinox RE243 and Valinox WP142) in a TT condition and two plate heats (TK-VDM 114092 and ATI/Allvac B25K-2). The TK-VDM 114092 plate was obtained in a TT condition while the Allvac B25K-2 bar was obtained in a MA condition. The two CRDM materials have equiaxed and uniform GB structures with no banding. The two plate heats both are banded in the plate processing plane, a feature that is common in modern Alloy 690 plate (as well as in Alloy 600 plate).

2.1.2 Alloy 152(M)/52(M) Material Selection Approach

Because of the interest in testing several different high-chromium, nickel-base alloy welds relevant to nuclear construction, PNNL has obtained one weldment each of Alloys 152, 152M, 52, and 52M. All the weldments were made available by EPRI and were made in support of the qualification of these weld metal materials for light water reactors (LWRs). Microstructure examinations and SCCGR testing for most of these materials have been performed previously [2,3,5,6].

2.1.3 Base Microstructure and Properties

Detailed base microstructure characterization of the Alloy 690 materials was previously performed by PNNL and is covered in detail in a NUREG report [4]. Among the weld metals, only the Alloy 152 and Alloy 52 base microstructures were examined in detail [5].

2.1.4 Tensile, Hardness, and SCCGR Susceptibility

Material strength and SCC susceptibility in the form of hardness, 360°C YS, and SCCGR are summarized in Table 4. While YS is the best estimate of overall material strength, hardness measurements were performed to look at spatial variability in material strength, in particular for the weld metals.

Table 4. Hardness, 360°C yield strength, and SCCGR results of the materials.

Material	ID	Condition	Hardness (kg/mm^2)	YS@360°C (MPa)	SCCGR@360°C (mm/s)†	% IG
Alloy 690 CRDM	RE243	TT	155	**	<1e-09	3
		15% CF	240	415, 420	~3e-09‡	37‡
Alloy 690 CRDM	WP142	TT	163	**	<1e-09	3
		15% CF	247	445, 455	**	**
Alloy 690 Plate	114092	TT	165	**	<1e-09	<5
		15% CF	260	460	**	**
Alloy 690 Plate	B25K-2	MA	173	**	1.1e-09	5
		15% CF	270	515	**	**
Alloy 152 U-groove	MHI 307380	AW	**	**	<1e-09	40
		15% CF	225–345	500	~2.2e-09	50
Alloy 52 U-Groove	MHI NX2686JK	AW	**	**	<1e-09	11
		15% CF	225–315	470	~5.5e-09	80
Alloy 52M Butter	ENSA DPM Butter	AW	**	**	**	**
		15% CF	240–300	430	~2e-09	20
Alloy 152M U-Groove	EPRI 444537/WC83F8	AW	**	**	**	40
		15% CF	255–345	550, 560	~1.5e-09	70

† 25-30 MPa$\sqrt{m}$
** Not evaluated
‡ For 12% CF material

2.2 Material Condition for Testing

2.2.1 Cold Work

As indicated by the test matrix, the SCCI tests are being conducted on these materials in a 15% homogeneously cold forged (CF) condition. It is useful to recall that a defining aspect of initiation events in service components often involves tensile loading of a highly CW surface layer. French researchers [7-9] have suggested that a strain reversal process produces very high stresses along with high levels of strain. Test specimens such as U-bends, bent beams, and even tensile specimens enable a highly stressed CW layer on a mildly CW bulk substrate to be evaluated in a way that is relevant to service components. However, a critical consideration for SCCI testing is the associated relationship between the CW layer thickness and the crack depth needed to produce a stress intensity factor (K) level sufficient for propagation. While the effect of CW depth has been considered in phenomenological analysis of SCCI times [9], the effect of damage depth has not been generally addressed in the literature as a consideration for SCCI test specimen design or test methodology, even though it has a profound effect on the time-to-initiation. Instead, experimental studies tend only to reach the conclusion that tensile-strained CW surfaces of Alloy 600 specimens reduce the SCCI time compared to polished (i.e., undamaged) surfaces [10,11].

Uncertainties exist concerning the representative CW depth and degree of damage in LWR service components. The depth of the CW layer is variable, as is the applied stress and the component thickness that determine the stress intensity factor after the formation of a crack.

The wide range of CW layer depths that have been observed in Alloy 600/182 service components suggests that a conservative approach would be to assume a worst-case depth that could be as high as approximately 0.7 mm as reported from service component observations [11]. Based on the available literature, this depth exceeds that needed to produce SCCI in susceptible Alloy 600/182 service components and establishes a condition under which SCC growth controls the lifetime of the component. This variability in the service component CW layer depth makes using a surface CW specimen less desirable when similar stresses and strains can be achieved much more easily and in a more quantitative manner for specimens with homogeneous levels of cold deformation.

Thus, PNNL believes that the most effective means of evaluating the material response is to use a homogeneously CW specimen rather than a specimen with a complex CW surface layer. While it is clearly important to understand the effect of the CW damage layer on SCCI for components in service, understanding the material response to CW is a necessary first step for this program.

An important aspect to consider for this program is that it strives to measure SCCI times and not through-thickness responses of the specimen. In service components where CW may exist only in a surface layer, Alloy 690 and its weld metals may exhibit crack initiation followed by very low growth as the crack extends into the softer base material. SCCI times measured in homogeneously CW tensile specimens are only meant to be an indicator of SCCI response and not an indicator of susceptibility to through-thickness crack growth.

The selection of the appropriate level of CW is important to consider. It has been reported that highly damaged, CW layers under very high stresses are relevant to plant SCCI conditions. However, the level of deformation in these layers is likely not uniform. Measurements of hardness or stress for field components are not readily available, but examples of laboratory measurements [12,13] and finite element modeling-based predictions [14] show that the damage does decrease with depth, typically with an inverse dependence.

Fifteen percent CW achieved by cold forging was selected to best represent the surface damage layer. The 15% CF Alloy 690 materials have a 360°C YS of ~400–500 MPa, while the Alloy 152(M)/52(M) materials are in the range of 450–550 MPa. The choice of 15% CW as the baseline condition also stems from the expected maximum strain levels in heat affected zones and weld repairs [15]. From a practical perspective during the planning for assessing FOIs for Alloy 690/152(M)/52(M) materials, 15% CW was expected to shorten the initiation time of susceptible Alloy 600/182 to approximately 2,000 hours or less, thereby making it possible to determine a useful Alloy 690/152(M)/52(M) FOI within the time frame of this project.

For the base metals in plate form, the forging plane is coincident with the processing plane. Specimens were cut from these forged materials so that the axis of the specimen is parallel with the forging direction. The forging plane and processing plane will both cut across the diameter of the gauge section. This will allow cracking to take place along the most susceptible plane of the CF material. CRDM materials that tend to show more equiaxed grain structures will be forged in such a way as to be able to extract specimens from the available material. All welds were forged in the transverse direction with specimens aligned as shown in Figure 1, again resulting in the crack initiation plane being along the most susceptible orientation relative to the cold forging and the weld microstructure.

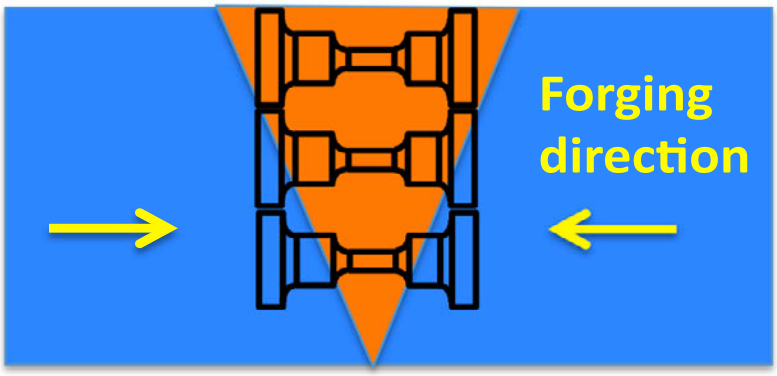

Figure 1. Orientation of forging direction and tensile specimens cut from weldments.

2.2.2 Surface Condition

The baseline surface condition is a highly polished 1 μm finish. Based on nuclear reactor operational experience, ground surfaces reduce initiation time; however, analysis of available information does not suggest that the resulting nanocrystalline microstructure or surface roughness is the cause of the reduced initiation times. As discussed in the previous section, grinding, possibly in conjunction with other fabrication processes such as bending or hammering, elevates the material strength and creates membrane surface tensile stresses that are strong promoters of SCCI. Increases in initiation time associated with the polishing of service components is not due to removal of the nanocrystalline, uneven surface; rather, it is due to removal of the high-strength, membrane tensile loading. SCCI testing at PNNL of tensile specimens with ground and highly polished surfaces supports this conclusion [16]. Constant load tensile initiation tests on CW Alloy 600 with either ground or highly polished surfaces have exhibited nearly the same initiation times. In fact, the specimens with ground surfaces have consistently exhibited slightly longer SCCI times [16]. Microstructural examinations indicate that the slightly longer initiation time is due to better availability of chromium from the high GB surface area in the nanocrystalline layer, and this promotes the formation of a more passive oxide layer. With this understanding, the decision was made to use a 1 μm (or better) surface finish that allows for much better identification of surface cracks.

3.0 Experimental – Test Setup

This test was conducted in a PNNL 3-string test system that has been described in detail in previous reports [17,18]. The load train for this style of test system utilizes a single servoelectric motor to apply load. The strings hang from a 3-bar linkage as shown in the sketch and photo in Figure 2. The load is balanced evenly among the three strings using a balance plate between the three strings and the central pullrod. As described in the 2017 status report, an improved balance plate design was implemented shortly after this test was started.

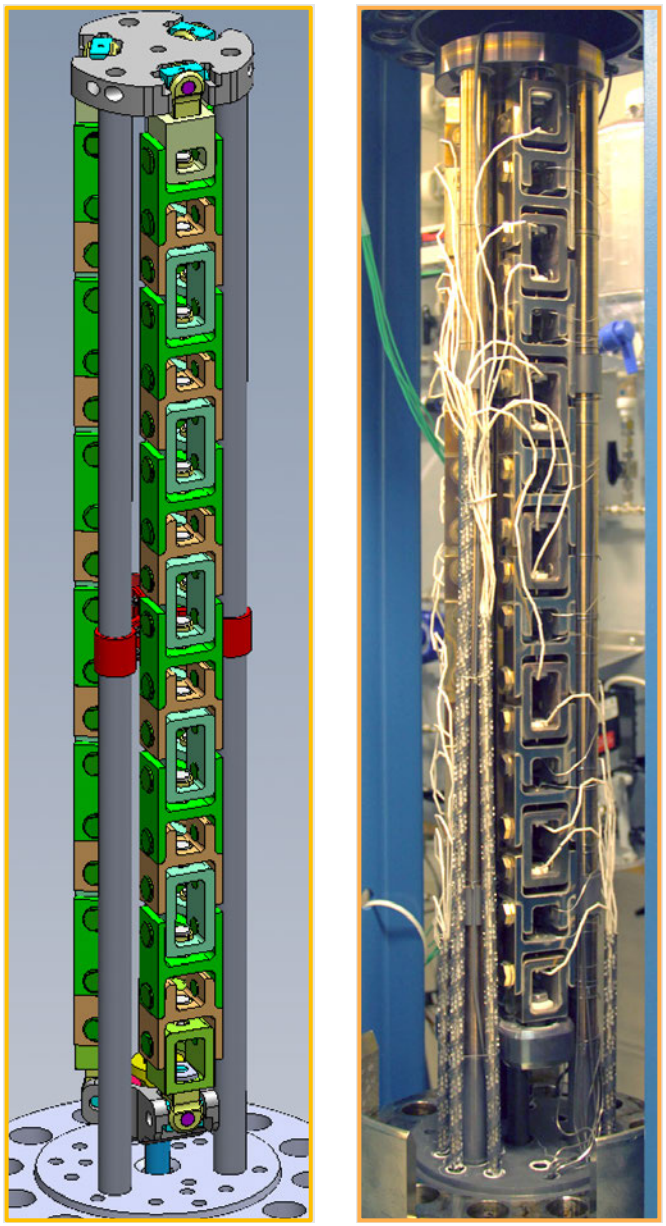

Figure 2. Sketch and photo of a three-string load line. The photograph is the Alloy 690/152(M)/52(M) specimen load line after an early inspection at 350 hours of exposure.

The test environment was simulated PWR primary water with 1,000 ppm boron, 2 ppm lithium, and 25 cc/kg hydrogen at 360°C. This combination of temperature and dissolved hydrogen content puts the corrosion potential at the nickel/nickel oxide (Ni/NiO) stability boundary. Testing at elevated temperature compared to typical PWR primary water temperature, and testing at the Ni/NiO stability boundary both serve as test accelerants. This was the typical condition used by PNNL for PWR primary water SCCGR testing.

As will be seen in the test results plot, the test was stopped and restarted several times. Some of these were planned stops to examine specimens or perform maintenance while other stops were due to various service-related outages. Some of these outages were planned (e.g., building outages to update the building electrical system) while others were not planned (e.g., storms causing a blackout). All the electronics, including the servo motor, are fed by an uninterruptible power supply that can maintain power to the equipment for up to approximately 2.5 hours during an unplanned outage.

Custom software was created for SCCI testing at PNNL. This software interfaces with and controls both the servo and the DCPD electronics, and it logs all pertinent data. Over the course of the program, the performance of the software was frequently improved, and features were added. Updates include the ability to read and control a second failsafe load cell, automatically unload the test systems when an extended power outage occurs, and the signal-to-noise ratio has been substantially improved with a revised DCPD electronics control approach.

4.0 Results – SCC Initiation Test Data

4.1 Overview

This 36-specimen test was started in January 2016 and consists of specimens machined from four heats of Alloy 690 and four Alloy 152(M)/52(M) welds. There are three specimens each of the Alloy 690 heats. The intent was to test six specimens each of the weld metals; however, because of a material limitation, there are only five Alloy 152 specimens. A seventh Alloy 52M specimen was tested because ample extra material from this weld was available.

One specimen of each Alloy 690 heat and two of each Alloy 152(M)/52(M) welds (12 specimens total among all the materials) were instrumented for DCPD detection of initiation while the other 24 specimens were instrumented for detection of failure. The 12 specimens instrumented for detection of initiation are in a non-referenced DCPD configuration that does not subtract DCPD voltage changes due to alloy resistivity evolution and creep. A non-referenced configuration was used because at the time when the test was started, the maximum number of DCPD signals that could be monitored by the software was only twelve. These specimens were all in String 1.

Dimensional measurements and selected details on each specimen are given in Table 5. The specimens were arranged in the autoclave so that for each material, the smallest gauge diameter was instrumented for DCPD. This arrangement was selected to enable the best chance of observing the highest strains that might occur during loading, and if any initiations were to occur, it would most likely happen in the smallest gauge diameter specimens that are being monitored.

Testing was stopped at 2.4, 4.0, and 5.7 years to perform specimen examinations.

4.2 First Specimen Load-up

The first specimen load-up is used to set the stress and strain on the specimens. This takes place after the specimens are at full temperature in the test system. The target metric is to obtain 0.2–0.3% plastic strain on each specimen, but for this test in which many different materials are in the load train, there is an expectation that it will be impossible to hold all specimens to the 0.2–0.3% plastic strain metric and that the range of applied plastic strain among the specimens could be 1–2%. YS measurements at 360°C made on each material were used to set the gauge diameter of each SCCI specimen and to provide an idea of the load that will be obtained on the specimens. Gauge diameters were selected with the goal of each specimen reaching its YS at 1,000 lb load on the specimen.

During the first load-up, unexpected, negative DCPD-indicated strain response was observed on 4 of the 12 instrumented specimens as shown in Figure 3. The load on the specimens was approximately 860 lb which was well below the target yield load of 1,000 lb, so there was little concern that something undesirable was happening with these specimens. However, this type of behavior had not been previously observed, and because the cause could not be immediately determined, the specimens were unloaded. After finding no issues with the test setup outside the autoclave, another load-up attempt was performed the next day.

The same behavior was observed during the second attempt, but this time, it happened with all 12 specimens. Load-up was continued to approximately 930 lb to see if the strain response would change, but it did not, so the test was stopped again.

Table 5. Selected information on the Alloy 690/152(M)/52(M) specimens being tested in NRCI1. The rows correspond to each string. The specimens in String-1 (S1) were instrumented for DCPD.

	1 A690 114092	2 A52M ENSA	3 A52M ENSA	4 A690 WP142	5 A52 MHI	6 A52 MHI
S1	*IN107, A690 TK-VDM*	*IN110, A52M ENSA DP*	*IN113, A52M ENSA DP*	*IN116, A690 Valinox*	*IN119, A52 MHI*	*IN122, A52 MHI*
	HT# 114092, B#1, S#2	B#4, S#1	B#3, S#4	HT# WP142, B#3, S#3	B#1, S#1	B#2, S#4
	1 um Finish, 460 MPa	1 um Finish, 430 MPa	1 um Finish, 430 MPa	1 um Finish, 450 MPa	1 um Finish, 470 MPa	1 um Finish, 485 MPa
	30.51, 12.26, 3.54	30.52, 12.20, 3.65,	30.48, 12.29, 3.66	30.46, 12.26, 3.57	30.44 ,12.37, 3.44	30.48, 12.22, 3.47
	MUX1	MUX2	MUX3	MUX4	MUX5	MUX6
S2	IN108, A690 TK-VDM	IN111, A52M ENSA DP	IN114, A52M ENSA DP	IN117, A690 Valinox	IN120, A52 MHI	IN123, A52 MHI
	HT# 114092, B#1, S#1	B#3 S#1	B#4 S#2	HT# WP142, B#3, S#1	B#2, S#2	B#2, S#5
	1 um Finish, 460 MPa	1 um Finish, 430 MPa	1 um Finish, 430 MPa	1 um Finish, 450 MPa	1 um Finish, 470 MPa	1 um Finish, 485 MPa
	30.52, 12.25, 3.55	30.52, 12.22, 3.67	30.46, 12.23, 3.67	30.48 12.21, 3.59	30.50 12.25, 3.47	30.52 12.26, 3.47
	FC1	FC2	FC3	FC4	FC5	FC6
S3	IN109, A690 TK-VDM	IN112, A52M ENSA DP	IN115, A52M ENSA DP	IN118, A690 Valinox	IN121, A52 MHI	IN124, A52 MHI
	HT# 114092, B#1, S#3	B#3 S#2	B#4 S#4	HT# WP142, B#3, S#2	B#2, S#3	B#2, S#6
	1 um Finish, 460 MPa	1 um Finish, 430 MPa	1 um Finish, 430 MPa	1 um Finish, 450 MPa	1 um Finish, 470 MPa	1 um Finish, 485 MPa
	30.44, 12.29, 3.56	30.49, 12.24, 3.67	30.52, 12.21, 3.67	30.50 12.21, 3.58	30.45 12.31, 3.47	30.47 12.13, 3.47
	FC13	FC14	FC15	FC16	FC17	FC18

	7 A690 RE243	8 A152M IHI	9 A152M IHI	10 A152 MHI	11 A690 B25K-2	12 A152 MHI
S1	*IN125, A690 Valinox*	*IN128, A152M IHI*	*IN131, A152M IHI*	*IN134, A152 MHI*	*IN137, A690 Allvac*	*IN140, A152 MHI*
	HT# RE243, B#1, S#1	B#1, S#1	B#1, S#4	B#1, S#2	HT# B25K-2, S#1	B#1, S#4
	1 um Finish, 415 MPa	1 um Finish, 555 MPa	1 um Finish, 555 MPa	1 um Finish, 500 MPa	1 um Finish, 515 MPa	1 um Finish, 500 MPa
	30.31, 12.15, 3.72	30.45, 12.73, 3.22	30.49, 12.45, 3.24	30.48, 12.35, 3.37	30.45, 12.35, 3.32	30.47, 12.40, 3.37
	MUX7	MUX8	MUX9	MUX10	MUX11	MUX12
S2	IN126, A690 Valinox	IN129, A152M IHI	IN132, A152M IHI	IN135, A152 MHI	IN138, A690 Allvac	IN141, A152 MHI
	HT# RE243, B#1, S#2	B#1, S#2	B#1, S#5	B#1, S#3	HT# B25K-2, S#1	B#1, S#5
	1 um Finish, 415 MPa	1 um Finish, 555 MPa	1 um Finish, 555 MPa	1 um Finish, 500 MPa	1 um Finish, 515 MPa	1 um Finish, 500 MPa
	30.50, 12.24, 3.72	0.48, 12.60, 3.22	30.50, 12.55, 3.26	30.49, 12.40, 3.37	30.54, 12.49, 3.34	30.43, 12.31, 3.37
	FC7	FC8	FC9	FC10	FC11	FC12
S3	IN127, A690 Valinox	IN130, A152M IHI	IN133, A152M IHI	IN136, A52M ENSA	IN139, A690 Allvac	IN142, A152 MHI
	HT# RE243, B#1, S#3	B#1, S#3	B#1, S#6	DPM, B#3, S#3	HT# B25K-2, S#2	B#1, S#1
	1 um Finish, 415 MPa	1 um Finish, 555 MPa	1 um Finish, 555 MPa	1 um Finish, 430 MPa	1 um Finish, 515 MPa	1 um Finish, 500 MPa
	30.45, 12.20, 3.72	30.49, 12.77, 3.22	30.50, 12.46, 3.26	30.46, 12.15, 3.67	30.53, 12.44, 3.34	30.43, 12.40, 3.39
	FC19	FC20	FC21	FC22	FC23	FC24

Smallest gauge diameter
Instrumented for SCCI
SEM surface exams at 2.4, 4.0 yrs
SEM surface & FIB trench GB exams at 2.4, 4.0, 5.7 yrs
FIB trench GB exams at 5.7 yrs
SEM surface exams on all specimens at 5.7 yrs

This time the test was completely stopped, and the autoclave was opened to examine the load line, the specimens, and the DCPD wiring. No issues were observed with the specimens or the load line. However, several of the DCPD current wire spot welds to the specimens were found to have failed. The cause was determined to be inadequate spotwelding voltage.

During these two attempts to bring the specimens up to load, DCPD-indicated plastic strain was observed for some specimens, and in particular, IN107 (Alloy 690 114092), IN137 (Alloy 690 B25K-2), IN134 (Alloy 152), IN128 (Alloy 152M), and IN131 (Alloy 152M), all exhibited some plastic strain ranging from 0.1–0.35%. This indicated that some specimens were yielding below their expected test load of 1,000 lb.

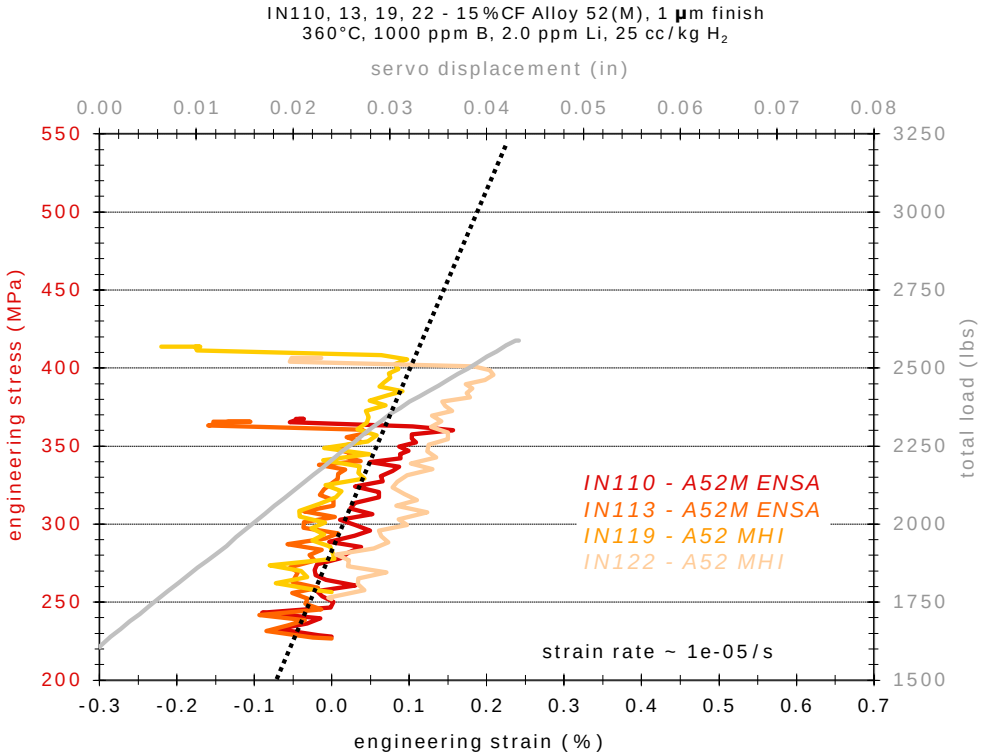

Figure 3. DCPD-indicated strain repones of the Alloy 52(M) specimens during the initial attempt at the first load-up.

The third attempt at load-up was successful, as shown in Figures 4-6. The final applied load on each specimen was approximately 965 lb. During this loading run, all specimens exhibited only elastic strain except for IN128 (Alloy 152), which exhibited a plastic strain jump of about 0.8%. When this strain jump occurred, it was decided to stop any further load-up. Since all the specimens were previously at the same load and with a small amount of plastic strain, reaching the yield stress for one specimen (the Alloy 152M specimen) means that all the other specimens were also essentially at their yield stress, and loading was stopped at that point. The lack of any plastic strain in the other specimens was due to the applied strain (and resulting work hardening) that occurred during the prior two attempts to load up the specimens.

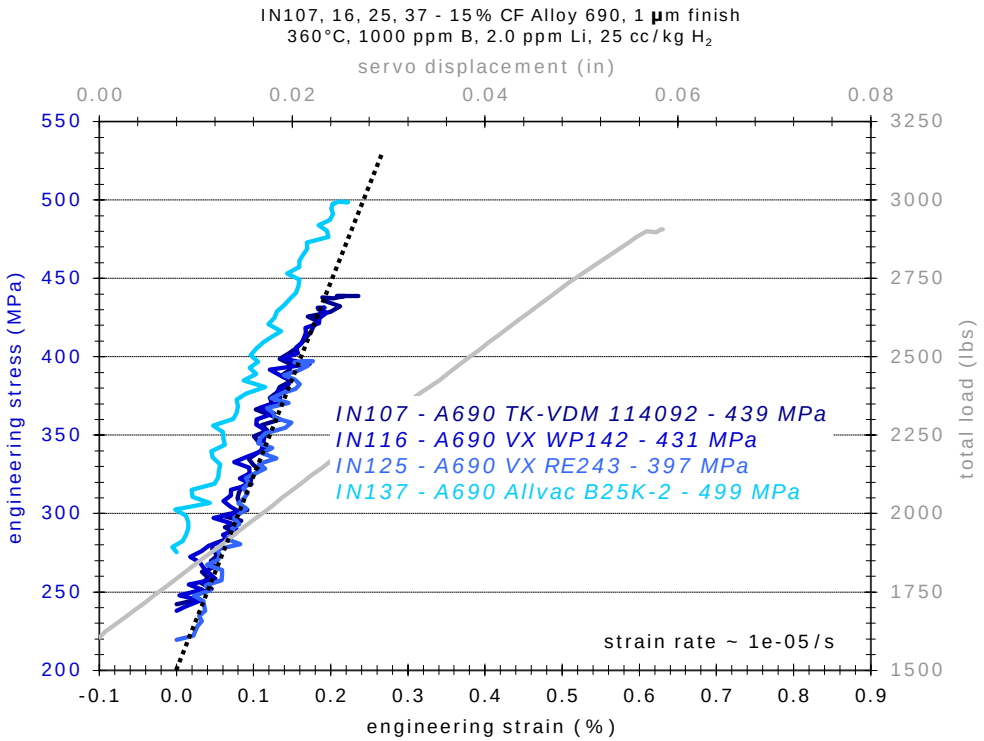

Figure 4. Stress versus strain curves for the four DCPD-instrumented Alloy 690 specimens during the successful first load-up.

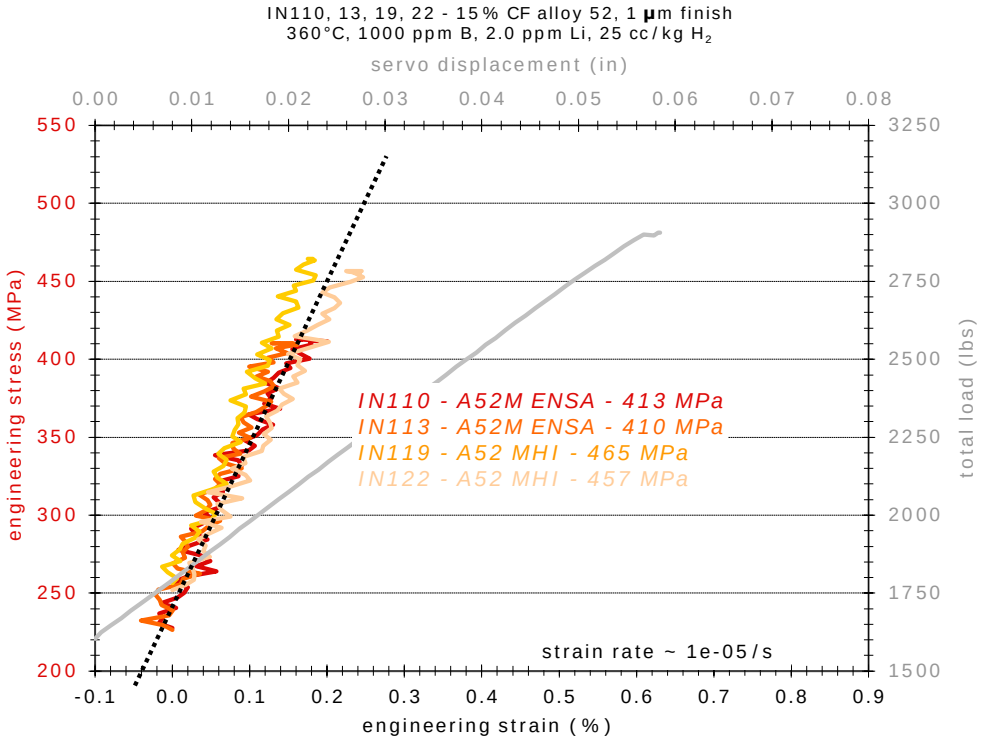

Figure 5. Stress versus strain curves for the four DCPD-instrumented Alloy 52(M) specimens during the successful first load-up.

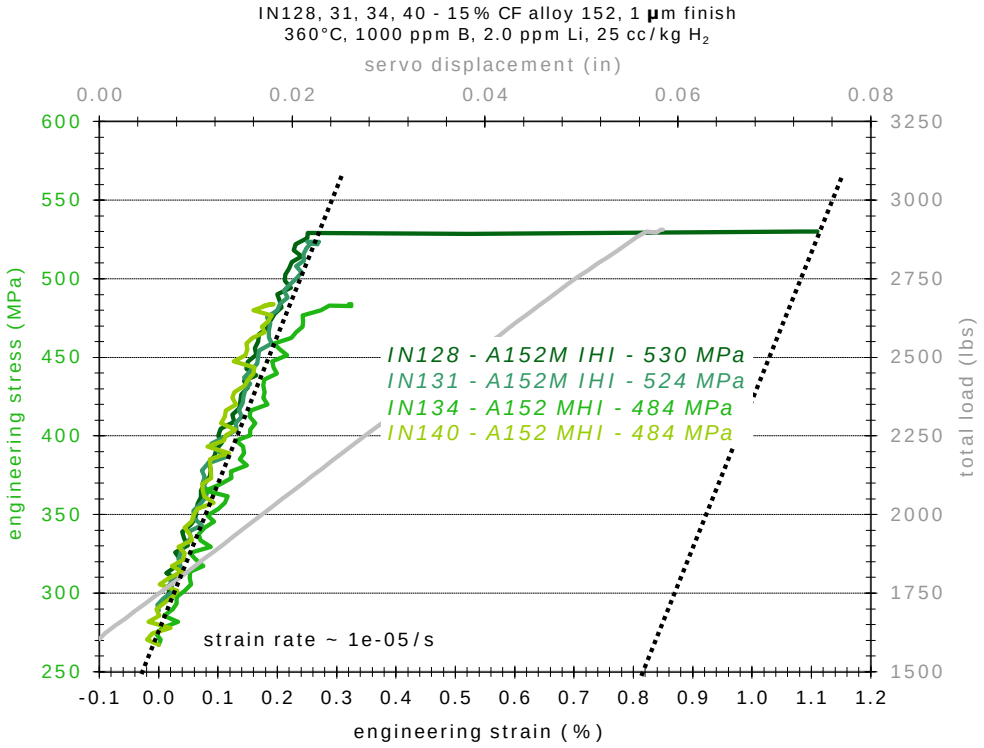

Figure 6. Stress versus strain curves for the four DCPD-instrumented Alloy 152(M) specimens during the successful first load-up.

4.3 SCC Initiation Specimen Response

The responses of the 12 DCPD-instrumented specimens are presented in Figures 7–9 up to the current test time of 50,163 hours (5.7 years).. All twelve of the DCPD-monitored specimens exhibited a non-referenced strain response that is primarily due to resistivity evolution and creep of the materials and is not indicative of SCC initiation, in particular, none of the specimen traces exhibited a shift to a positive rate of curvature that is indicative of SCCI.

Portions of the traces contain spikes in the values or periods of increased noise levels. These are primarily due to changes in DCPD system performance during the test and are not representative of specimen behavior. A few of the spikes are also due to building operational excursions that affected test temperature (DCPD readings change with test temperature) and room temperature (the output of the DCPD electronics have a slight room temperature sensitivity).

Actuator position is provided in the plots as a means to provide an alternative assessment of specimen response. Actuator position will increase as the specimens undergo elongation due to creep or cracking. Actuator position will change to a positive rate of curvature after specimen initiation occurs, just was with the DCPD readings. This is most useful for monitoring the combined response of the specimens not instrumented for DCPD. As can be seen in the plots, the curvature remained negative for the duration of the testing. Excursions in servo position are due to changes in room temperature which cause changes in load line length as the load frame changes length.

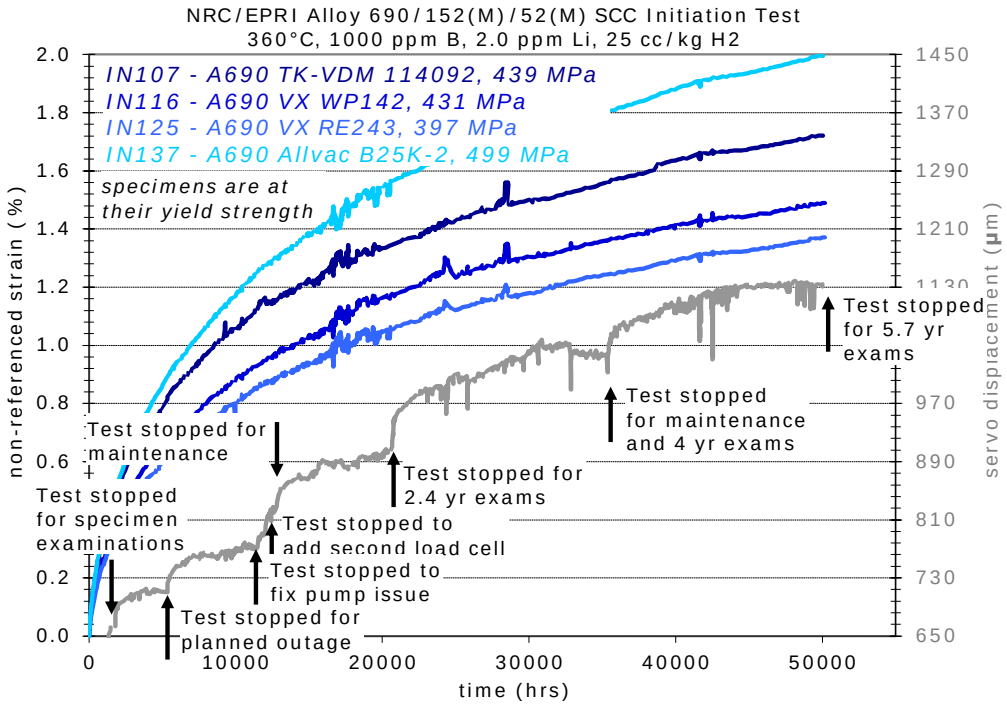

Figure 7. DCPD response of the four DCPD-instrumented Alloy 690 specimens in NRCI1. The gray line is the servo displacement. Temporary rapid increases in displacement occur after the test is restarted.

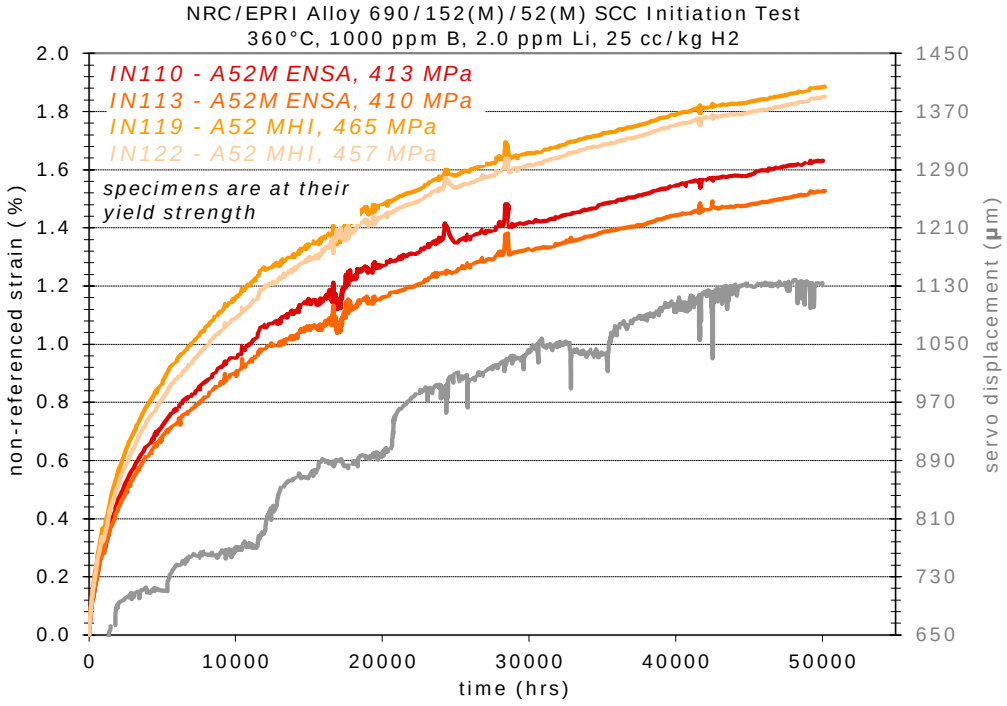

Figure 8. DCPD response of the four DCPD-instrumented Alloy 52(M) specimens in NRCI1. The gray line is the servo displacement. Temporary rapid increases in displacement occur after the test is restarted.

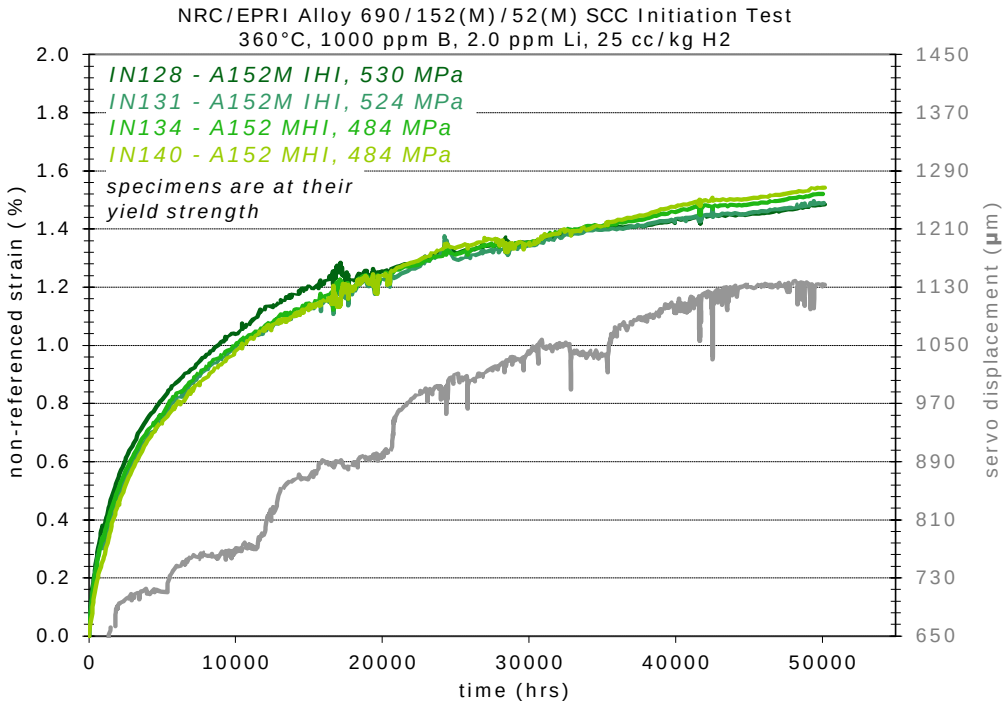

Figure 9. DCPD response of the four DCPD-instrumented Alloy 152(M) specimens in NRCI1. The gray line is the servo displacement. Temporary rapid increases in displacement occur after the test is restarted.

4.4 Creep Rate Measurements

Because the specimens did not exhibit any obvious cracking by DCPD or by mid-test specimen examinations, the recorded DCPD response is due only to a combination of specimen creep and resistivity evolution material. The resistivity evolution contribution can be measured by performing a DCPD observation at low load where creep is expected to be much lower. This resistivity contribution is then subtracted from the DCPD response at full load to obtain an estimate of creep rate. Two such measurements were performed on the specimens, once at 12,000 hours and then again at 50,163 hours just before the test was ended. In both cases, the servo-load was removed from the specimens leaving just the tare load due to water pressure on the pullrod. The tare load puts the specimens at approximately 45% of their YS. Power law creep behavior with a stress exponent greater than three will dominate near 100% YS, so a reduction of load to 45% of YS will cause a significant reduction in creep rate, leaving primarily resistivity evolution.

Creep strain rate estimates at 12,000 hours of exposure for the DCPD-instrumented specimens are presented in Table 6. The strain rate ranges from 2.8×10^{-9} to 11×10^{-9} %/sec, representing 0.09-0.35% strain per year. It appears that the Alloy 152 and 152M materials have the highest average creep rate, likely due to the higher average applied stresses on these specimens. There is limited data in the literature for comparison, but a creep strain rate published by Attanasio [19] shows a similar creep strain rate for Alloy 690 in high temperature water.

Table 6. Creep strain rates measured on Alloys 690/152(M)/52(M) at approximately 12,000 hours of exposure in high temperature water.

ID	Material	Heat	Full Load Stress (MPa)	Total Strain Rate (%/sec)	Material Resistivity Contribution (%/sec)	Creep Strain Rate (%/sec)
IN107	690	TK-VDM 114092	439	1.4×10^{-8}	6.9×10^{-9}	7.1×10^{-9}
IN116	690	Valinox WP142	431	7.3×10^{-9}	2.4×10^{-9}	4.9×10^{-9}
IN125	690	Valinox RE243	397	7.3×10^{-9}	4.5×10^{-9}	2.8×10^{-9}
IN137	690	Allvac B25K-2	499	1.3×10^{-8}	7.3×10^{-9}	5.7×10^{-9}
IN110	52M	ENSA	413	1.1×10^{-8}	8.3×10^{-9}	2.7×10^{-9}
IN113	52M	ENSA	410	9.7×10^{-9}	6.9×10^{-9}	2.8×10^{-9}
IN119	52	MHI	465	9.7×10^{-9}	6.9×19^{-9}	2.8×10^{-9}
IN122	52	MHI	457	9.9×10^{-9}	7.1×10^{-9}	2.8×10^{-9}
IN128	152M	IHI	530	1.1×10^{-8}	3.5×10^{-9}	7.5×10^{-9}
IN131	152M	IHI	524	1.1×10^{-8}	5×10^{-10}	1.1×10^{-8}
IN134	152	MHI	484	1.1×10^{-8}	7×10^{-10}	1.0×10^{-8}
IN140	152	MHI	484	1.1×10^{-8}	3.5×10^{-9}	7.5×10^{-9}

Creep strain rate estimates at 50,163 hours of exposure for all 12 DCPD-instrumented specimens are presented in Table 7. The resistivity evolution contribution of the Alloy 152(M) specimens was observed to be slightly negative which is the opposite of the expected response. The fact that this behavior occurred only for one class of material suggests that it is not an artifact of the DCPD system and instead is due to shift from a resistivity increase with time to a resistivity decrease. The creep strain rates ranged from 2.2×10^{-9} to 3.9×10^{-9} %/sec, representing 0.07–0.12% strain per year. For this time interval, it was the Alloy 52(M) specimens that had the higher creep rate, but only by a small margin.

Table 7. Strain rates measured on Alloy 690, 52, and 152 at approximately 50,163 hours of exposure in high temperature water.

ID	Material	Heat	Full Load Stress (MPa)	Total Strain Rate (%/sec)	Material Resistivity Contribution (%/sec)	Creep Strain Rate (%/sec)
IN107	690	TK-VDM 114092	439	2.8×10^{-9}	1.9×10^{-10}	2.6×10^{-9}
IN116	690	Valinox WP142	431	2.4×10^{-9}	1.9×10^{-10}	2.2×10^{-9}
IN125	690	Valinox RE243	397	2.4×10^{-9}	1.9×10^{-10}	2.2×10^{-9}
IN137	690	Allvac B25K-2	499	3.4×10^{-9}	1.9×10^{-10}	3.3×10^{-9}
IN110	52M	ENSA	413	4.2×10^{-9}	7.8×10^{-10}	3.4×10^{-9}
IN113	52M	ENSA	410	4.2×10^{-9}	7.8×10^{-10}	3.4×10^{-9}
IN119	52	MHI	465	4.7×10^{-9}	7.8×10^{-10}	3.9×10^{-9}
IN122	52	MHI	457	4.7×10^{-9}	7.8×10^{-10}	3.9×10^{-9}
IN128	152M	IHI	530	2.0×10^{-9}	-8.9×10^{-10}	2.9×10^{-9}
IN131	152M	IHI	524	2.0×10^{-9}	-8.9×10^{-10}	2.9×10^{-9}
IN134	152	MHI	484	2.3×10^{-9}	-8.9×10^{-10}	3.1×10^{-9}
IN140	152	MHI	484	2.3×10^{-9}	-8.9×10^{-10}	3.1×10^{-9}

One insight gained from the creep measurements is that it confirms that significant diffusive processes are occurring during the SCCI test. Creep cavities have been observed to form in moderately and highly CW Alloy 690, and this requires significant diffusive flow, so the creep measurements are an added indicator that indeed diffusive flow is occurring.

Analysis of the operating creep mechanism may provide additional insight into the creep cavity formation process. For these SCCI tests that were run at 360°C (~0.4T_m) and at the YS, the available creep deformation maps, which are available for non-CW Ni-binary alloys [20], and non-CW Alloy 690 [21], indicate that dislocation climb-glide will dominate the creep behavior. This mode of creep is not confined to grain boundaries and instead occurs throughout the material. As the name implies, it is a process whereby dislocations climb by diffusive processes and also glide due to athermal processes [22]. It is typically portrayed as an iterative process where dislocations will climb past obstacles and then glide until reaching another obstacle. The process then repeats. It involves a significant amount of dislocation movement, and it is hypothesized here that the dislocation movement drives dislocation recombination (e.g., like dislocation cell structure formation during thermal exposure of highly CW alloys) which produces vacancies as a by-product. Thus, the primary source of the vacancies for creep cavity formation is not the equilibrium vacancy concentration due to the alloy exposure temperature, but rather vacancies due to dislocation recombination.

GB cavity formation occurs most readily in CW Alloy 690 that has a high density of GB carbides. Prior to SCCI testing of such materials, the dislocation density around the GB carbides is very high and localized due to the cold working process (the carbides do not deform). Electron backscatter diffraction kernel average deformation maps confirm very high levels of deformation around GB carbides in CW Alloy 690 [4]. It is postulated that during SCCI testing, these dislocations undergo some recombination or reorganization which produces a locally high vacancy concentration in the vicinity of GBs that then allow for GB creep cavity formation. This mechanism would also contribute to SCC growth.

5.0 Results – Microstructure Observations

5.1 Experimental Setup for Specimen Examinations

SCC initiation behavior of four Alloy 690 heats and four Alloy 152(M)/52(M) weld metals was evaluated in a 15% CF condition in 360°C simulated PWR primary water in the NRCI1 test system. Prior to testing, the gauge surface of all specimens was polished to a 1-μm diamond paste finish.

The test was stopped at 2.4 years (20,659 hours), 4.0 years (35,414 hours), and 5.7 years (50,163 hours) for specimen examinations. The general approach to specimen examinations has been to conduct gauge surface examination by scanning electron microscopy (SEM) and to use a focused ion beam (FIB) instrument to perform FIB trench cross-section examinations of selected grain boundaries of selected specimens.

For the SEM gauge surface examinations, the entire gauge area and part of the fillet region (Figure 10) is documented using a JEOL 7600 SEM. Four rotations (90° to one another) are needed to document the entire gauge surface, and each rotation is a montage of about 160 images that are collected and stitched together using automation software on the microscope computer. SEM imaging is performed in high-kV backscattered electron (BSE) mode at a magnification of 200X, which allows the entire surface to be documented in a reasonable time frame with the ability to identity defects with a size down to approximately 500 nm.

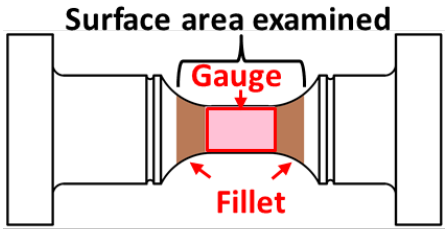

Figure 10. Schematic of the surface area of one rotation mapped in the SEM for pre-test examination. The gauge surface mapped is highlighted in red and the surface in the fillet region mapped is highlighted in taupe.

Depending on the surface examination result, FIB trenching was performed on selected specimens to document near-surface cross-section morphology on targeted GBs or intergranular (IG) damage precursor/defects observed on the surface. The GBs that were selected had a normal vector parallel or nearly parallel with the tensile axis and typically either had cavities, cracks, or defects that intersected the surface (Figure 11). An FEI Quanta 3-dimension field emission gun FIB/SEM dual beam system was employed for this task. In most cases, a trench with a depth of less than 10 μm was made, and serial milling of 10–30 μm along the length of a GB was performed to document the evolution of subsurface morphology.

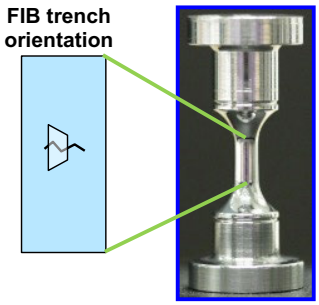

Figure 11. Orientation of FIB trench cross-sections relative to the SCCI specimens and grain boundaries.

The same set of specimens was examined at 2.4 and 4.0 years. At 2.4 and 4.0 years, the gauge surface of one specimen each of selected materials was examined by SEM, while FIB trench cross-section examinations were carried out on a subset of these specimens. After 5.7 years, the gauge surface of all 36 specimens was examined by SEM, and then a subset of these was examined by FIB trench cross-section. Every specimen that was examined by FIB trench cross-section at 2.4 and 4.0 years, was again examined at 5.7 years along with some additional specimens.

5.2 2.4/4.0-Year Surface and FIB Trench Cross-Section Examinations of Selected 15% CF Alloy 690 Specimens

Summary tables of the Alloy 690 specimen observations after 2.4 and 4.0 years is provided in Tables 8 and 9, respectively. One specimen of each Alloy 690 heat was subjected to FIB trench cross-section examination of selected GBs. After 2.4 years, spinel oxide (MO composition) had accumulated on the surface of some of the specimens, making it difficult to observe GBs by SEM. After 4.0 years, almost all specimens had a thick spinel oxide on the gauge surface. In cases where thick spinel oxide coverage was present, it was still possible to identify the location of some GBs due to differences in spinel oxide coverage on neighboring GBs.

Because of the formation of a nearly continuous MO spinel oxide on the surface, useful surface observations were not possible; however, selected FIB trenching was performed to reveal the grain boundaries to a depth of approximately 10 μm on one each of the Valinox (IN126) and TK-VDM (IN108) specimens. These materials were selected for examination because their fine, high density GB carbide distribution promotes GB cavity formation in more highly cold worked materials. Approximately 100-nm diameter pits were observed at the intersection of some GBs with the specimen surface, but no cavities were observed at any depth into the specimen.

The same two heats are also being tested in the U.S. Department of Energy (DOE) Light Water Reactor Sustainability (LWRS) Program task at PNNL but at higher CW levels. Short surface-breaking IG cracks were observed in the TT+21% CF Valinox and TT+21% cold rolled TK-VDM specimens after approximately 4.0 years of exposure with aggregations of GB cavities ahead of the crack tips. [23]. In addition, after only 1.1 year of exposure at YS, extensive GB cavities were observed in cross-sections of TT+31% CF Valinox and TT+31.9% CF TK-VDM specimens through destructive SEM examinations [24], and were later confirmed to have had led to DCPD detection of macroscopic crack initiation in the TT+31% CF Valinox material after 1.8 years of exposure [25] and in the TT+31.9% CF TK-VDM material after 3.2–3.7 years of exposure [23,26].

Table 8. Alloy 690 specimens examined after 2.4 years of exposure at their YS. All specimens in this list were subjected to gauge surface examinations.

ID	Material	Heat	YS (MPa)	FIB Trench Cross-Section of GBs	Notes
IN108	690	TK-VDM 114092	460	Yes	Surface cavities only
IN118	690	Valinox WP142	450		Surface cavities only
IN126	690	Valinox RE243	415	Yes	Surface cavities only
IN137	690	Allvac B25K-2	515		Surface obscured by oxide

Table 9. Alloy 690 specimens examined after 4.0 years of exposure at their YS. All specimens in this list were subjected to gauge surface examinations.

ID	Material	Heat	YS (MPa)	FIB Trench Cross-Section of GBs	Notes
IN108	690	TK-VDM 114092	460	Yes	Surface cavities hidden by oxide, no subsurface GB cavities
IN118	690	Valinox WP142	450		Surface cavities hidden by oxide
IN126	690	Valinox RE243	415	Yes	Surface cavities hidden by oxide, isolated subsurface GB cavities
IN137	690	Allvac B25K-2	515		Surface obscured by oxide

Examinations of more highly CW Alloy 690 SCC initiation specimens under the DOE LWRS Ni-base alloy SCC initiation task at PNNL revealed creep cavity formation along high angle GBs of 30% CW Alloy 690, and to a much lesser extent, in 20% CW Alloy 690 [27]. This mechanism has been observed to be responsible for SCC initiation in a small number of the 30% CW Alloy 690 specimens from that program. Therefore, the examination of the NRC/ERPI 15% CF Alloy 690 specimens focused on investigating to what extent cavity formation occurred after undergoing similar or longer length of exposure than the LWRS program specimens.

As reported previously [18], exposure of the NRC/EPRI specimens in 360°C simulated PWR primary water for 20,659 hours led to the formation of a thick iron-rich spinel oxide layer on much of the gauge surface of most specimens, making it difficult to observe GBs intersecting the gauge surface. Nevertheless, IG features were occasionally revealed in areas with thinner surface oxide coverage in a few specimens, and the specimen with the thinnest surface oxide layer from each material was selected for surface examination. As will be shown later, IG features such as surface cavities in the Alloy 690 or cracks in the weld metals were observed at GBs in specimens from multiple heats after the 2.4-year exposure. However, the surface oxide became thicker after 4.0 years, making it impossible to document surface damage evolution in all specimens. In such case, Serial FIB milling was performed on one TK-VDM and one Valinox RE243 specimen that were trenched previously at 2.4 years to check for GB cavity evolution after extended exposure.

5.2.1 IN118 – 15% CF Alloy 690TT CRDM Valinox WP142

The 15% CF Alloy 690TT Valinox heat WP142 specimen IN118 exhibited “postage stamp” features at GBs on the gauge surface after 2.4 years of exposure with examples at two locations provided in Figure 12. After a total of 4.0 years of exposure, the entire gauge surface

was covered by thick spinel oxides, obscuring detailed examination of the exposed grain boundaries as exemplified in Figure 13. This heat has a similar GB carbide distribution to the Valinox RE243 heat. Since the cavity distribution is believed to be similar to the Valinox RE243, no FIB trench cross-section examinations were performed on this specimen after 2.4 or 4.0 years of exposure.

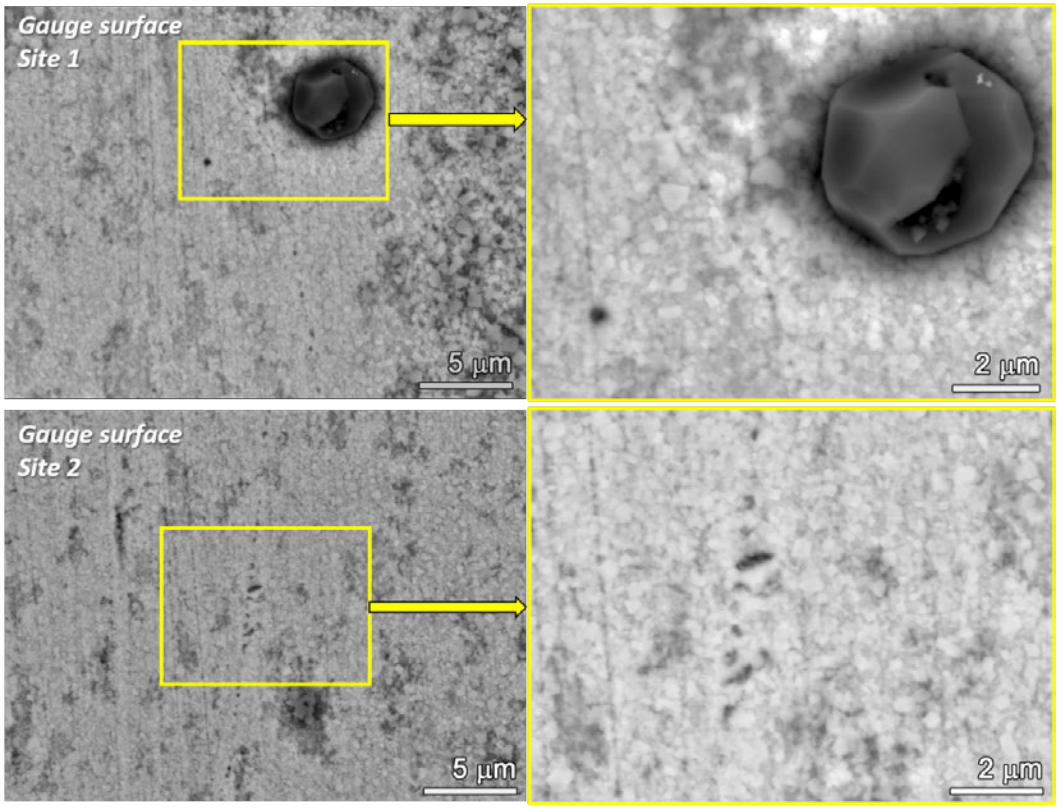

Figure 12. Representative SEM-BSE images of the gauge surface of the 15% CF Alloy 690 CRDM Valinox WP142 specimen IN118 after 2.4 years of exposure.

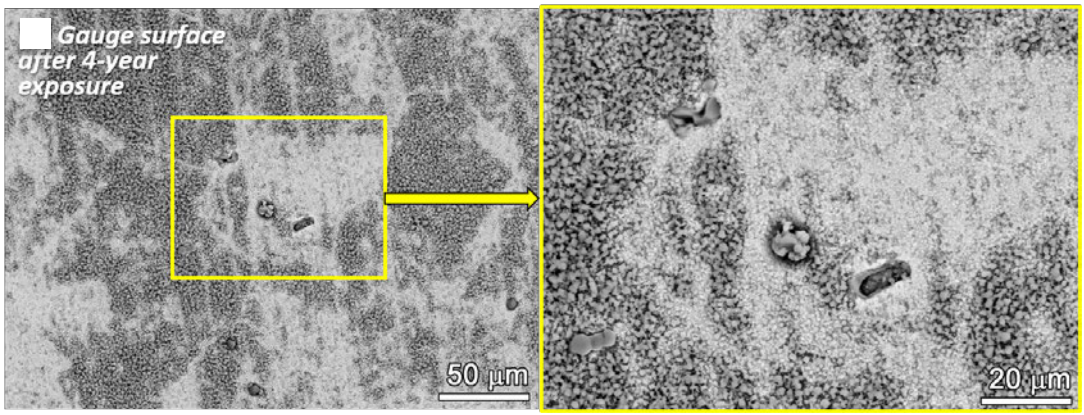

Figure 13. SEM-BSE images of typical gauge surface appearance in the 1 µm finish of the 15% CF Alloy 690TT CRDM heat WP142 specimen IN118 after 4.0 years of exposure.

5.2.2 IN126 – 15% CF Alloy 690TT CRDM Valinox Heat RE243

This a CRDM heat of Alloy 690 that has a semi-continuous distribution of 50–200 nm size GB carbides with a spacing of approximately 100 nm as shown for example in Figure 14. Cold forging or cold rolling this material will result in the production of cracked carbides and voids in progressively higher quantities with cold work level [4, 24].

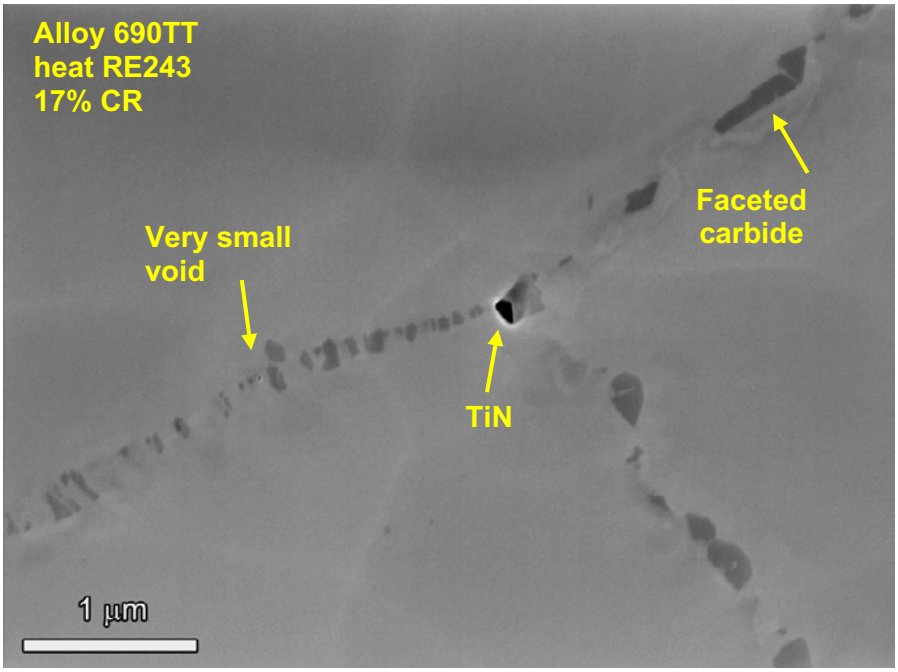

Figure 14. SEM-BSE observations of Alloy 690TT heat RE243 in a 17% CR condition.

Coupled surface and FIB trench cross-section examinations were performed on one specimen of the Valinox RE243 CRDM heat after 2.4 and 4.0 years of exposure. As shown in Figure 15, “postage stamp” features were commonly observed at GB intersections with the surface of this specimen after 2.4 years. Serial FIB milling was performed along the GB over a distance of about 18 µm with examples showing the cross-section morphology in Figure 16. The cavities observed on the surface were found to be no more than 100 nm in depth, and as with the Valinox RE243 specimen, no GB cavities were found below the surface.

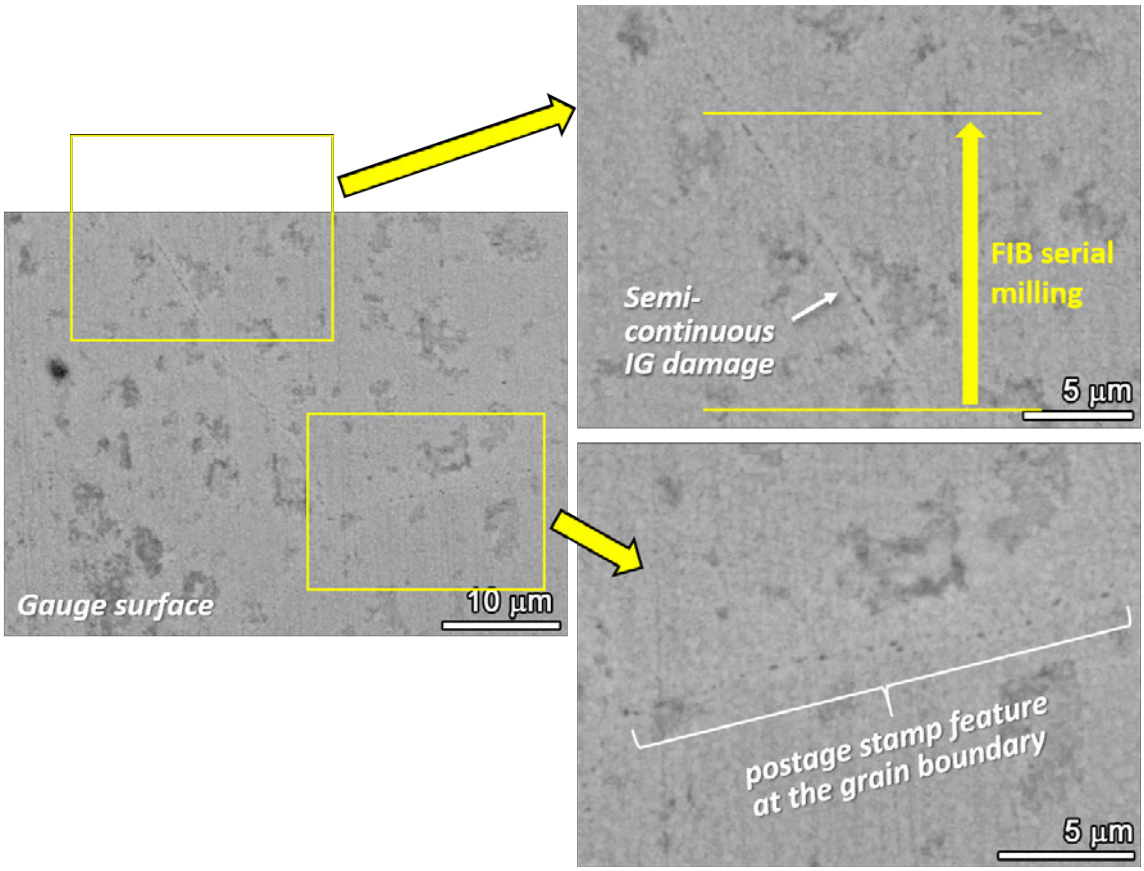

Figure 15. Representative SEM-BSE images of the gauge surface of the 15% CF Alloy 690 CRDM Valinox RE243 specimen IN126 after 2.4 years of exposure.

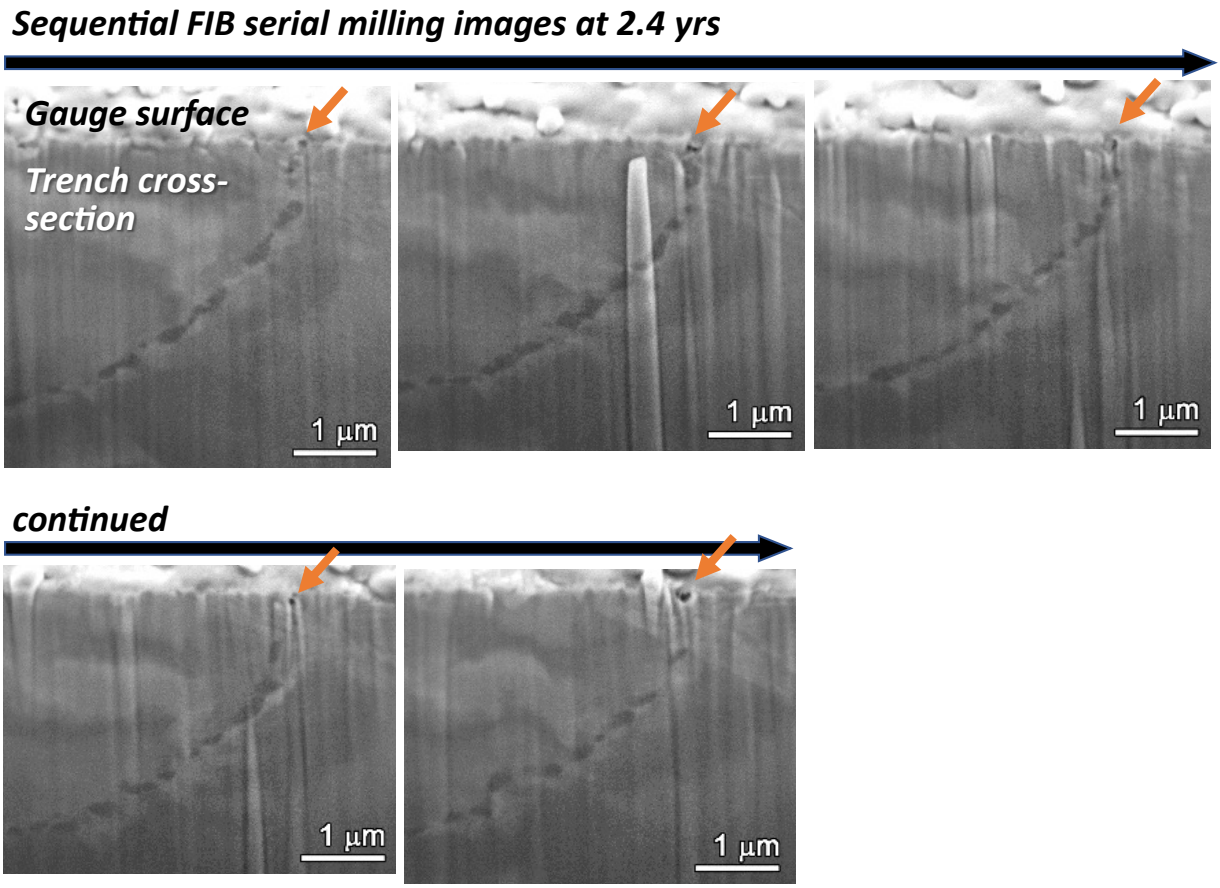

Figure 16. Selected FIB-SE serial trench cross-section images of IN126 after 2.4 years. These were taken along a selected portion of a GB highlighted in Figure 15. The small holes revealed at the GB intersecting the surface are highlighted by orange arrows.

The same region was examined again after 4.0 years of exposure. Similar to IN108 (TK-VDM 114092) after 4.0 years, this specimen was covered by thick spinel oxides that prevented observation of the GBs intersecting the surface (Figure 17b). While no GB cavities were observed in FIB trench cross-sections after 2.4 years, serial FIB trench cross-sections at two different GBs after 4.0 years in the same specimen consistently revealed a small number of GB cavities in multiple cross-sections with some examples provided in Figure 18. This suggests that the formation of GB cavities appears to be possible in Alloy 690TT at near-service relevant CW levels after long-term testing; however, the overall density at this point in time is inconsequently low and may simply be growth of cavities produced during cold forging. It should also be noted that this heat exhibited a higher areal density of GB carbides than the Alloy 690TT TK-VDM plate heat. High densities of GB cavities have been found to promote GB cavity formation and growth. This led to crack initiation of two 31% CF specimens from the same heat of Alloy 690 after 3.2–3.7 years of exposure [23,26].

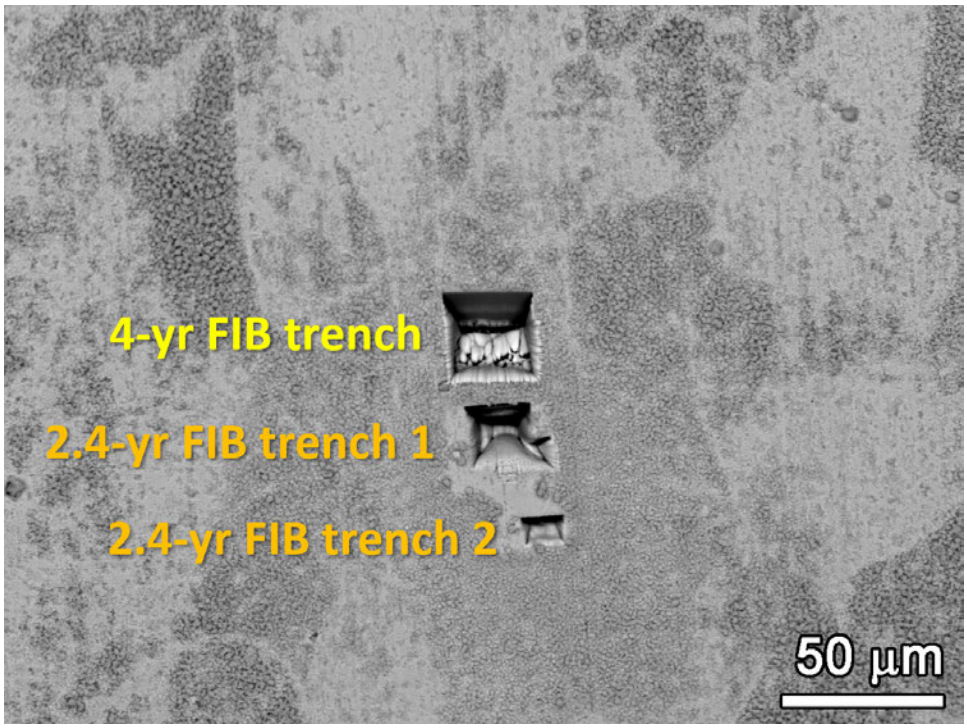

Figure 17. SEM-BSE images of typical gauge surface appearance in the 1 µm finish of the 15% CF Alloy 690TT CRDM heat RE243 specimen IN126 after 4.0 years of exposure in the same region shown in Figure 15.

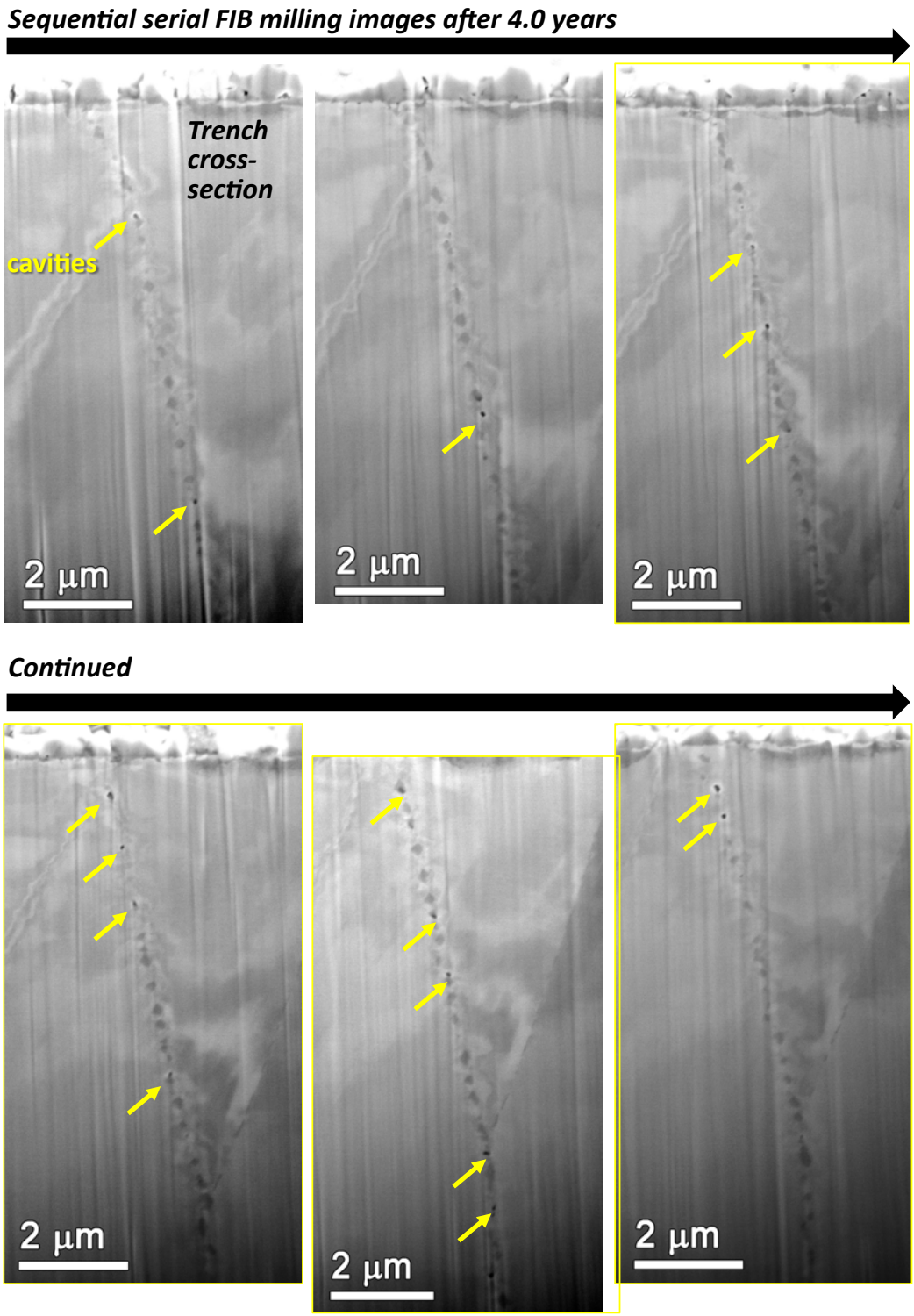

Figure 18. Selected FIB-SE serial trench images taken of IN126 along a randomly selected GB after 4.0 years of exposure. Cavities revealed in the cross-sections are highlighted in yellow.

5.2.3 IN108 – 15% CF Alloy 690TT plate TK-VDM Heat 114092

This a plate heat of Alloy 690 that has a semi-continuous distribution of 50-200 nm size GB carbides with a spacing of approximately 200 nm, as shown for example in Figure 19. Cold forging this material will result in the production of cracked carbides and voids in progressively higher quantities with cold forge level.

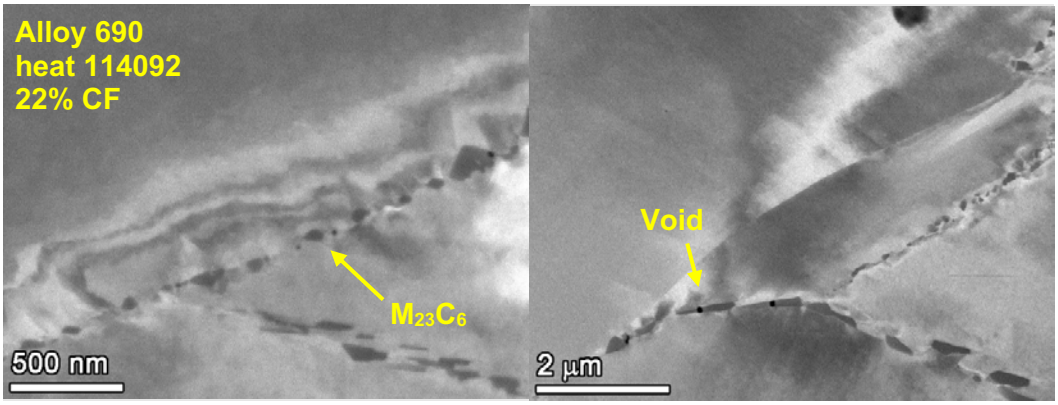

Figure 19. SEM-BSE observations of Alloy 690TT TK-VDM heat 114092 in a 22% CF condition.

As shown in Figure 20a, no obvious cracks were observed on the surface of IN108 after 2.4 years, but many of the visible GBs in this specimen exhibited a “postage stamp” appearance whereby the GBs intersecting the surface of the specimen are decorated with what appear to be nano-sized, discrete holes or cavities. To better understand the nature of these features, serial FIB trenching was performed as shown in Figure 21 to reveal cross-sections of a portion of the GB highlighted in the red box in Figure 20a for examination of the subsurface morphology of these “postage stamp” features. A total of approximately 100 images were taken of serially obtained cross-sections over a distance of approximately 10 µm along the GB with representative images shown in Figure 22. Small cavities were only found on the surface where the GB exhibits the “postage stamp” features. This same heat of material in a 21% CF condition was examined under the DOE LWRS program at PNNL after approximately the same exposure duration and found to contain not only surface cavities but also a very limited number of nano-sized cavities in cross-section [23].

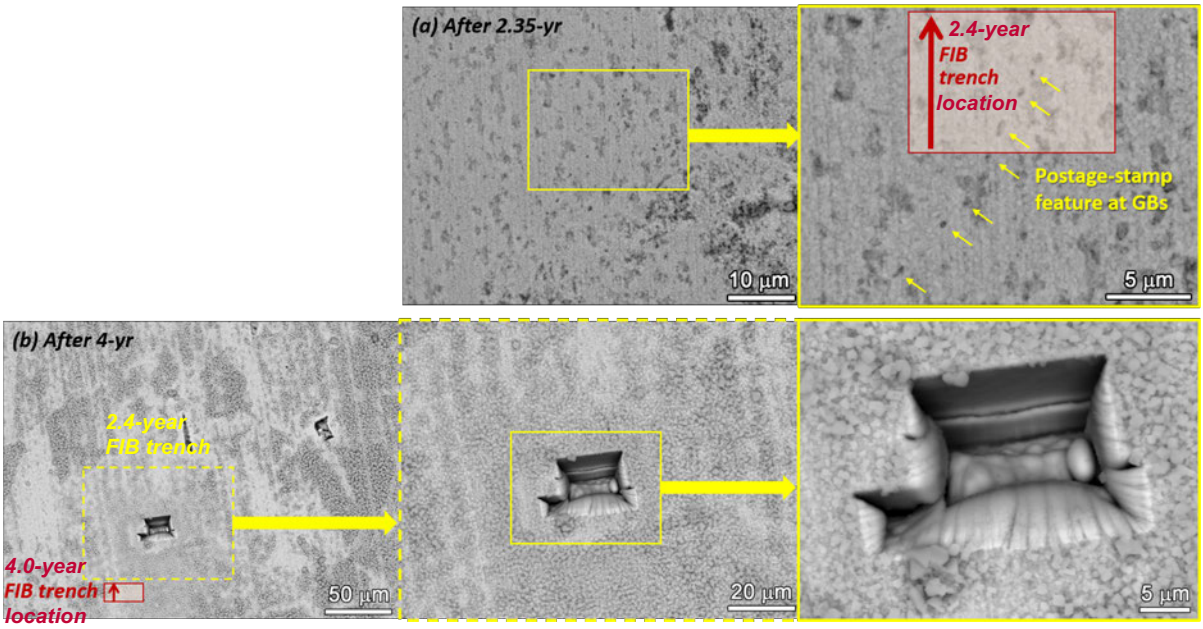

Figure 20. SEM-BSE images of typical gauge surface appearance of IN108 after (a) 2.4 and (b) 4.0 years of exposure. The images at 2.4 and 4.0 years were taken at similar locations.

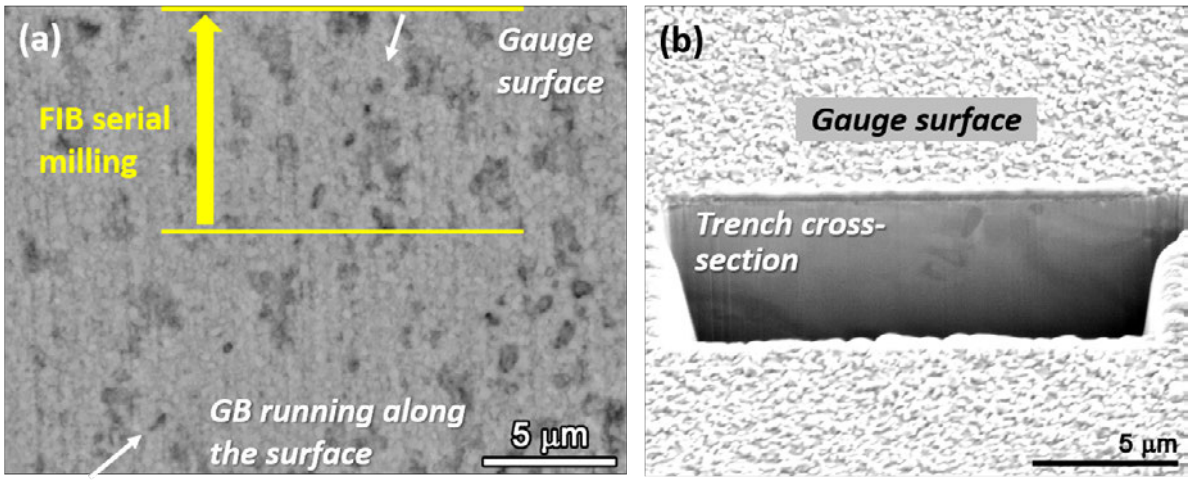

Figure 21. (a) SEM-BSE image of IN108 showing the location of the 2.4-year FIB trench with an arrow indicating the direction of FIB serial milling, and (b) FIB-SE image showing the starting cross-section of the trench in IN108.

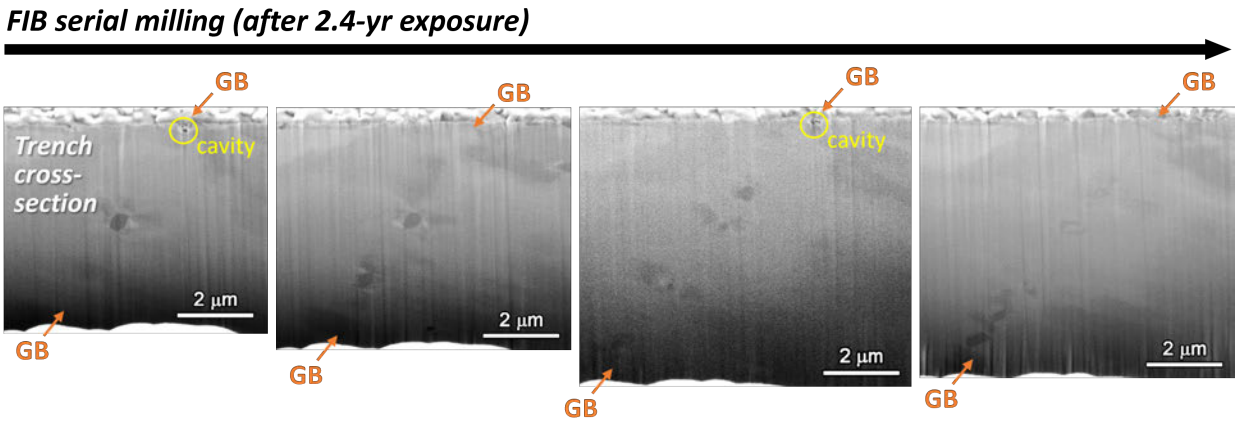

Figure 22. Selected FIB-secondary electron (SE) serial trench cross-section images taken along a selected portion of a GB highlighted in the red box in Figure 20(a) after 2.4 years of exposure in IN108.

SEM surface examination was again performed on the same specimen after 4.0 years of exposure as presented in Figure 20b. The observation was in the same location as the 2.4-year examination with the 2.4-year FIB trench noted in the image. After 4.0 years of exposure, the "postage stamp" features revealed above and below the 2.4-year trench are no longer visible due to formation of a thicker spinel oxide layer. While this thick surface oxide layer obscured the examinations of the surface, the 20 kV SEM accelerating voltage should be sufficient to resolve any open, small cracks despite the presence of the thick surface oxide. Thus, it is believed that no significant cracks were present after 4.0 years of exposure

To investigate whether cavities had grown or increased in quantity, serial FIB trenching was again performed along the same GB at the site marked by a red box in Figure 20b (left image) with representative images of the cross-sections shown in Figure 23. Although the orientation of the GB examined after 4.0 years (Figure 23) is different than the one observed at 2.4 years (Figure 22), the carbide density and size are similar between the two observations. No cavities were observed in the multiple cross-sections revealed during serial FIB milling, suggesting little or no cavity formation or growth in this material after a total exposure of 4.0 years. In comparison, the same material tested under DOE LWRS program in the 21% cold rolled condition exhibited multiple obvious short cracks at the surface associated with cavity evolution after 4.0 years of exposure [23]. Increased cavity formation and coalescence also led to macro-sized crack formation and DCPD detection of crack initiation at approximately 3.7 years of exposure in a 31% CF specimen from the same material [26].

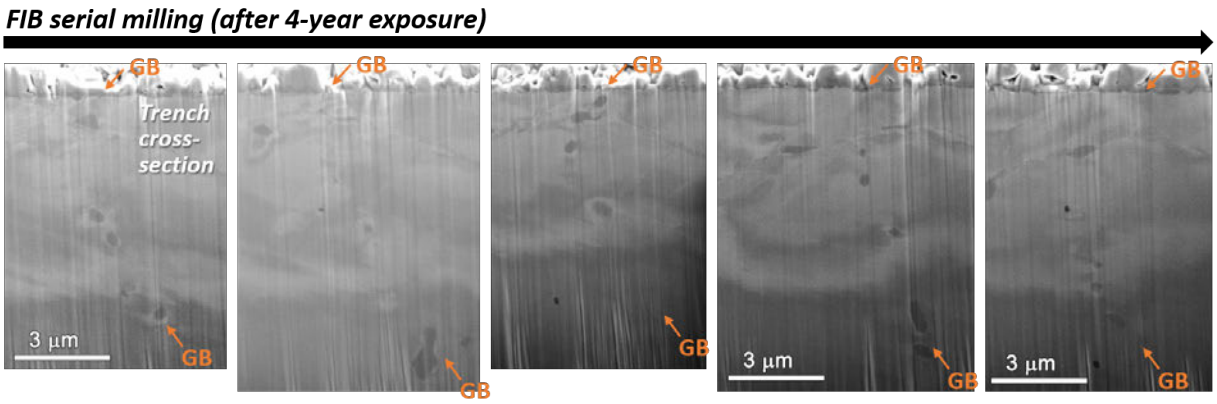

Figure 23. Selected FIB-SE serial trench cross-section images taken after 4.0 years of exposure of IN108 along the same GB trenched after 2.4 years. The GB included in this serial milling is highlighted in the red box in Figure 20(b).

5.2.4 IN137 – 15% CF Alloy 690MA Bar Allvac B25K-2

This MA material has a low density of unevenly distributed GB carbides along with a low density of matrix carbides as shown in Figure 24. When this material was cold rolled to 20% reduction for the NRC SCCGR project, very few cracked carbides and voids were observed. Based on our previous experience, such microstructures are much less susceptible to cavity formation as compared to materials featuring a semi-continuous distribution of nanometer-sized GB carbides.

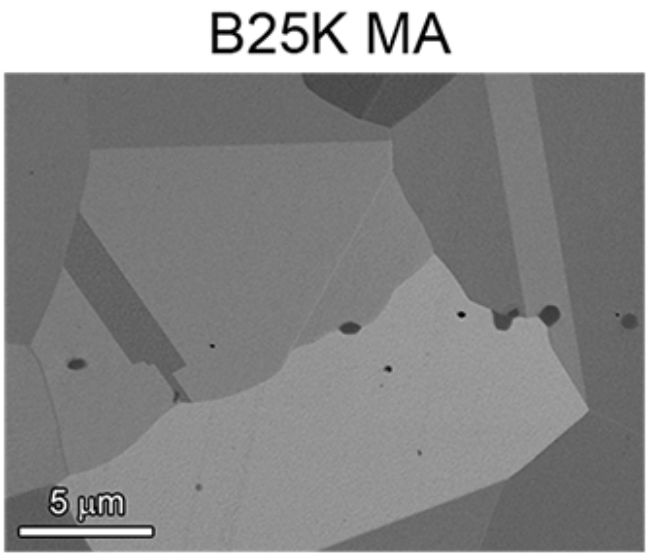

Figure 24. SEM-BSE image of the Allvac Alloy 690 B25K-2 microstructure.

As shown in Figure 25, after 2.4 years, the IN137 specimen exhibited a thick spinel oxide layer on the gauge surface, obscuring a clear examination of GB features. As expected, the surface was even more heavily covered in spinel oxides after 4.0 years with an example of the specimen surface provided in Figure 26 No FIB trenching or serial milling were performed on this specimen during the test interruptions.

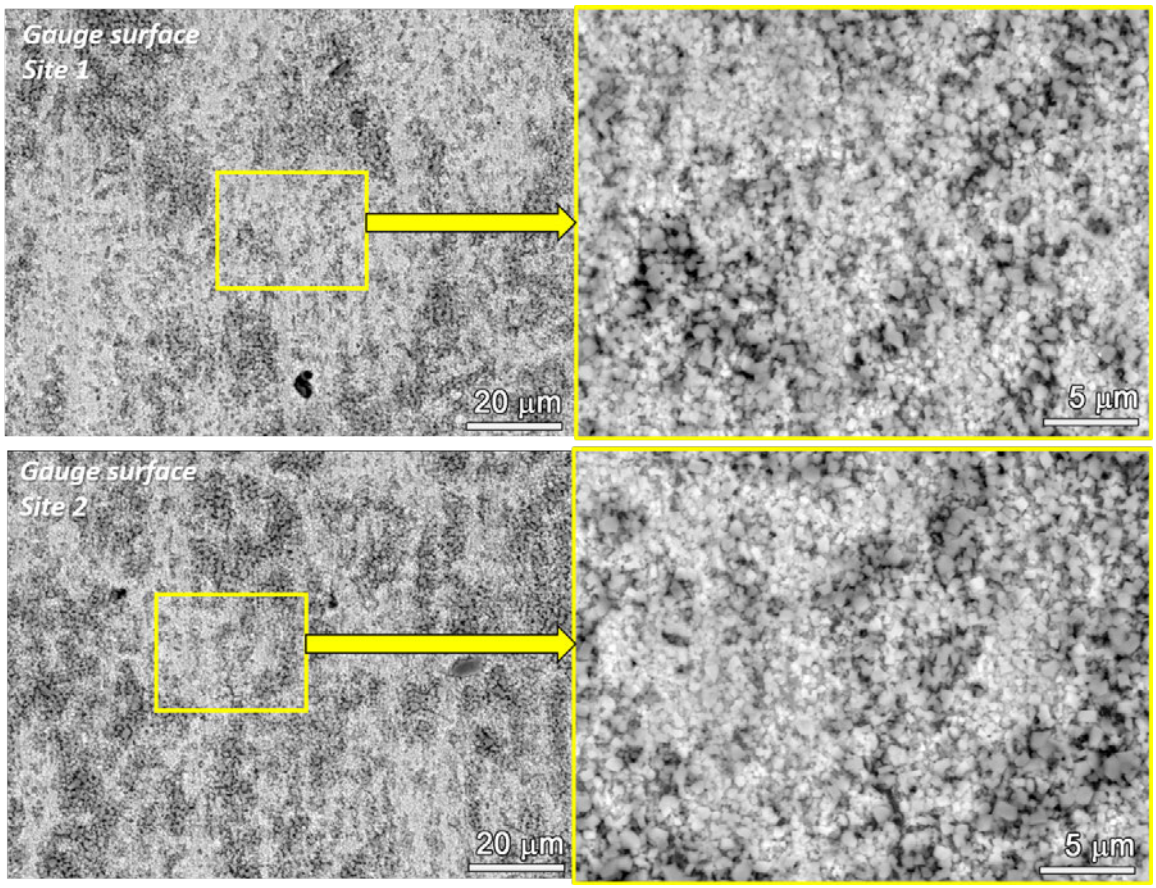

Figure 25. Lower and higher magnification SEM-BSE images of the gauge surface of the 15% CF Alloy 690MA bar Allvac B25K-2 specimen IN137 after 2.4 years of exposure.

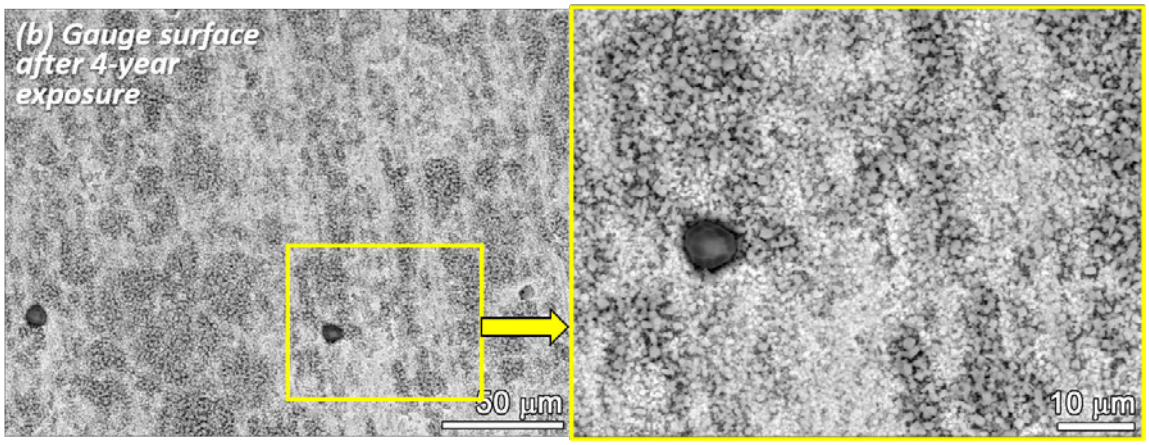

Figure 26. Lower and higher magnification SEM-BSE images of typical gauge surface appearance of the 15% CF Alloy 690MA bar Allvac B25K-2 specimen IN137 after 4.0 years of exposure.

5.3 5.7-Year Surface and FIB Trench Cross-Section Examinations of Selected 15% CF Alloy 690 Specimens

Gauge surface examinations were conducted on all 12 specimens after 5.7 years with a summary of key observations provided in Table 10. In general, there were indications of discontinuous dark contrast along isolated GBs that can represent either enhanced levels of GB oxidation or strings of cavities intersecting the specimen surface along a GB. Several specimens had crack-like features denoted by even darker contrast.

Table 10. Summary Alloy 690 SCCI specimen SEM gauge surface observations after 5.7 years.

Heat and Approximate Stress (MPa)	Spec ID	Material Condition	Observations
TK-VDM 114092, 440 MPa	General comments:		Spinel oxide covering 30-40% of surface of all 114092 specimens
	IN107	TT+15% CF	Indications of strong oxidation/cavities on isolated GBs, no crack-like features apparent
	IN108	"	Indications of postage stamp damage on isolated GBs, *two crack-like features in the fillet transition region*
	IN109	"	Indications of strong oxidation/cavities on isolated GBs, no obvious crack-like features
Valinox WP142, 430 MPa	General comments:		Spinel oxide covering 30-40% of surface of all WP142 specimens
	IN116	TT+15% CF	No strong oxidation/cavities or crack-like features visible
	IN117	"	Indications of strong oxidation/cavities on isolated GBs, no crack-like features apparent.
	IN118	"	Indications of strong oxidation/cavities on isolated GBs, *one crack-like feature near the fillet transition region*
Valinox RE243, 400 MPa	General comments:		Spinel oxide covering approximately 30% of surface of all RE243 specimens
	IN125	TT+15% CF	Indications of strong oxidation/cavities on isolated GBs, *two crack-like features*
	IN126	"	Indications of strong oxidation/cavities on isolated GBs, *one crack-like feature in the gauge*
	IN127	"	Indications of strong oxidation/cavities on isolated GBs, no obvious crack-like features
Allvac B25K-2, 500 MPa	General comments:		Spinel oxide covering approximately 20% of surface of all B25K-2 specimens
	IN137	MA+15% CF	Indications of strong oxidation/cavities on isolated GBs, no obvious crack-like features
	IN138	"	Indications of strong oxidation/cavities on isolated GBs, no obvious crack-like features
	IN139	"	Indications of strong oxidation/cavities on isolated GBs, no obvious crack-like features

Eight Alloy 690 specimens among heats RE243, 114092, and B25K-2 were examined by FIB trenching after the test was stopped at 5.7 years. Heat WP142 was not examined because it has essentially the same base microstructure as RE243. In most cases, a single GB was examined by FIB trenching on each specimen. In some cases, only snapshots were obtained,

while in others serial trenching and imaging were performed. A summary of the specimen examination history is provided in Table 11. The RE243 and WP142 heats have the highest GB carbide density followed next by heat 114092. Heat B25K-2 is essentially free of GB carbides. For those specimens subjected to FIB trench cross-section examinations, 2–3 GBs were examined per specimen at 2.4/4.0 years, while one GB was examined at 5.7 years.

Table 11. Alloy 690 SCCI specimen FIB trench examination matrix including the 5.7-year examinations.

Specimen ID	Material and Heat	2.4 Years	4.0 Years	5.7 Years
IN107	TK-VDM 114092			Snapshots
IN108	“	Y	Y	Snapshots, serial imaging
IN109	“			Serial imaging
IN125	Valinox RE243			Snapshots
IN126	“	Y	Y	Snapshots, serial imaging
IN127	“			Serial imaging
IN137	Allvac B25K-2			Snapshots
IN139	“			Snapshots, serial imaging

5.3.1 IN107 – 15% CF Alloy 690TT TK-VDM 114092

An example of a heat 114092 specimen (IN107) gauge surface is provided in Figure 27.

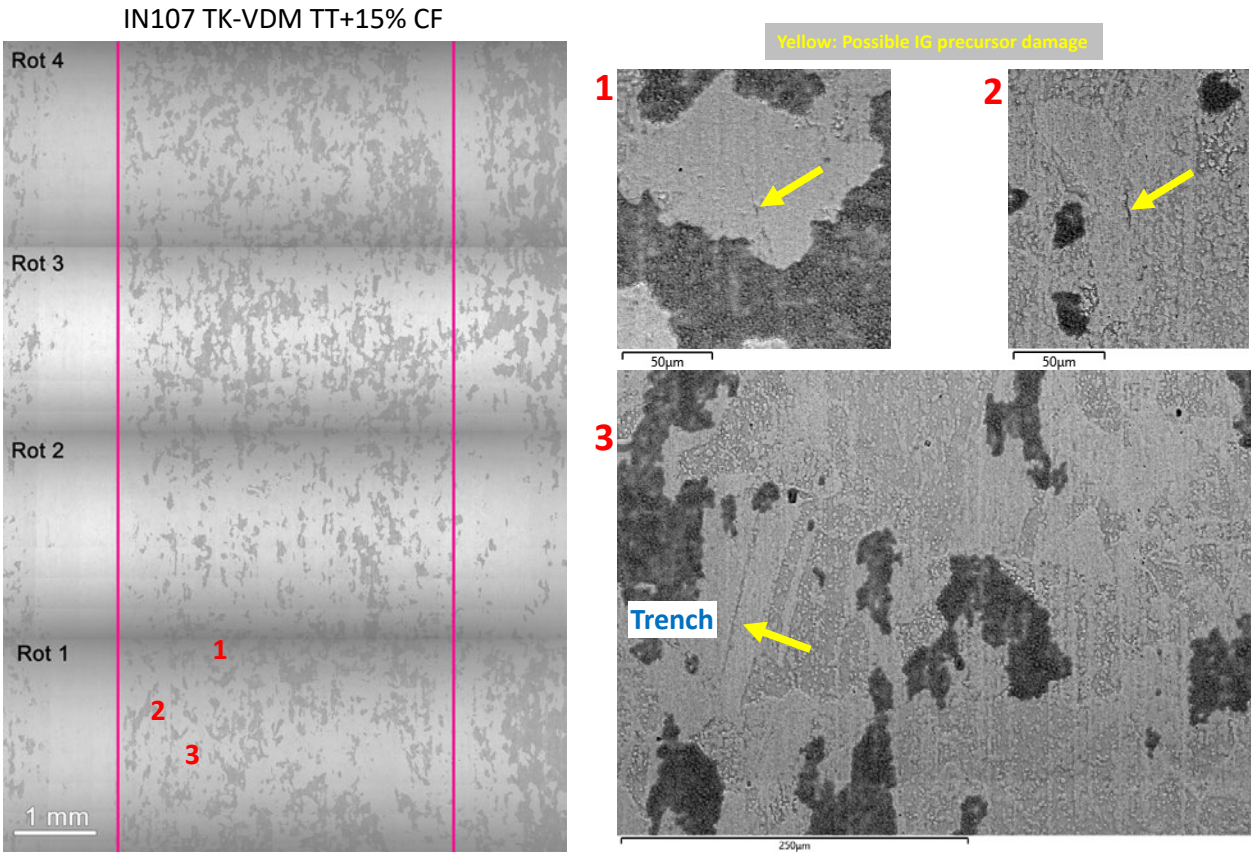

Figure 27. IN107 TK-VDM 114092-gauge surface summary.

The highlighted features are examples of enhanced oxidation or possible postage stamp GB cavities. A FIB trench cross-section of feature #3 is presented in Figure 28 where it is revealed that the contrast was due to the presence of a narrow twin band. This turned out to be a fairly common cause of enhanced linear contrast, and after this was understood, such twins could readily be identified in gauge surface observations and were not further examined.

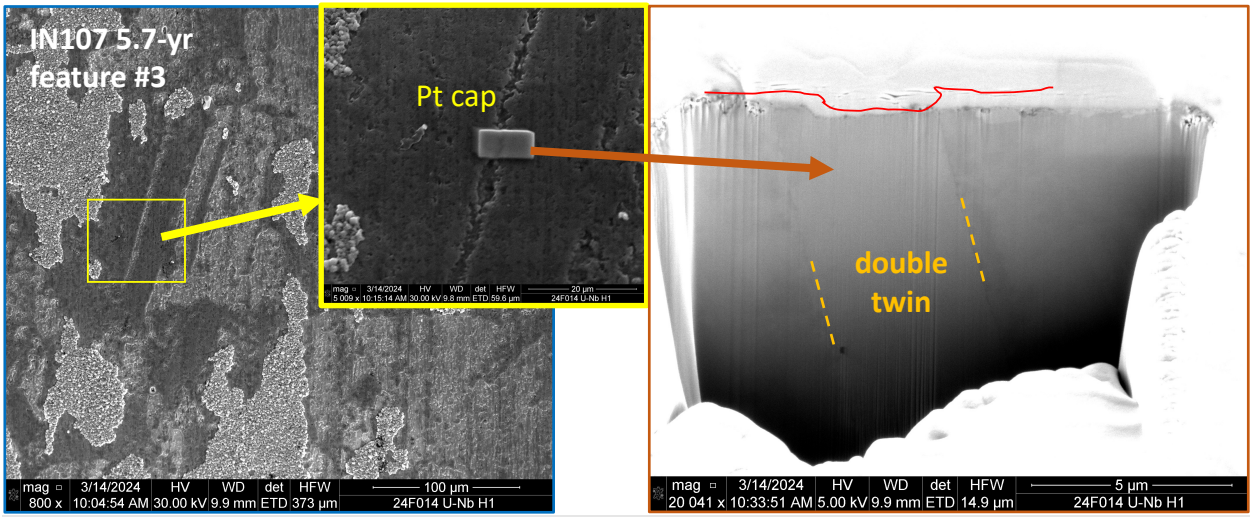

Figure 28. FIB trench of feature #3 observed on IN107 (heat 114092) after 5.7 years.

The exposed GBs on the surface of the heat 114092 specimens showed no obvious indications of cavity precursors, so a few GBs were randomly chosen for examination. The worst-case image of GB cavity formation is provided in Figure 29. A single large cavity and one small cavity are present. For this particular FIB trench cross-section series, a few other slices revealed a single cavity with a size closer to the smaller cavity in this image. The FIB trench cross-section series of IN109 had no GB cavities.

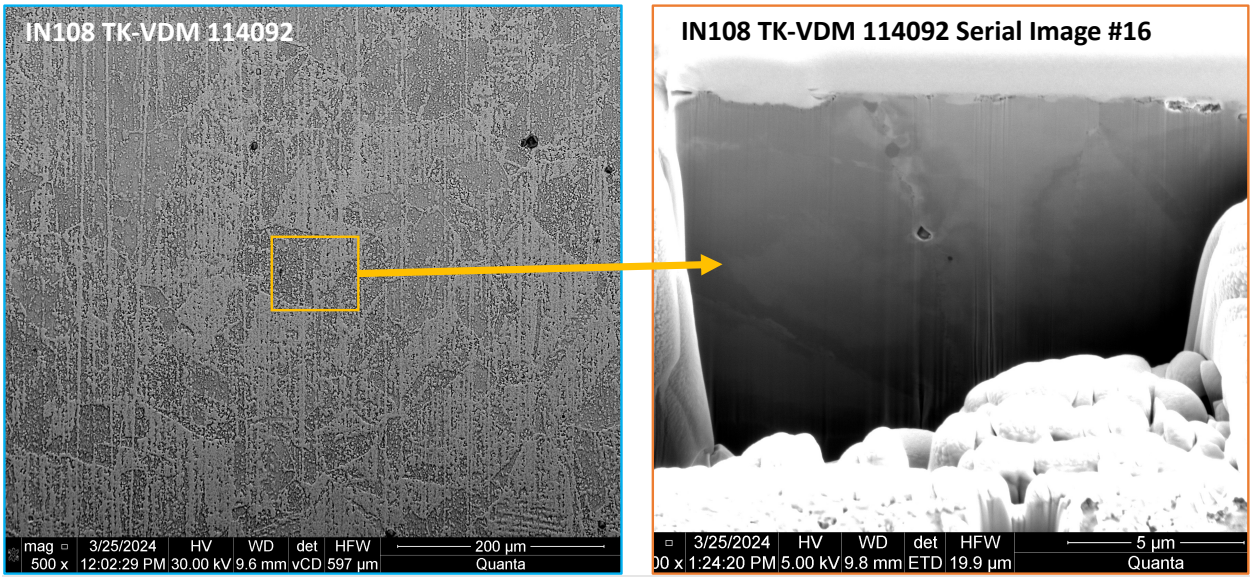

Figure 29. FIB trench cross-section image of a GB in IN108 showing worst-case cavity formation after 5.7 years.

5.3.2 IN126 – 15% CF Alloy 690TT Valinox RE243

Among the heat RE243 and WP142 specimens, there were further examples of GBs and twins with darker contrast, but one of the RE243 specimens—IN126—had what appeared to be an obvious crack as shown in Figure 30.

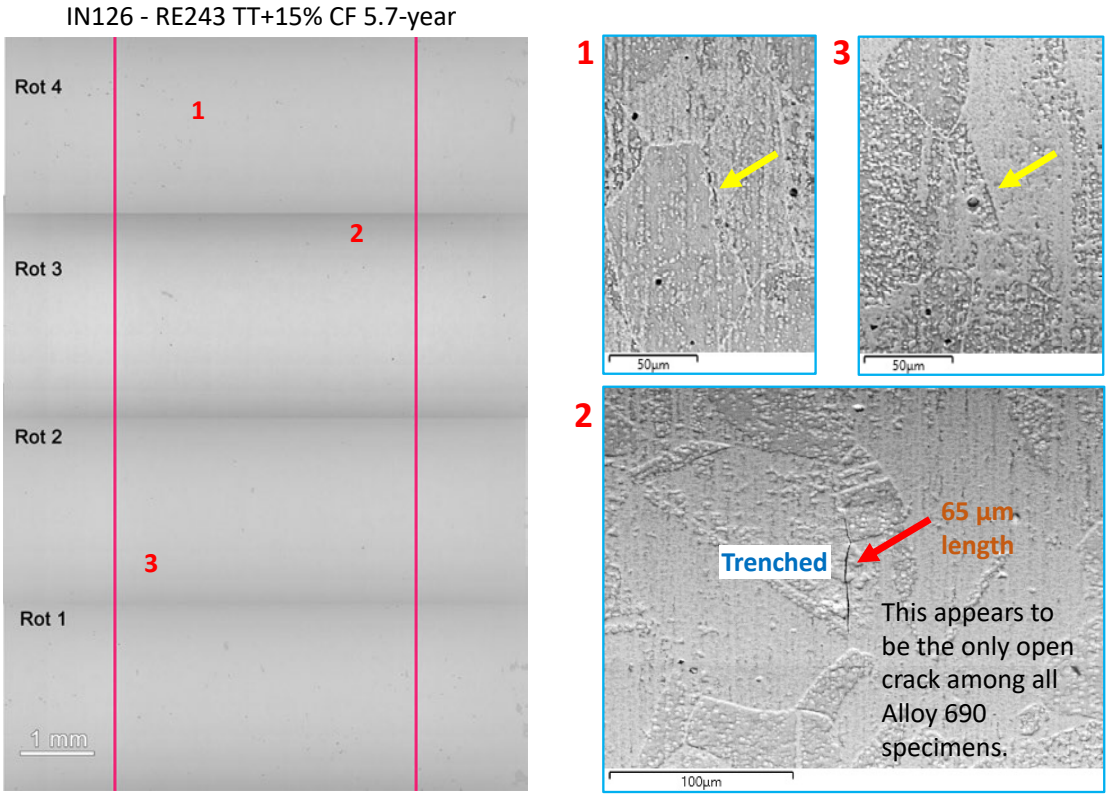

Figure 30. Gauge surface summary of IN126 which is heat R243. Three features of interest were observed with one appearing to be an obvious crack.

It is notable that even in the RE243 with the highest density of GB carbides and therefore the highest likelihood for GB cavity formation that there were only three suspect GBs. Detailed serial FIB trench cross-sectioning was performed on feature #2 with a subset of the cross-section images provided in Figure 31. A high density of large GB cavities is present down to a depth of 5 µm or more in many of the images, and higher resolution images such as shown in Figure 32 reveal that small cavities are present to a depth of >15 µm. The serial FIB trench images indicate that feature #2 is a shallow, 5 µm deep crack that formed as a result of GB cavity formation and coalescence. This is far too shallow of a crack to be of practical significance, but the rate at which the depth of the crack may be extending due to additional creep cavity formation cannot be determined from these images. Subjecting the specimen to additional SCCI testing would be the best means to accomplish this. Despite the formation of this shallow crack, which suggests that SCCI has the potential to occur in 15% CF material, it is important to keep in mind that this was the only obvious crack in all 12 of the Alloy 690 SCCI specimens.

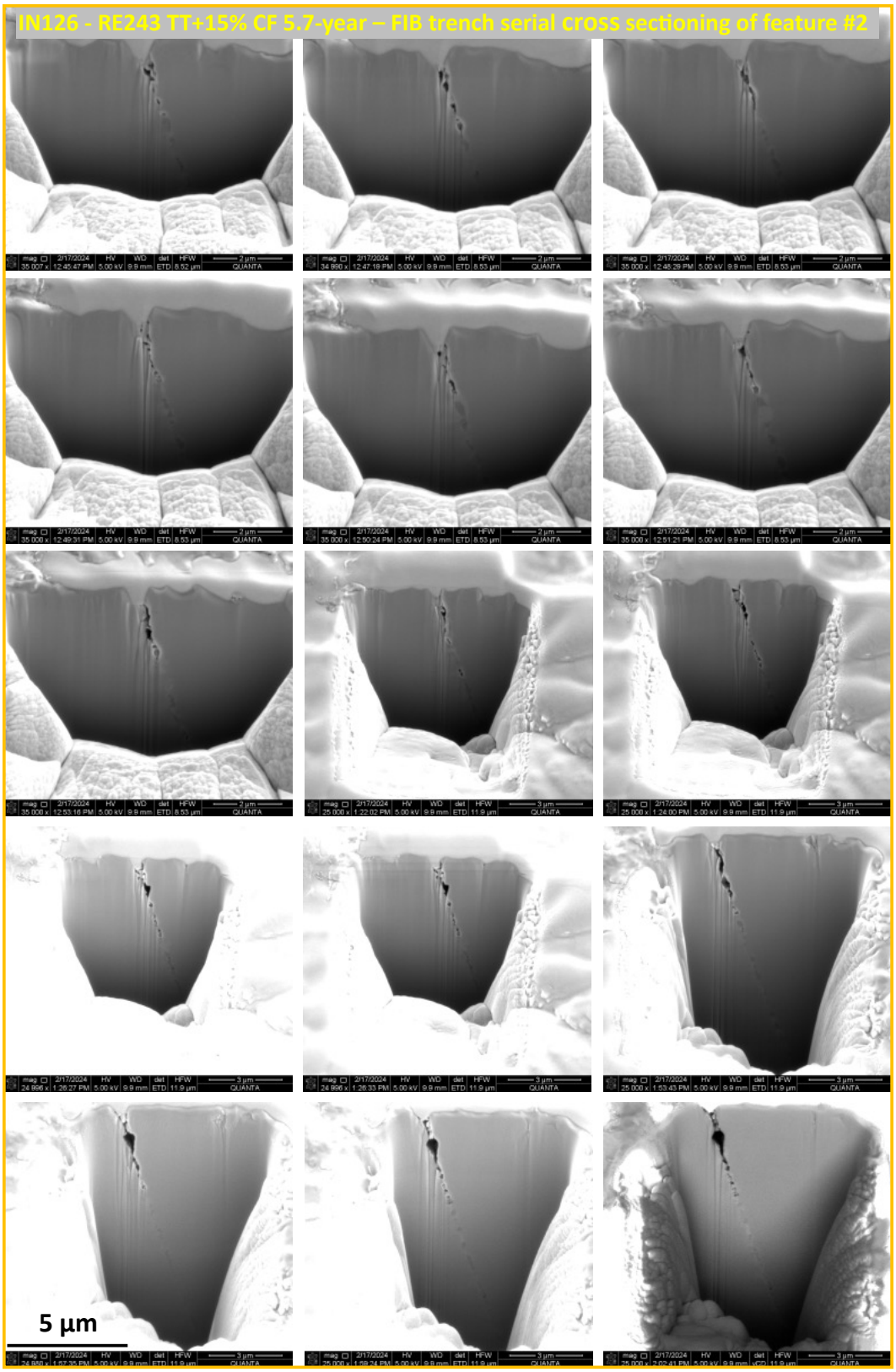

Figure 31. IN126 (RE243) feature #2 FIB trench serial cross-section image series. The progression of the images is to the right and then down.

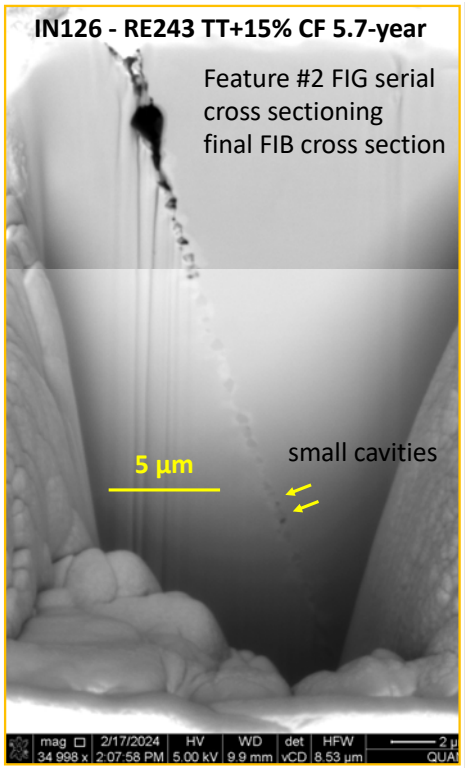

Figure 32. IN126 (RE243) feature #2 final cross-section showing cavities to a depth of >15 µm.

5.3.3 IN137 – 15% CF Alloy 690 Allvac B25K-2

As previously mentioned, the heat B25K-2 specimens exhibited the least SCC susceptibility to high temperature water exposure. The only boundaries with dark contrast appeared to be double twin boundaries as shown, for example, in Figure 33 which is a gauge surface summary of the IN137 B25K-2 specimen. Both features are straight lines running across a clear region surrounded by mostly darker (more heavily oxidized regions). This is highly suggestive that these are double twin boundaries, and FIB trench cross-sectioning confirmed that feature #2 is a double twin boundary. To obtain information from a high angle GB, one such boundary aligned to the stress was selected for FIB trench serial cross-section imaging. Within the 34 images that were obtained over tens of micrometers along the crack, no carbides or cavities were observed. Typical example images are shown in Figure 34. Note that in image 29 (right-hand image in Figure 34), two GBs are intersecting, confirming that this is not a twin boundary.

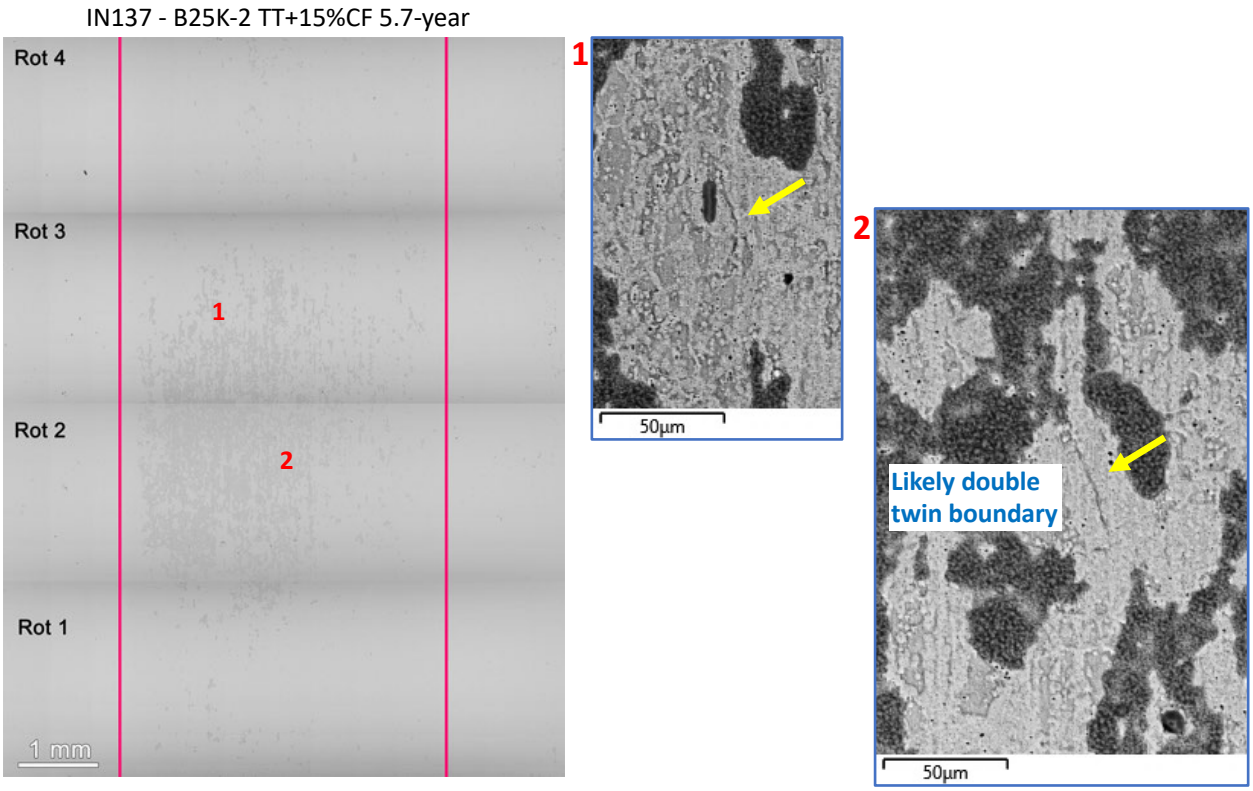

Figure 33. IN137 B25K-2 specimen 5.7-year gauge surface summary.

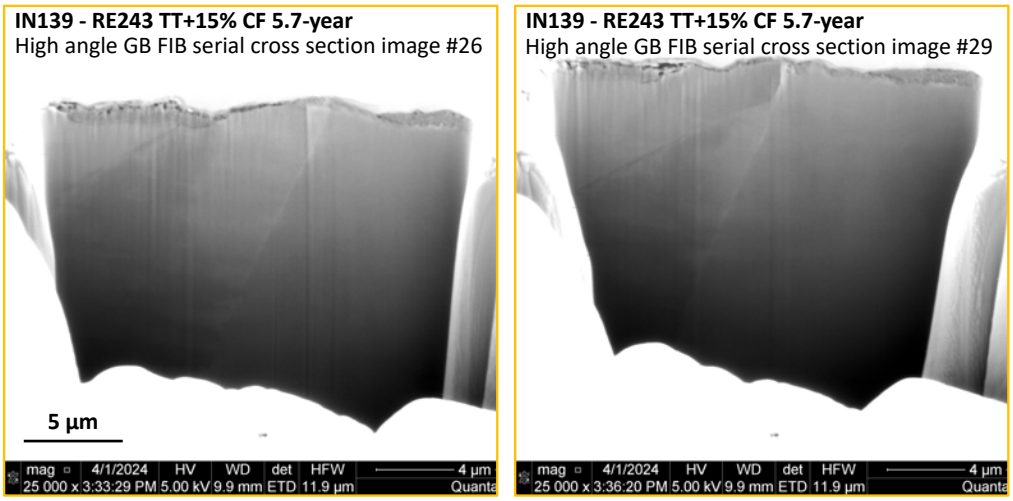

Figure 34. IN139 B25K-2 select FIB serial cross-section images of a high angle GB showing no carbides and no creep cavities.

5.4 2.4/4.0-Year Surface and FIB Trench Cross-Section Examinations of Selected 15% CF Alloy 152(M)/52(M) Specimens

Summary tables of the Alloy 152(M)/52(M) specimen observations after 2.4 and 4.0 years are provided in Tables 12 and 13, respectively. One specimen of each weld metal was subjected to SEM gauge surface observations, and then among these four specimens, two were subjected to

FIB trench cross-section examination of selected GBs. After 2.4 years, spinel oxide (MO composition) had accumulated on the surface of some of the specimens, making it difficult to observe GBs by SEM. After 4.0 years, almost all specimens had a thick spinel oxide on the gauge surface. In cases where there was thick spinel oxide coverage, it was still possible to identify the location of some GBs due to differences in spinel oxide coverage on neighboring GBs.

Table 12. Alloy 152(M)/52(M) specimens examined after 2.4 years of exposure at their YS. All specimens in this list were subjected to gauge surface examinations.

ID	Material	Heat	YS (MPa)	FIB Trench Cross-Section of GBs	Notes
IN112	52M	ENSA DPM	430	Yes	Possible surface cavities
IN124	52	MHI	485		Surface obscured by oxide
IN128	152M	IHI	555	Yes	No surface cavities, a few cracks, likely preexisting, ≤1 μm deep
IN142	152	MHI	500		Surface obscured by oxide

Table 13. Alloy 152(M)/52(M) specimens examined after 4.0 years of exposure at their YS. All specimens in this list were subjected to gauge surface examinations.

ID	Material	Heat	YS (MPa)	FIB Trench Cross-Section of GBs	Notes
IN112	52M	ENSA DPM	430	Yes	Near-continuous, <100 nm deep oxide penetration at many GBs
IN124	52	MHI	485		Surface obscured by oxide
IN128	152M	IHI	555	Yes	Cracks, likely preexisting, some unknown depth, subsurface crack-like defects
IN142	152	MHI	500		Surface obscured by oxide, small pits/holes likely due to precipitate dissolution or fall-out

5.4.1 IN112 – 15% CF Alloy 52M ENSA DPM

Similar to the three Alloy 690TT specimens (IN108, IN118, and IN126), GBs in the 15% CF Alloy 52M ENSA DPM specimen IN112 also has some “postage stamp” features on the surface after 2.4 years of exposure (Figure 35), but these features were not as extensive as seen in the Alloy 690TT specimens. Two nearby regions along a GB were examined in cross-section by serial FIB trenching after 2.4 years on a GB that did not have a clear indication of postage stamp features (Figure 36). Serial milling along the direction of the GB covering a distance of approximately 5 μm was performed in one of the trenches as illustrated by the sequence of images in Figure 36b, and the other trench was made for a quick examination of the cross-section morphology of the investigated GB. A high density of IG precipitates was revealed in both locations, but no IG defects were observed in either of them.

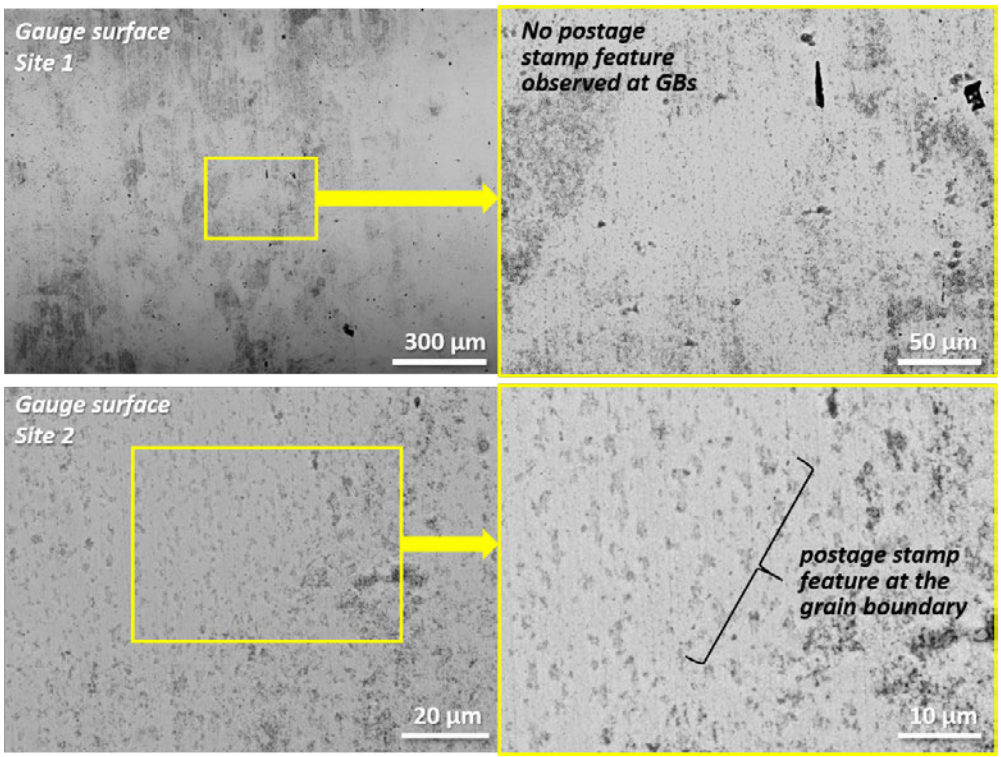

Figure 35. Representative SEM-BSE images of the gauge surface of the 15% CF Alloy 52M ENSA DPM specimen IN112 after 2.4 years of exposure.

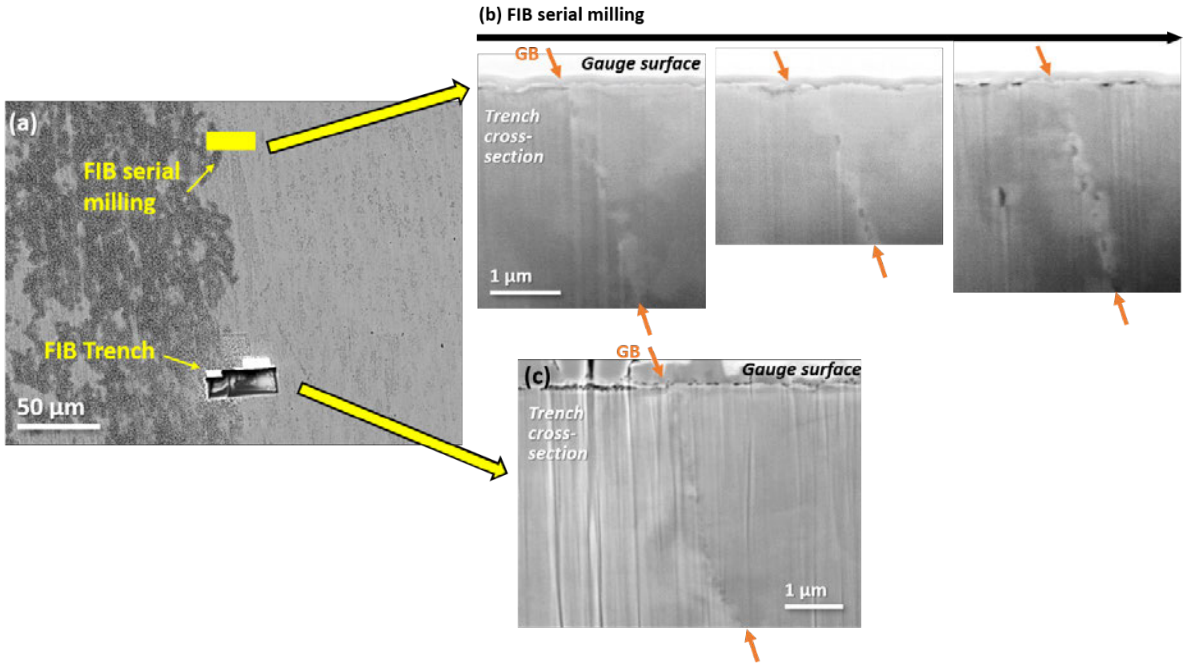

Figure 36. (a) SEM-BSE image showing the location of the two FIB trenches in IN112 made at the 2.4-year test interruption, (b) examples of the FIB-SE images taken during the serial FIB milling along the selected portion of a GB identified in (a), and (c) FIB-SE image showing the cross-section of the trench at the location identified in (a).

This specimen was examined again at the 4.0-year test interruption. Four sites were examined in detail in the vicinity where the FIB trenches were made after 2.4 years of exposure (Figure 37).

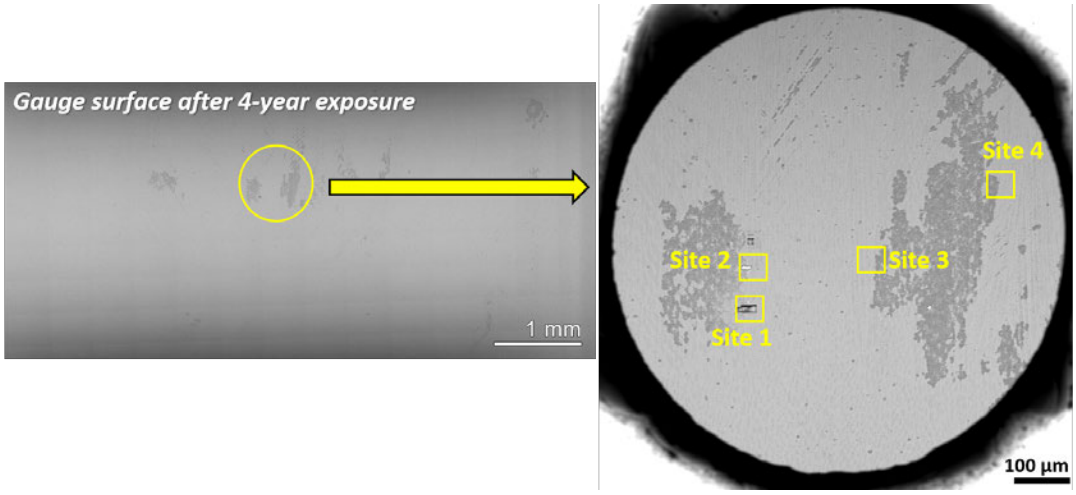

Figure 37. Representative SEM-BSE images of the gauge surface of the 15% CF Alloy 52M ENSA DPM specimen IN112 after 4.0 years of exposure.

In general, the surface oxide in this specimen is thin enough to allow the SEM to probe the GB appearance at the surface of the specimen. As shown in Figure 38, the GBs appeared as a dark line of contrast at all four sites. This is different from the occasional, discrete postage stamp-like features observed after 2.4 years, indicating a progression in GB microstructure, at least near the surface of the specimen.

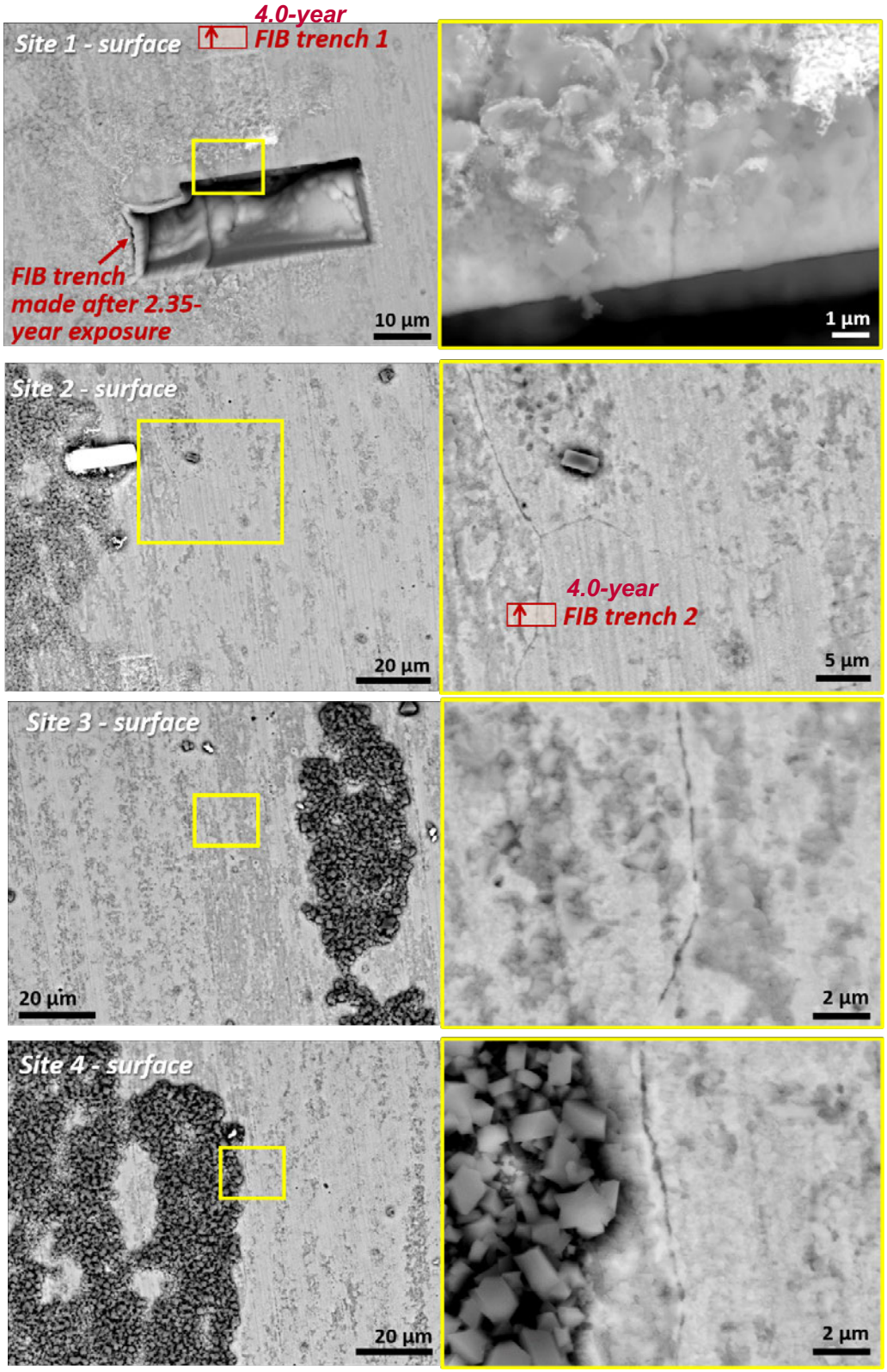

Figure 38. Detailed examination of surface morphology at the four sites highlighted in Figure 37 in IN112 after 4.0 years of exposure.

To better understand this continuous dark line contrast, two small FIB trenches were made at locations marked at Sites 1 and 2 in Figure 38, and serial milling was performed in both trenches with results shown in Figures 39 and 40, respectively. The dark contrast appears to be due to very shallow GB oxidation to a depth of no more than 100 μm. Both GBs feature a high density of very small, nm-sized IG precipitates, but no cavities or cracks are present.

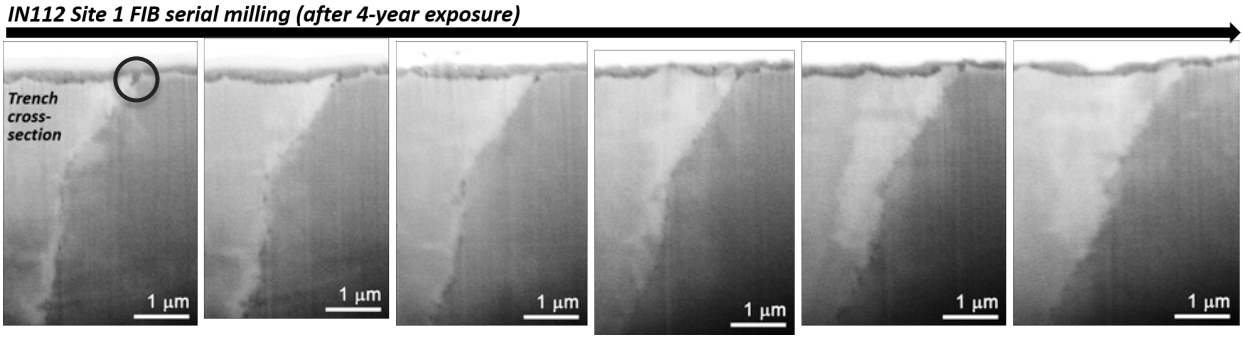

Figure 39. Selected FIB-SE images taken during the serial FIB milling along a trench made after 4.0 years of exposure along the same GB where the first trench was made after 2.4 years of exposure in IN112 (Figure 38 Site 1). An example of the shallow GB oxidation is within the black circle.

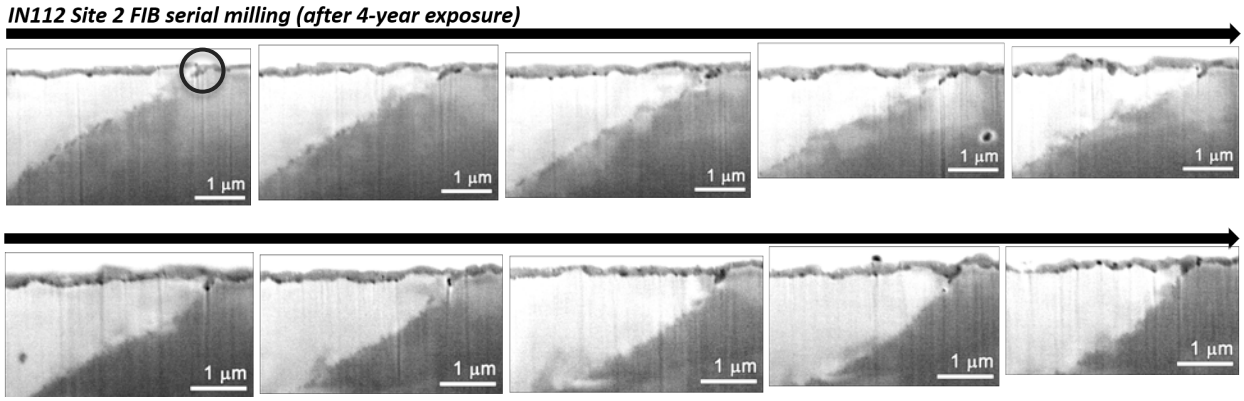

Figure 40. Examples of the FIB-SE images taken during the serial FIB milling along a randomly selected GB at Site 2 (the exact region is marked in Figure 38) after 4.0 years of exposure in IN112. An example of the shallow GB oxidation is within the black circle.

5.4.2 IN124 – 15% CF Alloy 52 MHI specimen IN124

Only gauge surface examinations were performed on this specimen. A non-uniform distribution of surface oxides was present on the gauge surface after both 2.4 and 4.0 years of exposure. As shown in both Figures 41 and 42, the grains were partially revealed possibly due to grain orientation-dependent formation of spinel oxides, and potential location of GBs could be traced by identifying the edge between regions of spinel oxide with significant difference in contrast such as those presented in higher magnification images in these two figures. However, even at regions where GBs likely reside with thinner surface oxides, IG damage were not identifiable after either 2.4 or 4.0 years of exposure.

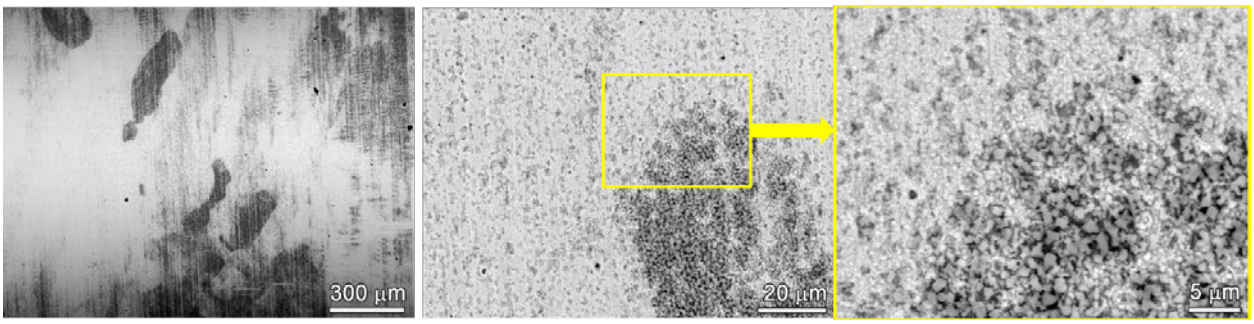

Figure 41. Representative SEM-BSE images of the gauge surface the 15% CF Alloy 52 MHI specimen IN124 after 2.4 years of exposure.

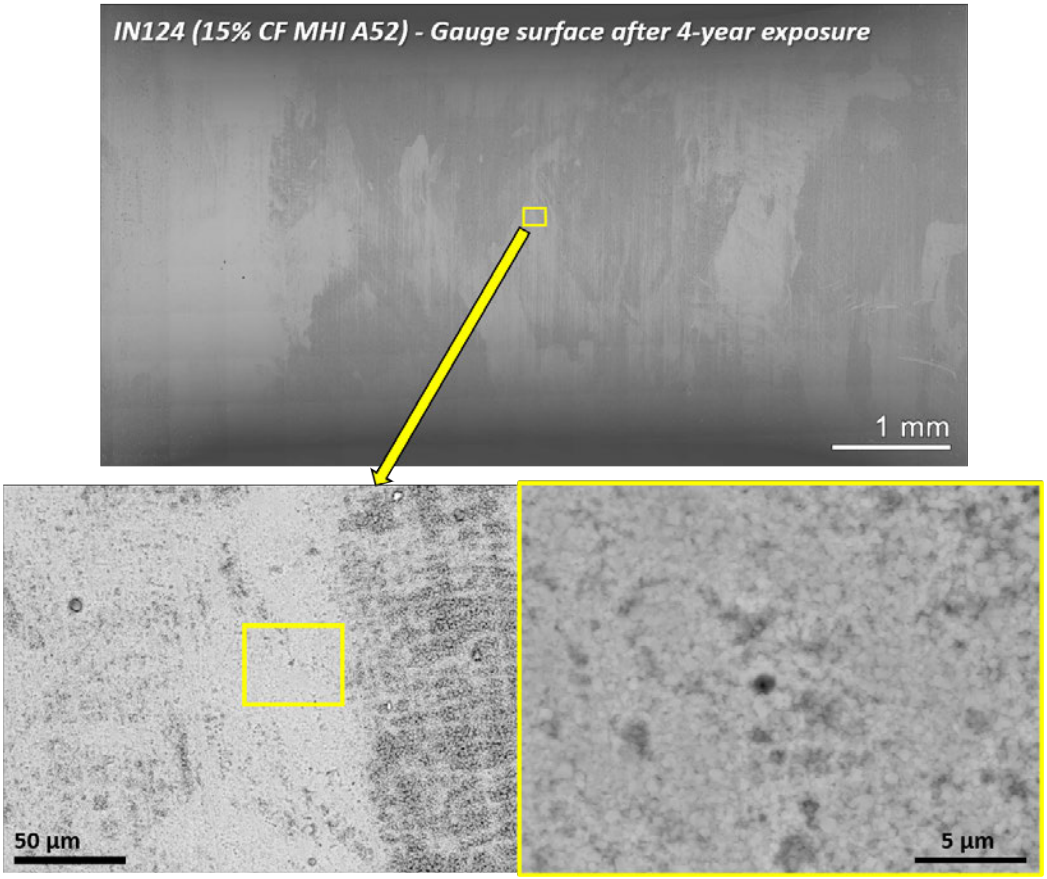

Figure 42. Representative SEM-BSE images of the gauge surface of the 15% CF Alloy 52 MHI specimen IN124 after 4.0 years of exposure.

5.4.3 IN128 – 15% CF Alloy 152M IHI

During the gauge surface observations after 2.4 years of exposure, a crack-like feature was found in the low-magnification SEM-BSE montage of the 15% CF Alloy 152M IHI specimen IN128, and therefore higher resolution SEM examination was performed in the vicinity of this feature (labeled Crack 1 in Figure 43). Details of this crack can be seen in the SEM-BSE and SE images presented in the bottom right of Figure 43.

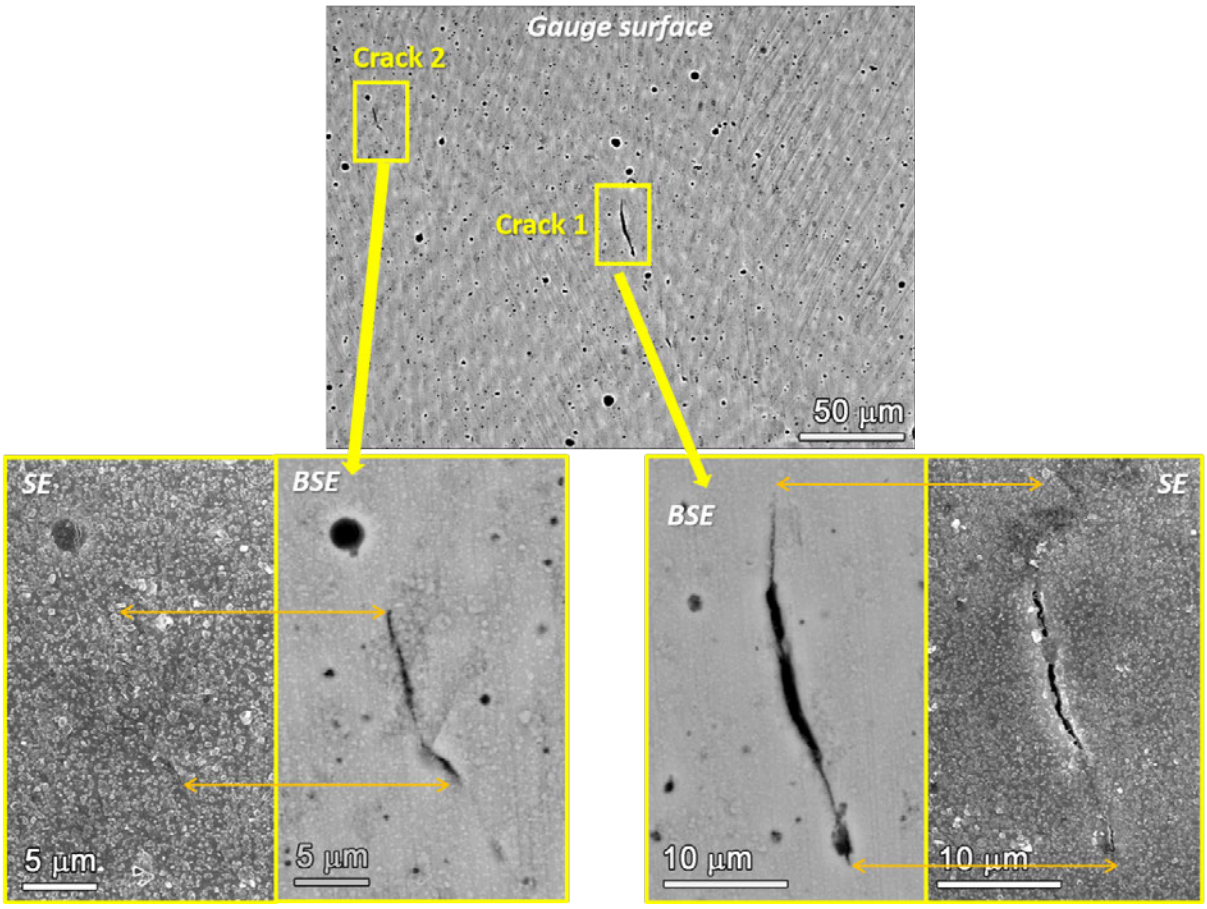

Figure 43. SEM-BSE/SE images of the two small cracks identified in the gauge surface of the 15% CF Alloy 152M IHI specimen IN128 after 20,659 hours of exposure.

The BSE image revealed a total crack length on the surface of approximately 25 µm, but in the SE image only the more widely opened middle-section of this crack is visible because of a smaller interaction volume associated with the secondary electrons. Another smaller, approximately 15 µm long crack-like feature was spotted to the left of Crack 1 (denoted as Crack 2 in Figure 43) during the higher resolution SEM examination. This crack had not been observable in the low-magnification SEM-BSE montage image. The detailed morphology of this crack is presented in the bottom left of Figure 43. It appears to be an IG crack since slip bands (denoted by slightly varying bands of darker and brighter contrast almost orthogonal to the crack) can be seen in the BSE image.

To better understand these IG cracks, FIB was employed to make shallow trenches of approximately 6 µm in depth at two locations on Crack 1 as shown in Figure 44(a). The first trench was made at the lower tip of Crack 1 to examination the cross-section morphology of the crack. As shown in Figure 44(b), no crack opening was observed, and instead only a shallow but wide IG oxidation with a penetration depth of approximately 500 nm from the surface was found. While this depth is extremely shallow, the open nature of this feature suggest that it is a crack. No other IG defects such as cavities were observed in the near-surface region. To preserve this crack-like feature for future exposure and documentation of its evolution over time, a second trench was made approximately 10 µm away from the lower tip of the crack, and serial milling across a span of approximately 5 µm on the surface was performed.

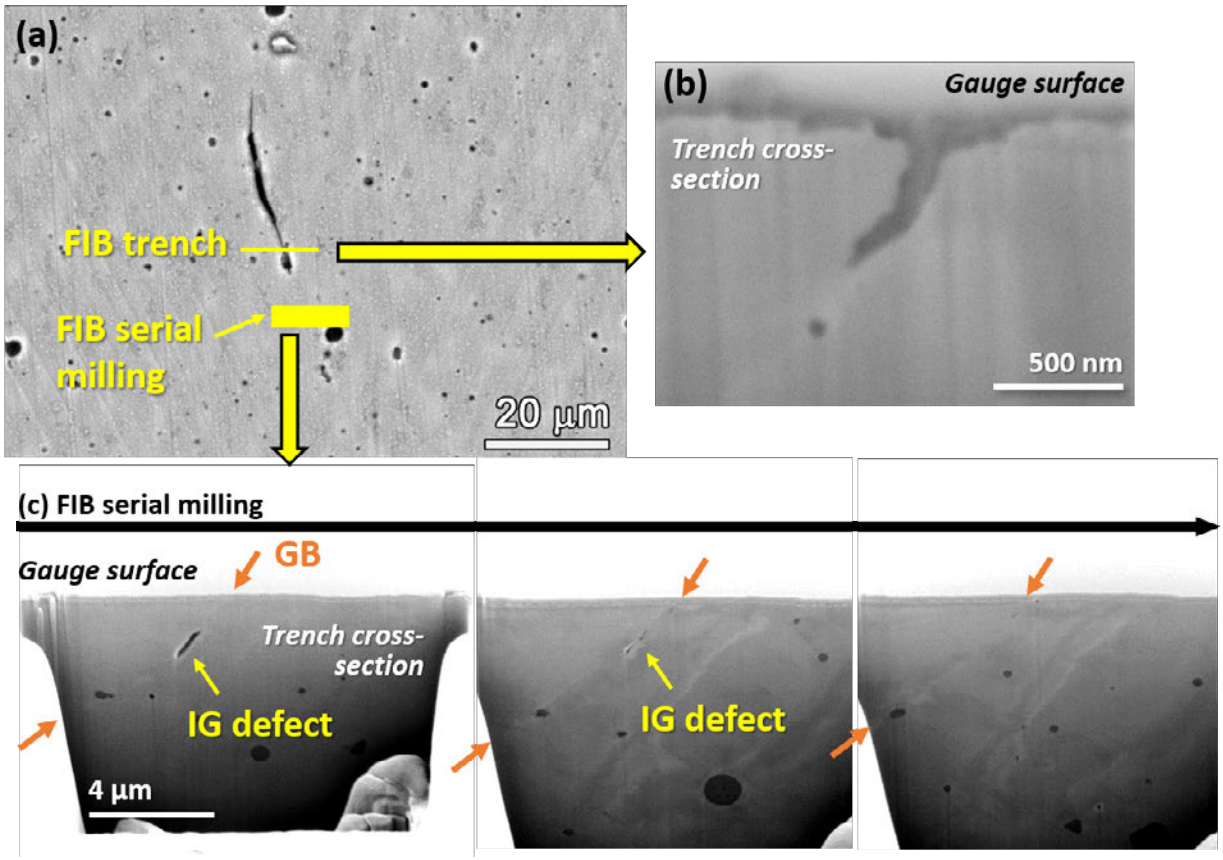

Figure 44. (a) SEM-BSE image showing the location of the two FIB trenches in IN128, (b) FIB-SE image showing the cross-section of the trench at the location identified in (a), and (c) examples of the FIB-SE images taken during the serial FIB milling along the selected portion of a GB identified in (a).

No indication of GB cavities or intergranular oxidation was present in these cross-section images. However, a subsurface, lack-of-fusion type defect was revealed during the serial milling at approximately 2 µm below the surface along the GB (Figure 44c). This suggests that the surface crack may be associated with the subsurface welding defect, thereby making the surface crack a preexisting crack rather than a new crack formed during the long-term exposure. However, more examinations are needed to confirm this deduction.

After 4.0 years of exposure, higher resolution imaging was performed at additional sites to see whether more cracks could be identified (Figure 45). As shown in Figure 46, at least one crack-like feature was observed in each site, suggesting that this specimen may indeed exhibit a higher than usual density of cracks. However, it should be noted that all the crack-like features have a very short surface length. The longest crack in this specimen was observed at Site 1 (Figure 46(a)) and had a total surface length of approximately 30 µm. Not all of these cracks were recorded in detail during the 2.4-year test interruption, making it difficult to determine when these cracks formed. Nevertheless, some insights regarding this matter could be obtained by coupled SEM-FIB examinations of the two cracks that were documented at both test interruptions.

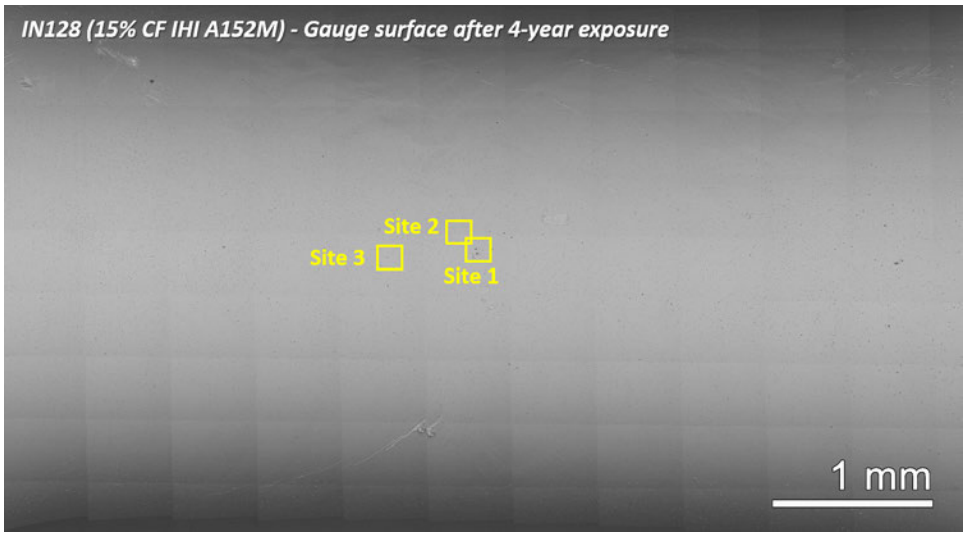

Figure 45. SEM-BSE low-magnification montage of the gauge surface of one rotation of the 15% CF Alloy 152M IHI specimen IN128 after 4.0 years of exposure. Sites examined at higher resolution for cracks are highlighted.

As shown in Figure 47, two sites were documented in detail after 4.0 years of exposure. Site 1 corresponds to the site that was examined in detail after 2.4 years (Figure 44) while at Site 2, basic imaging was performed at 2.4 years and detailed examinations were conducted at 4.0 years. At either site, no obvious change in morphology or size was found in any of the identified cracks, indicating little or no apparent growth of these cracks over extended exposure. To get an idea of the depth of the cracks and their subsurface morphology, serial FIB milling was employed on the largest crack (Crack 1) and a small crack (Crack 2) after 4.0 years of exposure.

For Crack 1, the FIB milling started from beyond one end of the crack and traversed through the entire tighter portion of the crack as enclosed in the red box in Figure 47(a), covering a total length of approximately 10 μm. A total of 112 FIB-SE images were taken during the serial milling. Figure 48 illustrates selected images showing the evolution of the subsurface morphology of Crack 1 from the start to the end of the milling. It can be seen that the crack started shallow and gradually grew deeper as the milling moved its way along the tighter portion of the crack to a total depth of approximately 5–6 μm. Interestingly, it appears that once the milling reached the transition between the tighter portion and more open portion of the crack as it appears on the surface, the crack suddenly went deep into the cross-section, and the total depth of the crack reached beyond the extent of the FIB trench. It was decided to stop milling at this point and the final milling face was examined in detail in an SEM for better resolution with results presented in Figure 49. It turns out that on this cross-section, the crack intersecting the surface and the crack at the bottom are not connected, but an examination at higher magnification revealed heavy oxidation around the bottom crack and clear decohesion between the neighboring grains. This is not typical of SCC morphology which usually becomes tighter with increasing depth, often ending with a sharp tip. Based on our experience, the deeper portion of the crack is a weld defect that existed before testing. Since it is heavily oxidized, it is reasonable to assume that the two cracks would link up if we continued milling, and that's how water got its way into the lower defect as we see it on the final milling face.

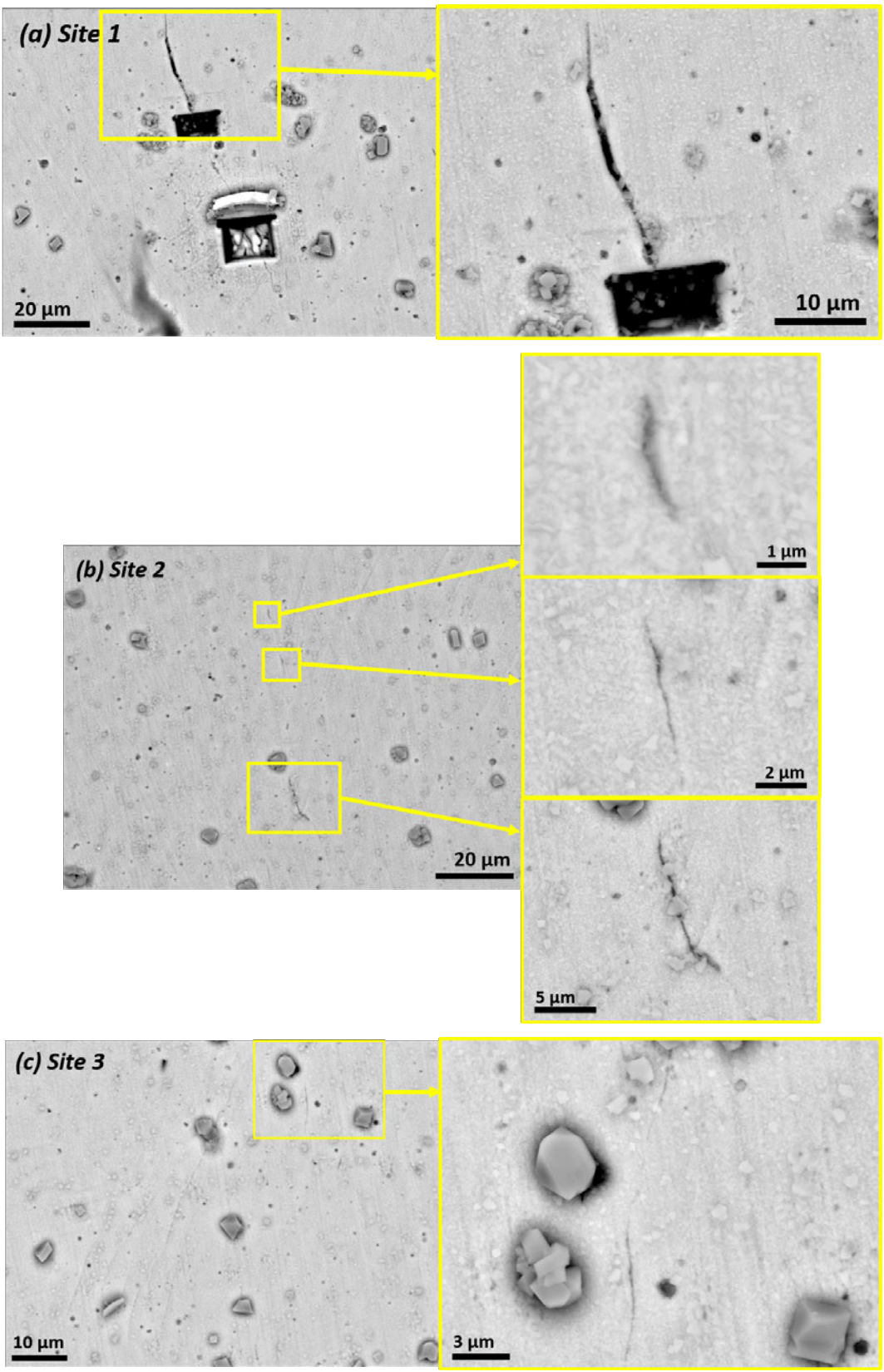

Figure 46. SEM-BSE images of the surface appearance at the three sites after 4.0 years of exposure. These sites are highlighted in Figure 45.

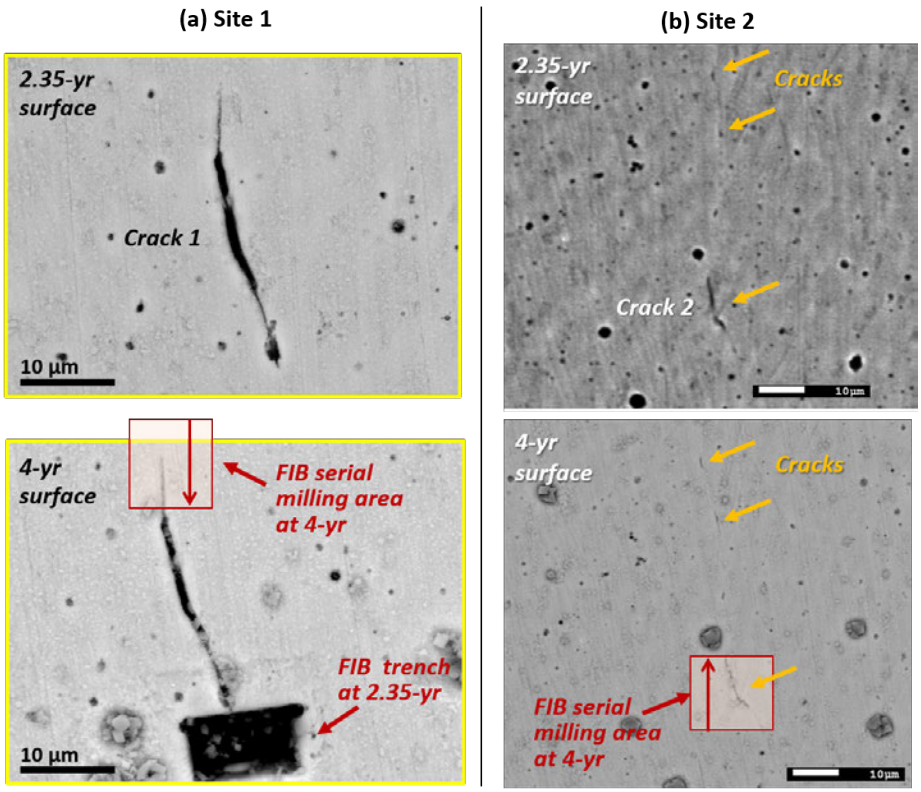

Figure 47. Comparison of the surface morphology of cracks observed at Sites 1 and 2 in IN128 after 2.4- and 4.0-year exposures.

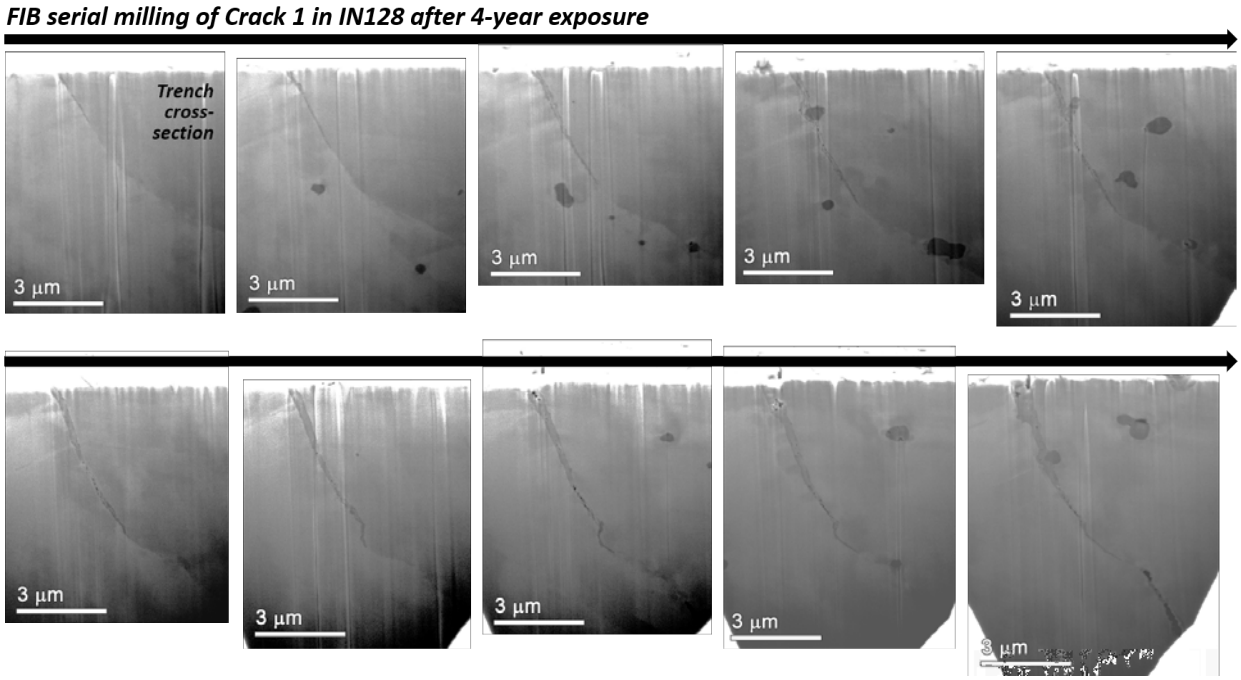

Figure 48. FIB-SE images taken during serial FIB milling of a portion of Crack 1 at Site 1 after 4.0 years of exposure in IN128. The FIB milling area is marked in Figure 47(a).

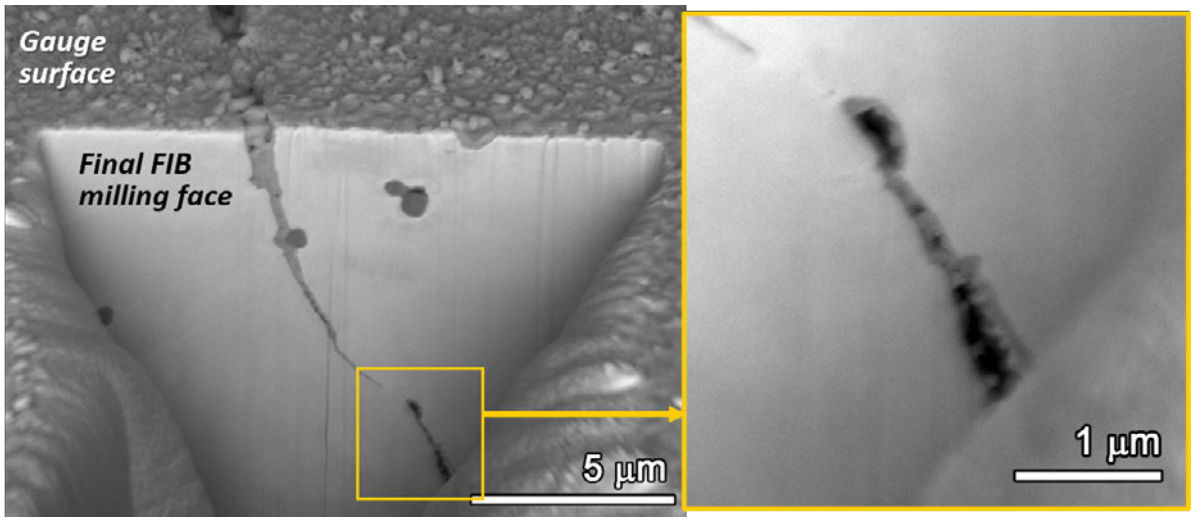

Figure 49. SEM-BSE image of the final milling face of the trench made on Crack 1 in IN128.

As shown in Figure 47(b), serial FIB milling was also performed on Crack 2 with images taken across the entire length of this short crack over a distance of approximately 15 µm. A total of 137 images were recorded. As shown in Figure 50, the first few FIB cross-section images revealed unoxidized IG weld defects at portions both near and approximately 6 µm below the surface along the GB where the crack was found. The upper defect disappeared before the oxidized crack was intersected by FIB milling, while the lower defect persisted through a few more FIB milling slices and was never found connecting to the oxidized crack above it. While the oxidized crack encountered a few precipitates as the serial milling progressed, no GB cavities were identified either within or beyond this crack. The deepest section of the crack is presented in the first two images in the third row in Figure 50, showing a depth of approximately 5–6 µm. Towards the end of the milling, another IG defect appeared at a depth of approximately 8–10 µm from the surface. By the time the milling was stopped because almost the entire crack had been trenched away, there was no sign that the defect would link to the crack, especially as the crack depth was getting shorter.

The final milled cross-section of this crack was examined in SEM for better viewing of the details of the crack and the defect (Figure 51). Although the orientation of the trench cross-section was not optimal for electron dispersive spectroscopy examination, elemental maps were acquired for these two features showing obvious Cr-oxidation of the crack and a lack of Cr-oxide at the defect.

In summary for this Alloy 152M specimen, detailed SEM and FIB examinations after 2.4 and 4.0 years of exposure revealed that the defected GBs were heavily oxidized which is representative of preexisting weld defects. While no direct evidence was found to demonstrate that these subsurface defects are linked to IGSCC cracking, they may contribute to higher IGSCC susceptibility at local GBs due to induced locally higher stresses and possibly because GB chemistry in the vicinity of these defects may be suboptimal, e.g., depleted in chromium or having a high concentration of impurity elements from welding (as evidenced by the significantly oxidized GBs). Additional chemistry examinations via atom probe tomography would be helpful in justifying this hypothesis. The IG cracks remained shallow even after 4.0 years of exposure without observable growth on the surface. These facts suggest that despite containing some very small IG cracks, this heat of Alloy 152M is very resistant to crack initiation, at least during the first 4.0 years of testing.

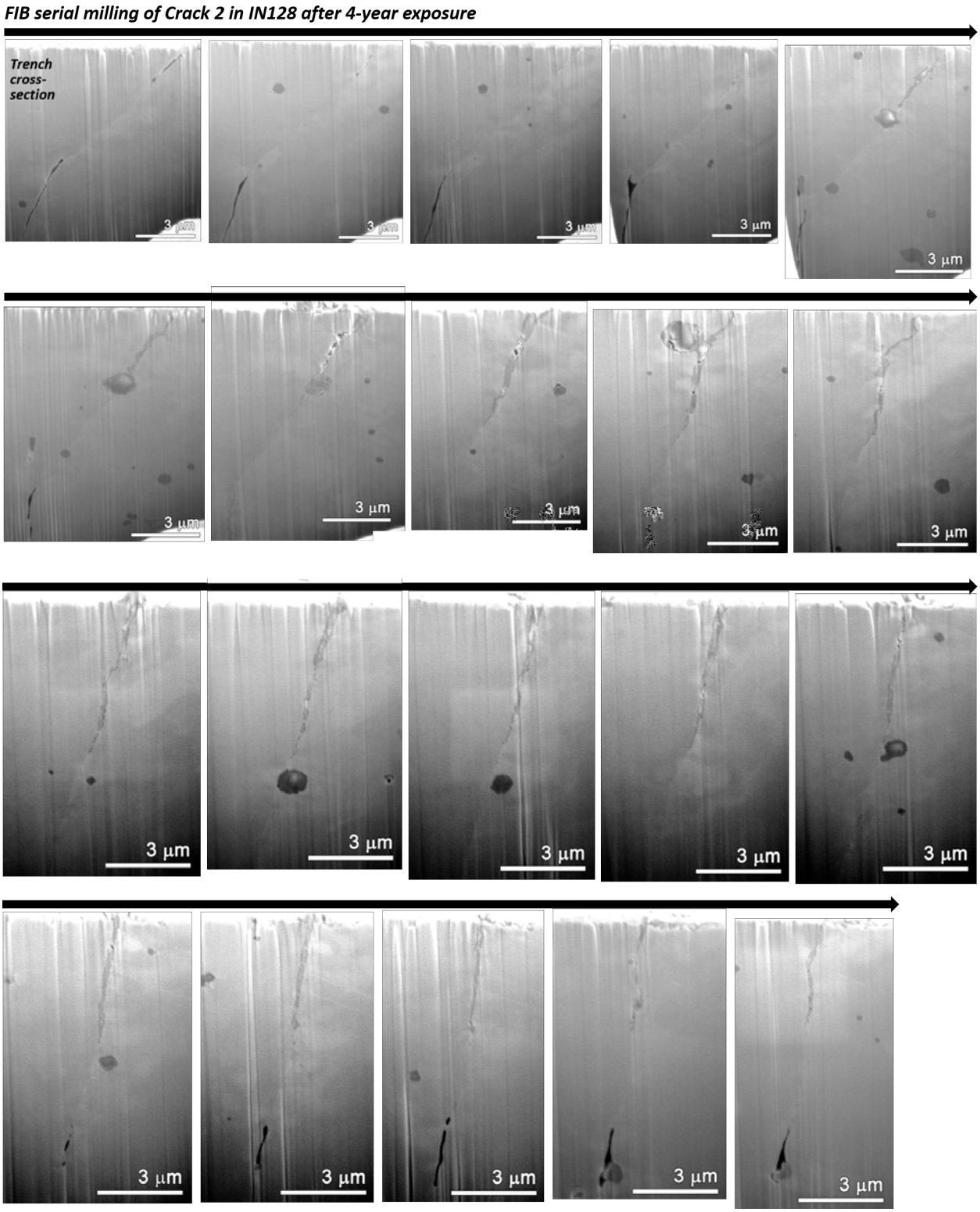

Figure 50. FIB-SE images taken during serial FIB milling of a portion of Crack 2 at Site 1 after 4.0 years of exposure in IN128. The FIB trench milling is marked in Figure 47(b).

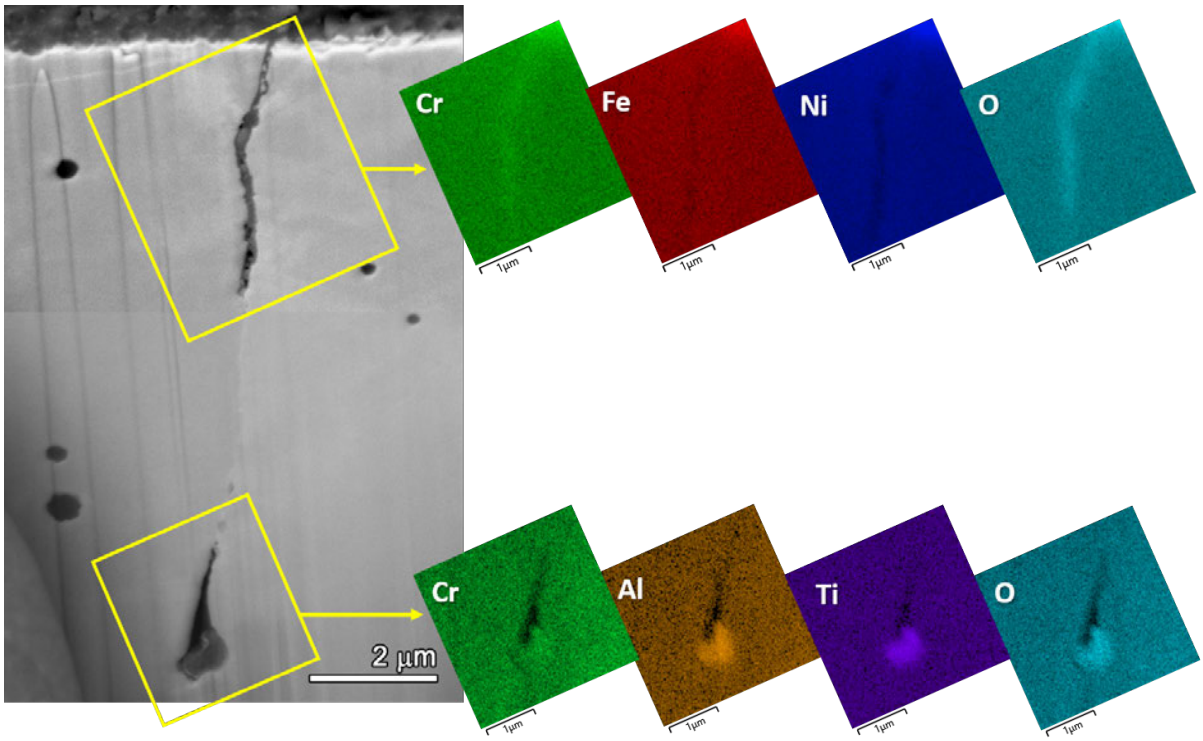

Figure 51. SEM-BSE image of the final milling face of the trench made on Crack 2 in IN128. Electron dispersive spectroscopy elemental maps also are shown for the short crack linking to the surface and the defect found below the crack on the same GB.

5.4.4 IN142 – 15% CF Alloy 152 MHI

Only gauge surface observations were performed on this specimen. Similar to the 15% CF Alloy 52 MHI specimen IN124, the Alloy 152 MHI specimen IN142 exhibited a thick surface oxide layer at both the 2.4 (Figure 52) and the 4.0-year (Figure 53) test interruptions, which obscured a clear examination of the GBs intersecting the surface of the specimen. Despite some small pits/holes less than a few micrometers in size observed during high-magnification examination after 4.0 years of exposure (Figure 54), no other types of defects were observed. These features appear to be intragranular and could possibly be associated with precipitate drop-outs. Based on our experience with Alloy 182 SCC initiation, these features are considered to have little impact on crack initiation in the weld materials [18].

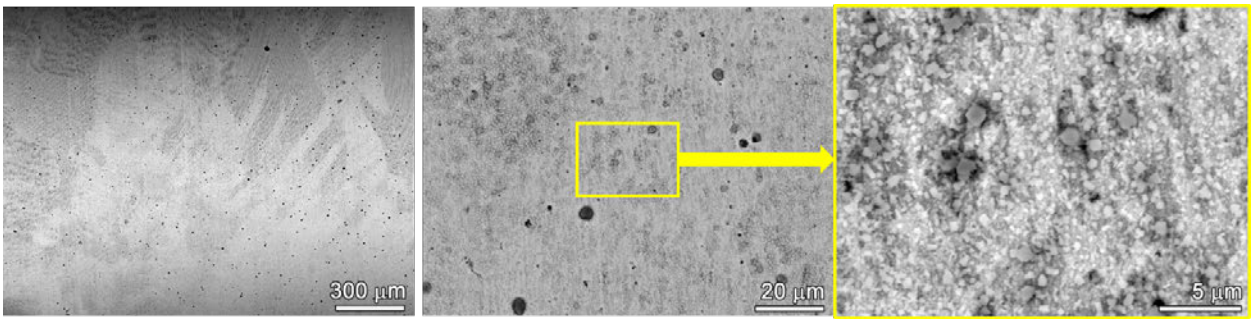

Figure 52. Representative SEM-BSE images of the gauge surface of the 15% CF Alloy 152 MHI specimen IN142 after 2.4 years of exposure.

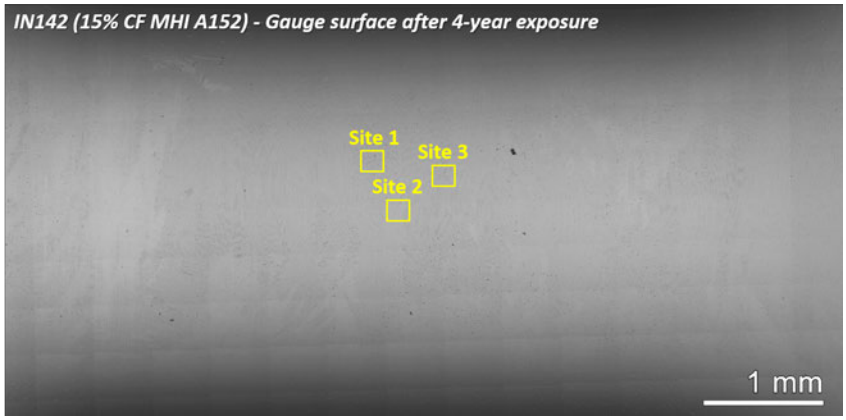

Figure 53. SEM-BSE low-magnification montage of the gauge surface of one rotation of the 15% CF Alloy 152 MHI specimen IN142 after 4.0 years of exposure. Sites examined at higher magnifications are highlighted.

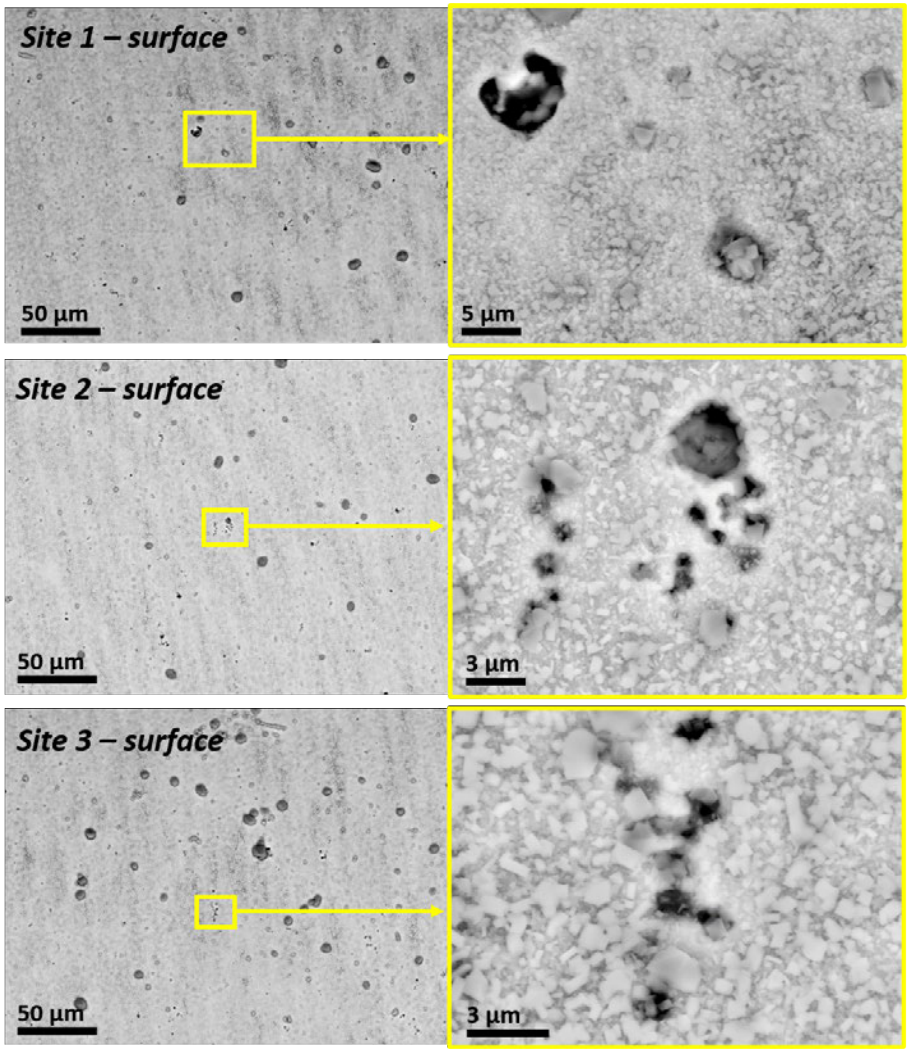

Figure 54. Higher magnification SEM-BSE images of the surface morphology at the three sites highlighted in Figure 53. Small pits/holes were observed at all three sites.

5.5 5.7-Year Surface and FIB Trench Cross-Section Examinations of Selected 15% CF Alloy 152(M)/52(M) Specimens

All 24 specimens were subjected to SEM-based gauge surface examinations with a summary of the observations provided in Table 14. Most of the specimens had a thick spinel oxide layer on the surface that prevented observation of anything but open cracks, and thus, only such features are noted in the table. The exceptions were the Alloy 152 specimens where only mild coverage was observed, and in this case, none of the specimens had crack-like features on the surface. In total, seven crack-like features were observed on six specimens. All six of the specimens with crack-like features were subjected to FIB trench serial cross-section imaging. Table 15 summarizes this and shows the relationship to the specimens that were FIB trenched at 2.4/4.0 years. Selected results are provided here.

Table 14. Summary Alloy 152(M)/52(M) SCCI specimen SEM gauge surface observations after 5.7 years.

Heat and Approx. Stress (MPa)	Spec ID	Material Condition	Observations of Significant Crack-like Features
Alloy 52M ENSA DPM, 410 MPa	General comments:		Thick spinel oxide obscuring the gauge surface, generally only possible to identify apparent large cracks
	IN110	15% CF	*One apparent crack-like feature near fillet*
	IN111	"	No obvious open crack-like features
	IN112	"	No obvious open crack-like features
	IN113	"	No obvious open crack-like features
	IN114	"	No obvious open crack-like features
	IN115	"	No obvious open crack-like features
	IN136	"	No obvious open crack-like features
Alloy 52 MHI, 460 MPa	General comments:		Thick spinel oxide obscuring the gauge surface, generally impossible to identify small features
	IN119	"	No obvious open crack-like features
	IN120	"	No obvious open crack-like features
	IN121	"	No obvious open crack-like features
	IN122	"	*One apparent open crack near fillet*
	IN123	"	*One apparent open crack near fillet*
	IN124	"	No obvious open crack-like features
Alloy 152M, 530 MPa	General comments:		Moderate amount of spinel oxide, some difficulty identifying small features
	IN128	"	*One apparent open crack near fillet*
	IN129	"	*One apparent open crack near fillet*
	IN130	"	No obvious open crack-like features
	IN131	"	No obvious open crack-like features
	IN132	"	No obvious open crack-like features
	IN133	"	*Two apparent open cracks near fillet*
Alloy 152 MHI, 485 MPa	General comments:		Low amount of spinel oxide
	IN134	"	No obvious open crack-like features
	IN135	"	No obvious open crack-like features
	IN140	"	No obvious open crack-like features
	IN141	"	No obvious open crack-like features
	IN142	"	No obvious open crack-like features

Table 15. Alloy 152(M)/52(M) SCCI specimen FIB trench examination matrix.

Spec ID	Material & Heat	2.4 yrs	4.0 yrs	5.7 yrs
IN110	Alloy 52M ENSA DPM			snapshots, serial imaging
IN112	“	Y	Y	
IN122	Alloy 52 MHI			snapshots, serial imaging
IN123	“			snapshots, serial imaging
IN128	Alloy 152M IHI	Y	Y	snapshots, serial imaging
IN129	“			snapshots, serial imaging
IN133	“			snapshots, serial imaging

5.5.1 IN110 – 15% CF Alloy 52M ENSA DPM

Only one Alloy 52M specimen was examined by FIB trench cross-section at 5.7 years. This specimen has a complex shape crack-like feature located in one of the fillets as shown in Figure 55. A FIB trench cross-section image at the end of one of the branches (Figure 55) revealed a heavily oxidized linear structure with voids away from the surface. A set of cross-section images taken from the middle of the same crack branch (Figure 56) revealed a complexly shaped feature that has no resemblance to a GB. This crack is most likely a weld fabrication defect that may be part GB and part lack-of-fusion structure. It is unclear whether the feature became heavily oxidized as a result of exposure to high temperature water or during weld fabrication.

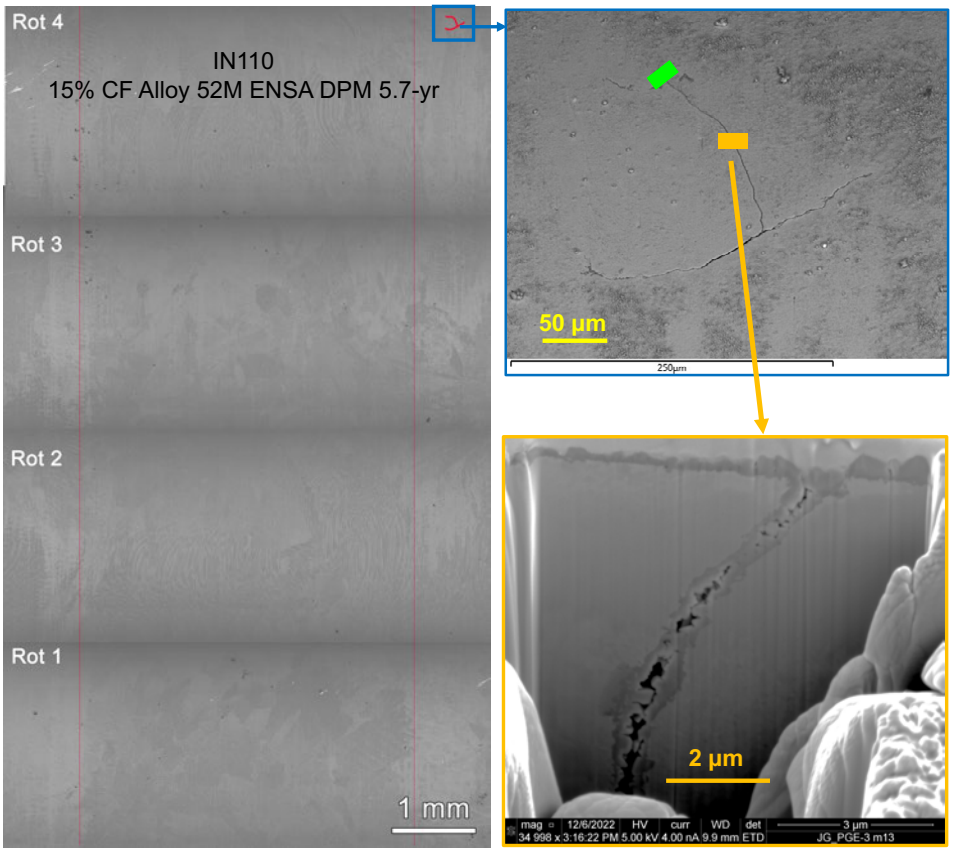

Figure 55. IN110 Alloy 52M ENSA DPM 5.7-yr FIB gauge surface and FIB trench. The morphology reveals that this was a preexisting weld fabrication crack.

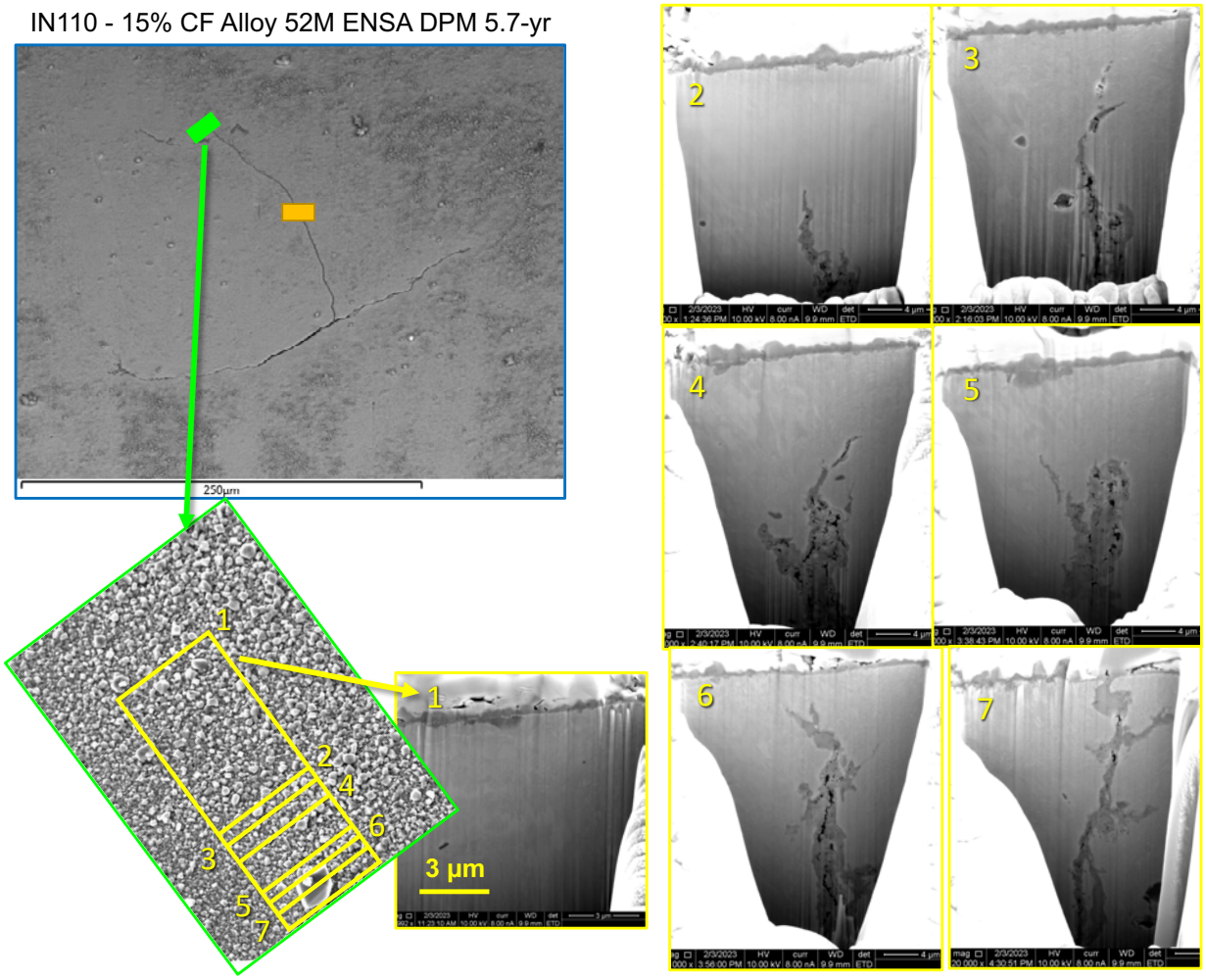

Figure 56. IN110 Alloy 52M ENSA DPM 5.7-yr FIB trench cross-section images.

5.5.2 IN122 – 15% CF Alloy 52 MHI

Two Alloy 52 MHI specimens were examined by FIB trench cross-section. The trenched GBs in both specimens had the same appearance, and for the purpose of illustration, IN122 is presented here, first with the gauge surface overview in Figure 57 and the FIB trench cross-section images provided in Figure 58. The GB cross-section has the same general appearance as the Alloy 690 RE243 specimen with significant quantities of GB cavities. There is no thick layer of oxidation on the GB as was observed in crack-like features that were probably weld fabrication defects such as was shown in the IN110 Alloy 52M specimen (Figure 56). The GB cavity in the Alloy 52 specimen has a approximately 150 µm length on the surface, and creep cavities extend to a maximum depth of approximately 10 µm. The degree of cavity formation in this Alloy 52 specimen is less than that of the Alloy 690 RE243 specimen, but a significant number of large cavities are present to a greater depth in this Alloy 52 specimen. While the Alloy 690 RE243 specimen has a 65 µm long, 5 µm deep crack, the feature in this Alloy 52 specimen has not yet become a crack despite having a greater length on the surface and large cavities to a greater depth than observed for the crack in the RE243 specimen.

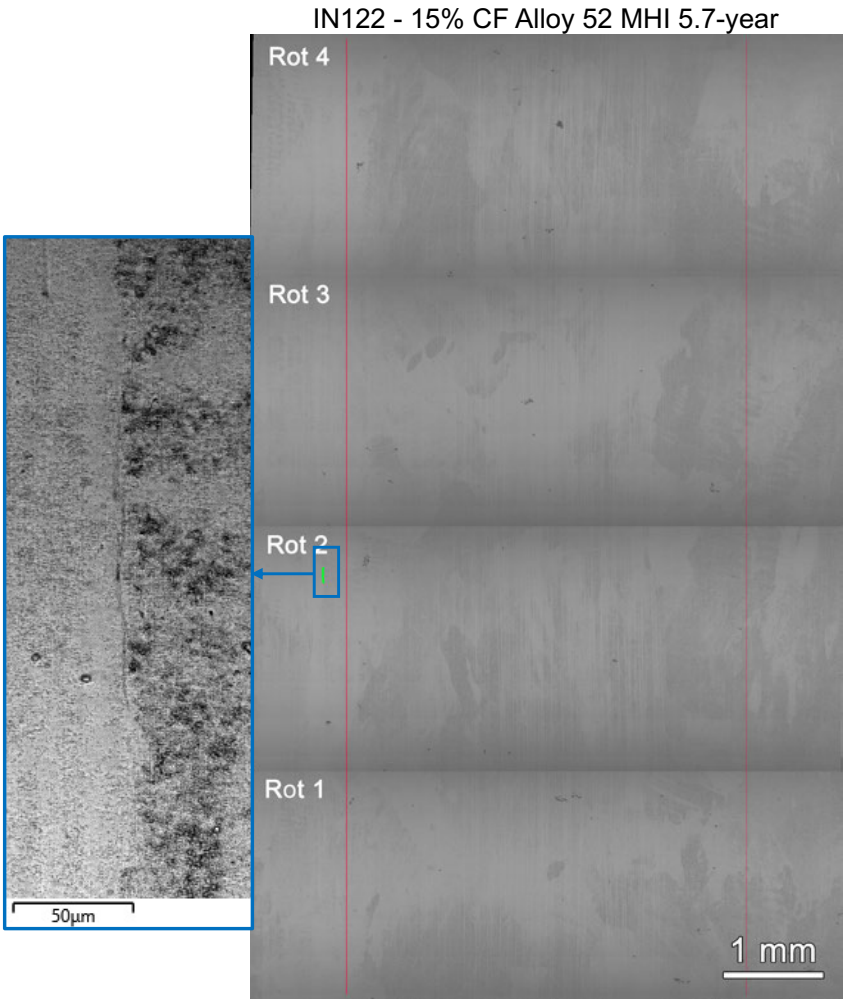

Figure 57. IN122 Alloy 152M MHI gauge surface after 5.7 years.

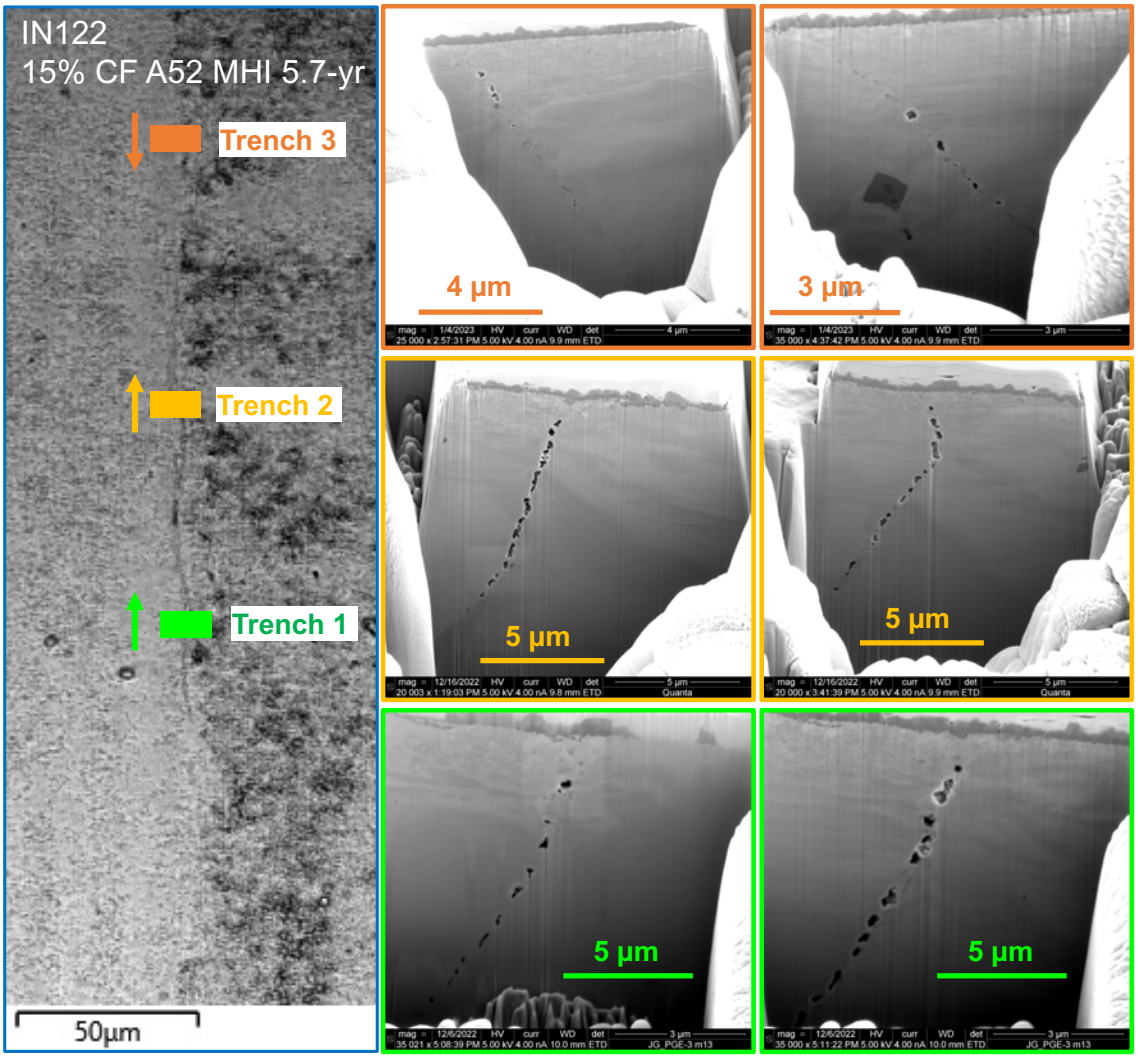

Figure 58. IN122 Alloy 52 MHI specimen showing FIB trench cross-sections of the only obvious crack in the specimen.

5.5.3 IN128 – 15% CF Alloy 152M IHI

IN128 was the only weld metal specimen that was examined at 2.4, 4.0, and 5.7 years. The gauge surface overview is provided in Figure 59. Four regions (sites) of interest were identified with this specimen. The gauge surface at Site 1 shows a linear set of surface-breaking cavities, likely following a GB. Sites 2–4 show a group of short (approximately 10 µm long) crack-like features. Site 3 was previously examined by FIB trenching at 2.4 and 5.0 years, and it was examined again after 5.7 years.

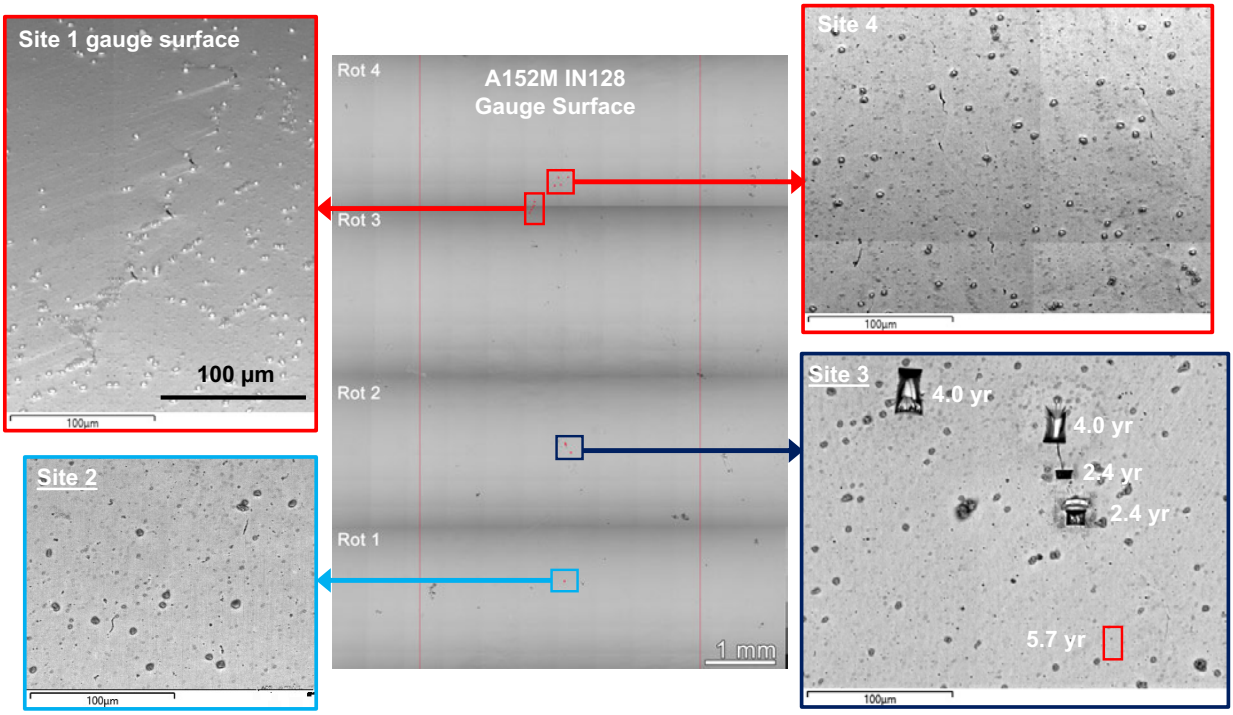

Figure 59. IN128 Alloy 152M 5.7-year gauge surface overview.

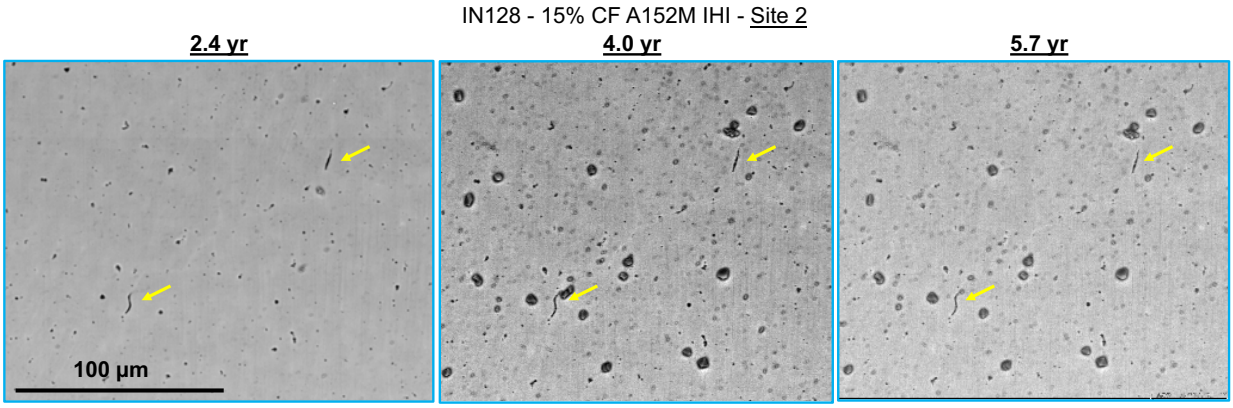

Figure 60. IN128 Alloy 152M Site 2 gauge surface appearance history.

A time evolution image series for Site 2 in Figure 60 shows that the surface appearance of the short crack-like features did not evolve between 2.4 and 5.7 years. The smooth shape of the crack on the surface suggests that it formed during weld fabrication. FIB trench cross-section analysis of this region was only conducted after 5.7 years on one of the features as shown in Figure 61. Cross-section images progressing from the end of the feature towards the middle reveal a GB that becomes progressively more open and filled with oxide. No cavities were present despite the presence of GB precipitates. Although the oxidation of this GB likely occurred during high temperature water exposure, this is most likely a preexisting weld fabrication defect rather than a feature that formed during SCCI testing.

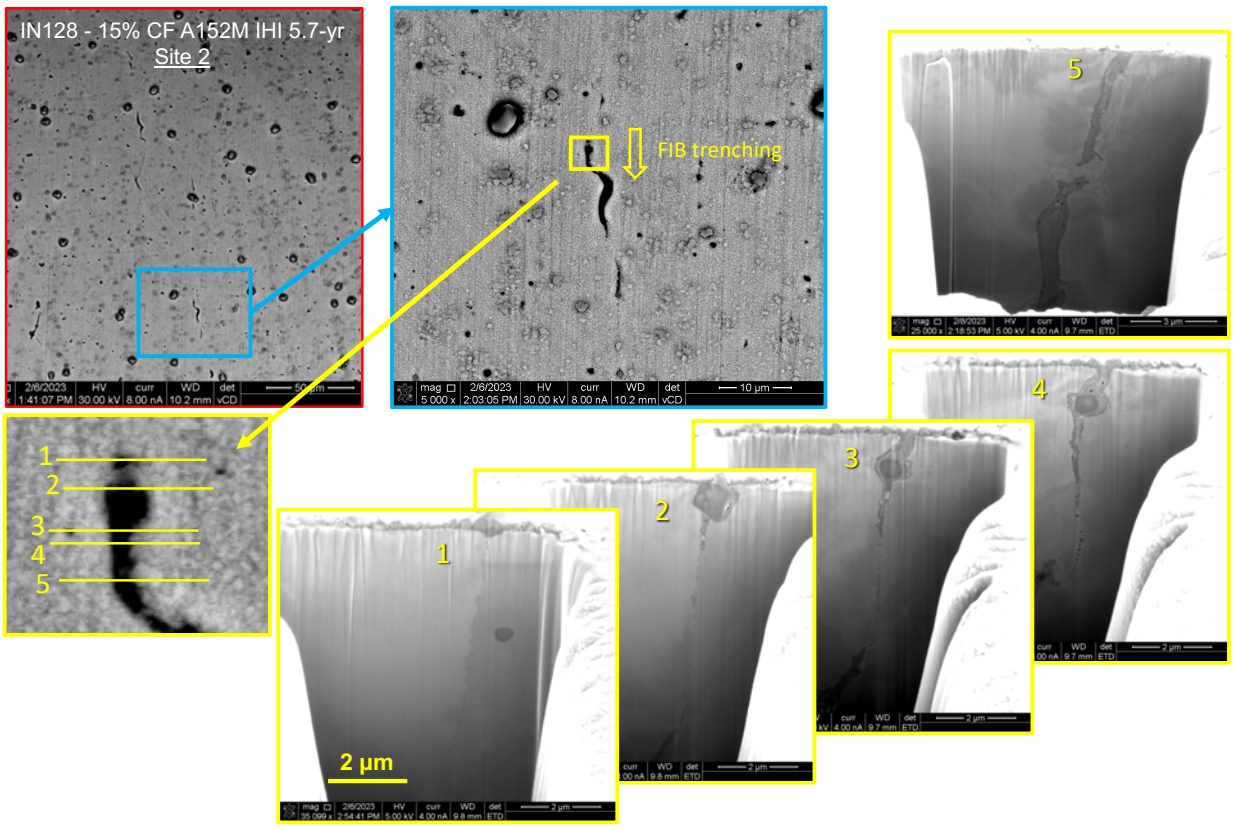

Figure 61. IN128 Alloy 152M FIB trench cross-section series after 5.7 years.

Gauge surface observations of Site 3 (Figure 62) similarly show a lack of time evolution of the linear defects. FIB trench cross-section imaging was performed on one of the features at a location adjacent to where an examination was performed after 4.0 years (Figure 63). The voids that were present have a linear appearance rather than appearing as spherical cavities. In trench #4, the boundary has a very smooth shape and appears to be filled with oxide or possibly some kind of precipitate. FIB serial trenching of this same boundary after 4.0 years is shown in Figure 50; this feature was also judged to be a very small preexisting weld fabrication defect.

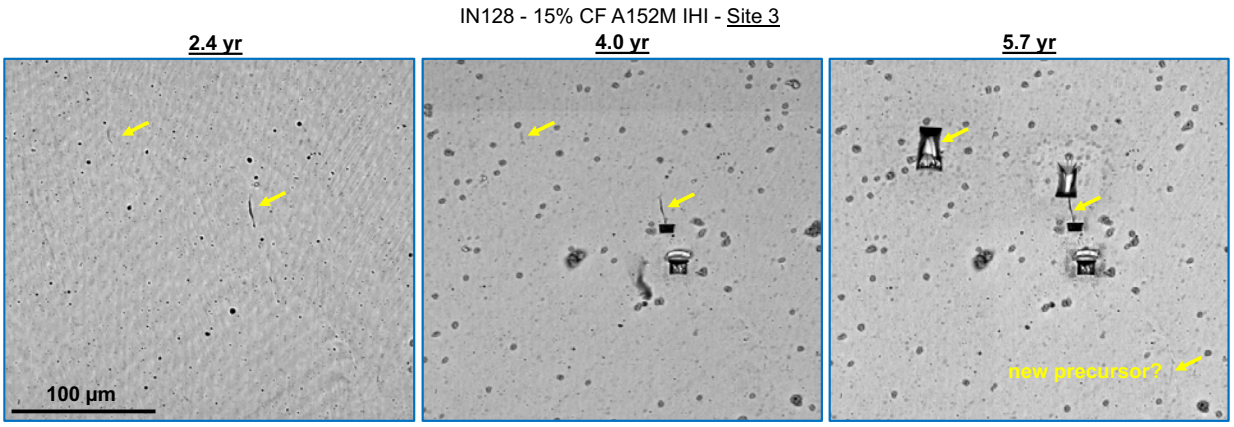

Figure 62. IN128 Alloy 152M Site 3 gauge surface appearance history.

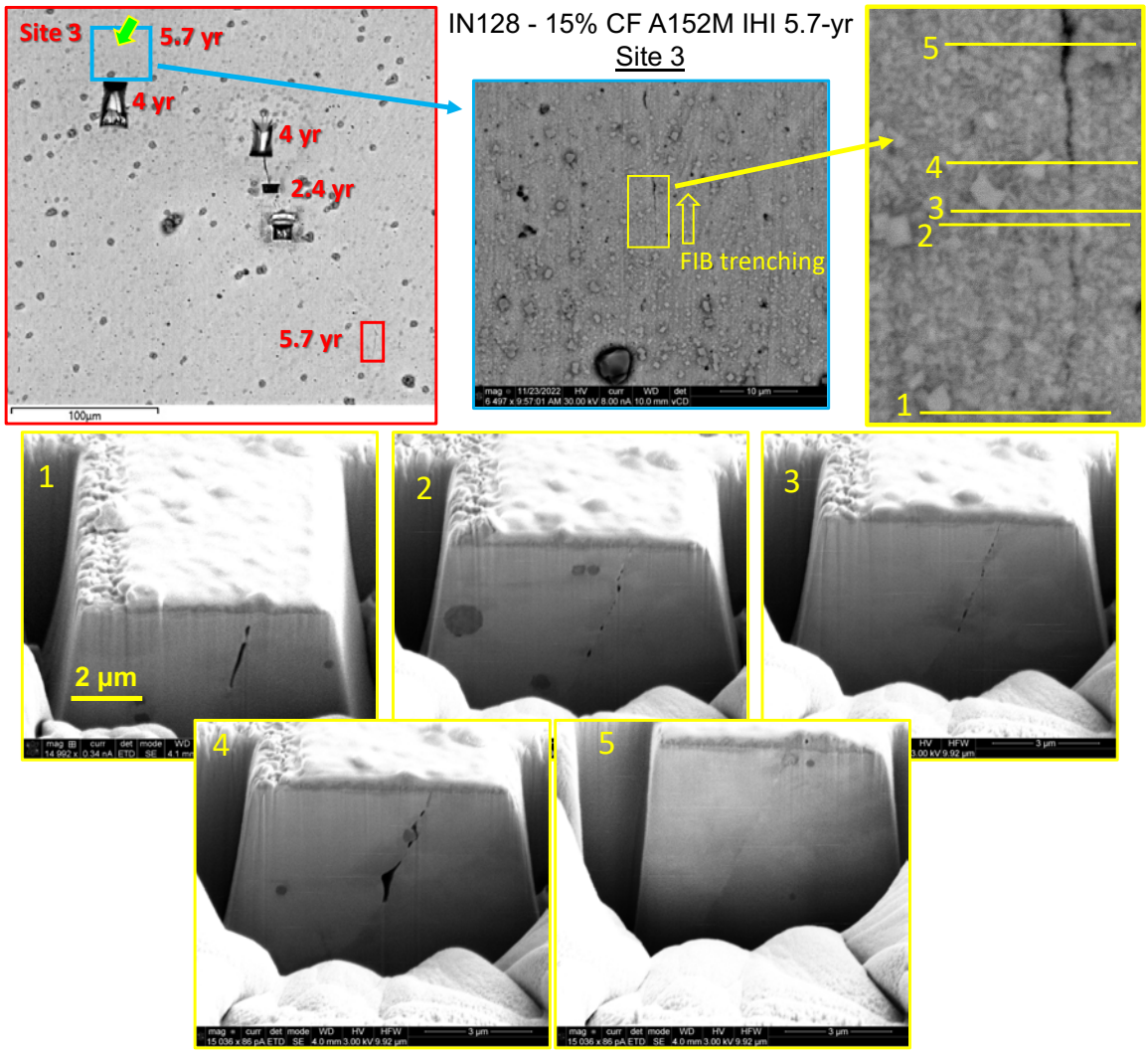

Figure 63. IN128 Alloy 152M Site 3 FIB trench cross-section series after 5.7 years.

5.5.4 IN133 – 15% CF Alloy 152M IHI

Whereas IN128 only had either very small crack-like features or crack precursor features, IN133 has two much longer crack-like features, with one being approximately 100 µm long and the other approximately 400 µm long as shown in Figure 64. Both were examined by FIB trench cross-section with the examination of the longer crack presented in Figure 65. Figure 65 shows a clearly open crack with depth beyond the field of view capable using FIB trenching. The crenulated appearance with the thick oxide suggests that this is another example of a preexisting weld fabrication defect. The shorter crack was not open but was filled with a very thick layer of oxide, also suggesting that it was a preexisting weld defect.

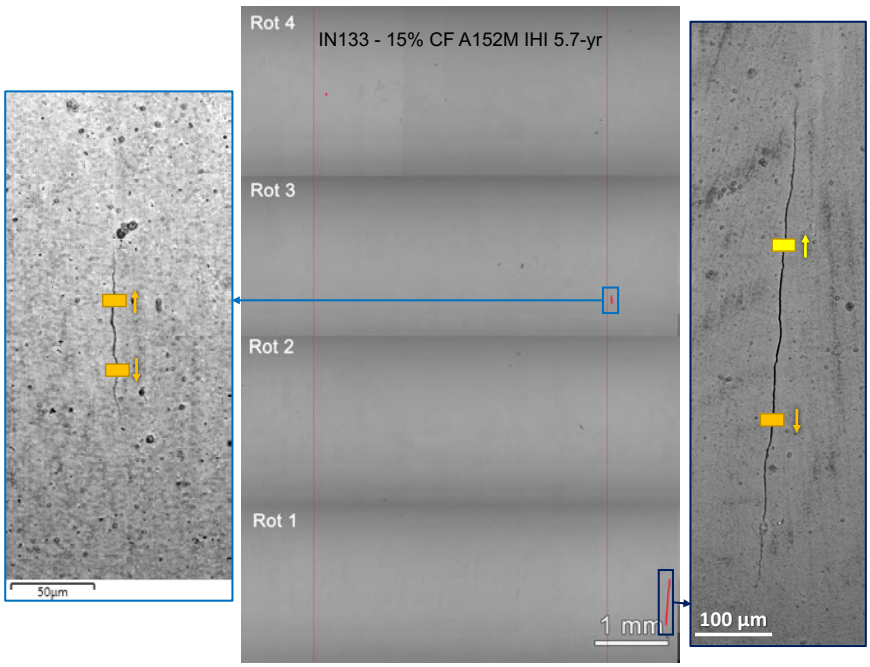

Figure 64. IN133 Alloy 152M IHI after 5.7 years showing the gauge surface montage and the location of two crack-like features.

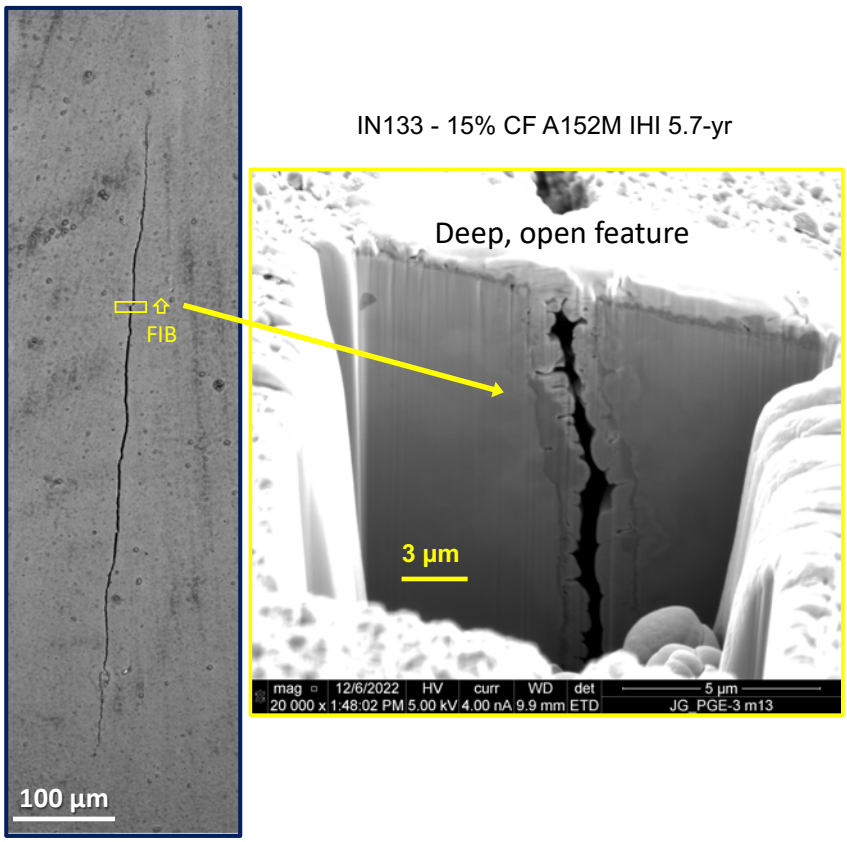

Figure 65. IN133 Alloy 152M IHI after 5.7 years showing the surface and FIB trench cross-section morphology of the larger crack-like feature.

5.5.5 IN129 – 15% CF Alloy 152M IHI

Gauge surface examination of this specimen (Figure 66) revealed that it had by far the longest and most open surface crack of all the Alloy 690/152(M)/52(M) specimens. The path length on the surface is approximately 1 mm, and the crack is clearly wide open with deformation bands emanating from both ends of the crack. The crack was sufficiently open to be detectable by x-ray tomography, and a top view of the crack in Figure 67 shows that the maximum depth is approximately 800 µm. The x-ray tomography image also reveals that the crack grew in the T-S orientation relative to the weld production path; this is one of the two most susceptible SCC growth directions for weld metals. An interesting aspect of the x-ray tomography image is that the crack path appears to be minimally branched suggesting that the majority of the crack was along a single, continuous boundary. This specimen was not monitored for crack initiation by DCPD, so there is no way to know with certainty whether this crack formed during SCCI testing and grew with time or was a preexisting defect.

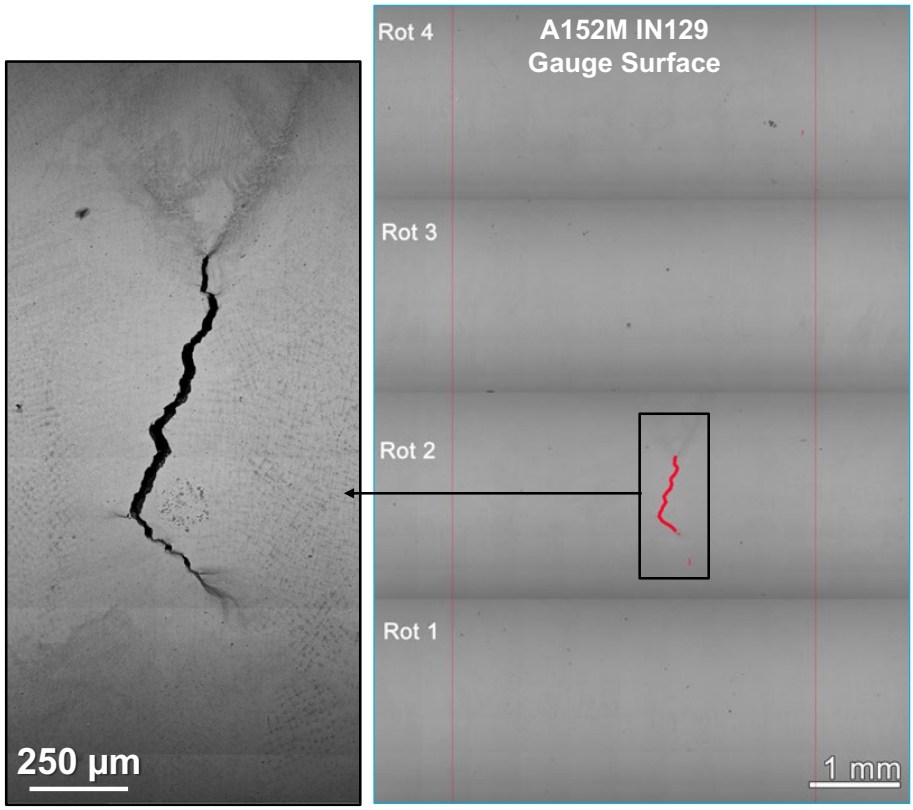

Figure 66. IN129 Alloy 152M IHI gauge surface montage and close-up of a single very large surface-breaking crack.

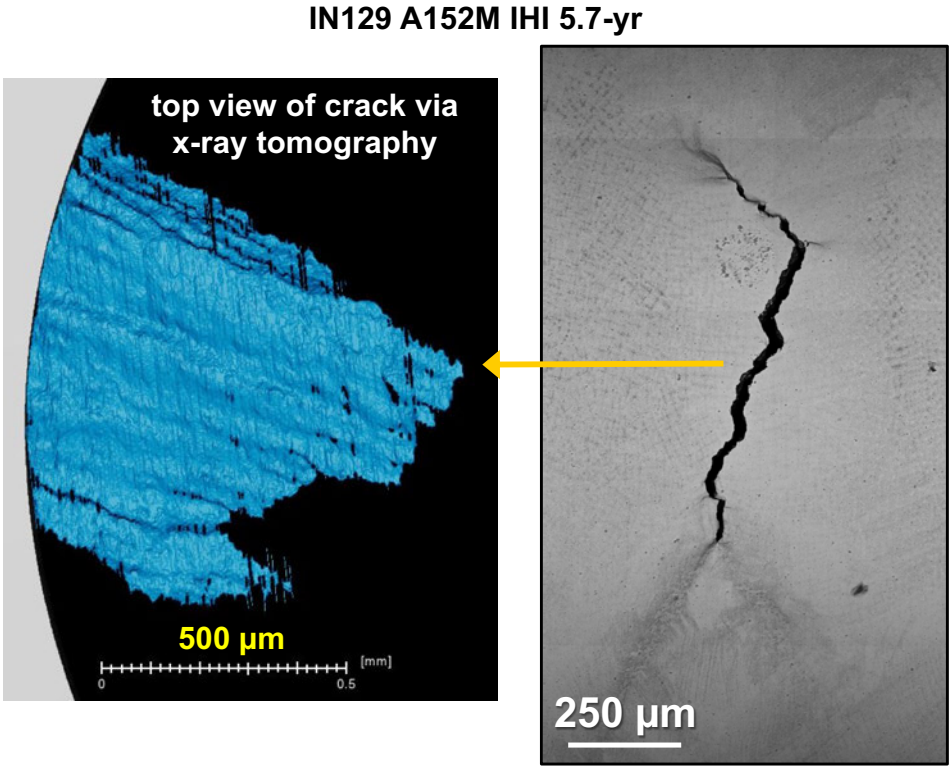

Figure 67. IN129 Alloy 152M IHI specimen showing very large crack after 5.7 years of SCCI testing.

The stress intensity at the middle of the crack and where the crack meets the surface of the specimen can be estimated from stress intensity factor (SIF) solutions in the literature. There are several studies in the literature with most of these based on finite element modelling of a sharp, elliptical shape crack in a linear elastic system [28-32]. Crack depth and shape have a significant effect on the predicted SIF. For elliptical cracks, the depth of the crack is given by the minor radius, a, and the width of the crack is based on the major radius, b. For a round bar of diameter D, the crack depth is given by the ratio a/D. For IN129, a/D = 0.25. Crack shape is represented by the ratio a/b. The projected width of the crack at the surface of the round bar is typically less than b. In the case of the crack in IN129, a/b is ~2.

Only one literature study was found to have estimated SIF values for a/b >1 [30], and the data from this work is reproduced in Figure 68 along with SIF values for a/b values up to 1.0 from another study for comparison [31]. A comparison of SIF values for a/b ≤1.0 shows that the two studies are in good agreement for a/b values ≤0.5 with the work of Astiz at a/D = 0.26 falling between the work of Shih at a/D = 0.2 and 0.3. At a/b = 1.0, the work of Astiz at a/D = 0.26 falls on the work of Shih at a/D =0.3. Some variability among similar studies is to be expected and should be considered part of the uncertainty in the K estimate. For a/b = 2.0, the work of Astiz predicts that the K value at the crack front midpoint for this specimen with a test stress of 527 MPa is 13 MPa√m while at the point where the crack intersects the surface, the estimated K value is 21 MPa√m. Since the crack is not a true elliptical shape, and the crack is somewhat blunted, these K values should be considered approximate.

Low SCCGRs of ≤$5x10^{-9}$ mm/s were measured at PNNL for 360°C tests on this weld metal in the 15% CF condition at 30 MPa√m. Low SCCGRs of <$5x10^{-9}$ mm/s were also measured during testing of 30% CW Alloy 690 at PNNL for K values ≤20 MPa√m [4]. The same 30% CW Alloy

690 materials exhibited SCCGRs of ~1x10^{-7} mm/s at 30 MPa√m, indicating a strong K dependence for Alloy 690 which is also likely for Alloy 152(M)/52(M). Thus, this SCCI specimen should be exhibiting SCCGRs well below 5x10^{-9} mm/s despite the very large crack. This would make it unlikely for the crack to grow to this size in 5.7 years.

While the available information suggests that this specimen had a large preexisting crack that did not grow significantly during 5.7 years of SCCI testing, further SCCI testing is recommended to confirm this hypothesis.

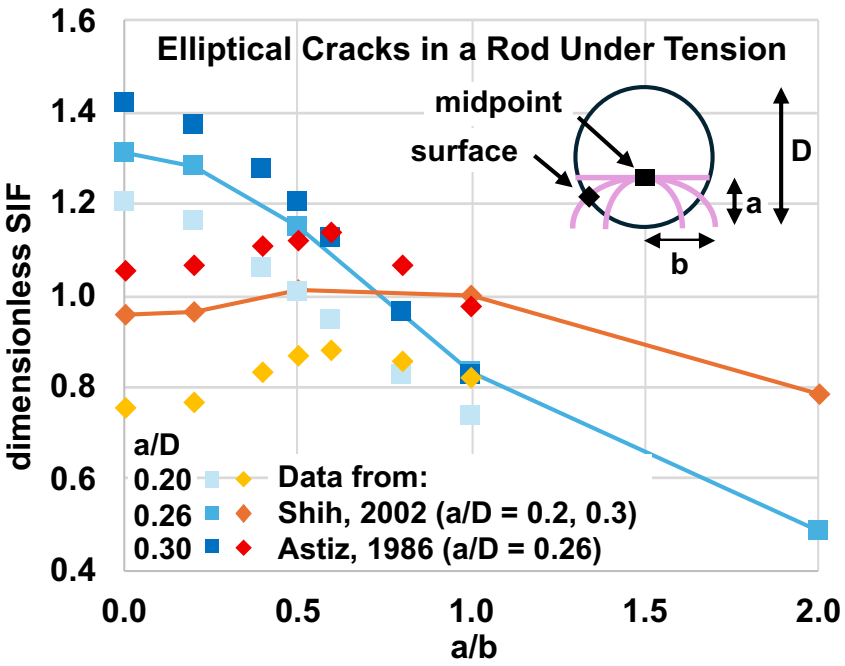

Figure 68. Dimensionless SIF values from Astiz [30] and Shih [31] for an elliptical crack. Note that “a” and “b” values are the ellipse minor and major radii rather than the values corresponding to where the crack meets the specimen surface.

6.0 Summary Discussion

6.1 Complimentary Data

The NRC/EPRI test on 15% CF Alloy 690/152(M)/52(M) specimens has the benefit of complimentary SCCI data on 12, 20, and 30% CW Alloy 690 that is being tested at PNNL for the DOE LWRS program [23-26]. Many of these specimens are made from the same heats of Alloy 690 as tested in the NRC/EPRI SCCI program. Key observations from the more highly CW Alloy 690 specimens from this program along with general knowledge of SCCI mechanisms in Alloys 600/182 are as follows:

- Alloys 600/182 undergo SCC initiation via GB oxidation and subsequent cracking or decohering of the oxide away from a grain. This process occurs continuously due to the oxide having a porous structure that allows oxygen diffusion from the water to the leading crack tip.
- The higher chromium level in Alloys 690/152(M)/52(M) produces a non-porous chromia oxide layer over surface-breaking GBs that prevents continuous GB oxidation, and thus it does not undergo SCCI by the same mechanism as Alloys 600/182.
- Alloy 690 undergoes SCCI by formation of stress-induced GB cavities that coalesce to form internal cracks that eventually extend to the surface of the specimen. This process may be enhanced near the surface of the specimen due to diffusion of chromium to the surface which leaves vacancies at the source of the chromium. If the depth of a surface-breaking crack generates a sufficiently high K value, it will exhibit SCC growth. More specific details of the timing between internal cavity formation and when these cracks link up to the surface are not yet known due to the very limited number of laboratory-observed SCCI events that have occurred.
- CW level and applied stress have a strong effect on cavity-induced crack initiation. After approximately 5 years of SCCI testing in the DOE LWRS program, only a small number of 30% CW specimens have exhibited SCCI, in particular, only 30% CW TT Alloy 690. The lowest SCCI time was approximately 1.8 years for a 30% CW TT Alloy 690 specimen. 20% CW TT Alloy 690 has exhibited GB cavity formation but thus far has not exhibited SCCI.
- GB carbide microstructure has a strong effect on the magnitude of GB cavity formation in CW Alloy 690. TT material with a high density of small GB carbides exhibits the greatest amount of GB cavity formation. MA material with few or no GB carbides does not exhibit GB cavity formation, and to-date, no CW MA Alloy 690 specimens have exhibited SCCI, and in fact, none of these have exhibited any substantial amount of GB cavity formation.

6.2 Alloy 690 Summary

The NRC/EPRI 15% CW Alloy 690 specimens extend the trends observed in the higher CW materials described above. The TT Alloy 690 heats (RE243 and WP142) with the highest GB carbide density were observed to begin undergoing GB cavity formation after 4.0 years of exposure. After 5.7 years, the RE243 heat sometimes exhibited a very high density of GB cavities within 5 μm of the surface. There was no indication that this high density extended to greater depths, but thus far, only FIB trench cross-section examinations have been performed, and these only provide microstructure information down to a maximum depth of 10–15 μm. Importantly, only a very small number of observed grain boundaries in these specimens

exhibited GB cavity formation, indicating that the GB cavity formation process was not yet widespread.

Alloy 690 Heat 114092 has a slightly lower density of GB carbides compared to heats RE243 and WP142. After 4.0 years of exposure, selected FIB trench cross-section observations revealed no GB cavities. After 5.7 years of exposure, only one of the observed GB cross-sections was found to have a few cavities. Alloy 690 B25K-2 which is nearly free of GB carbides exhibited had no GB cavities after 5.7 years.

6.3 Alloy 152(M)/52(M) Summary

As with the Alloy 690 specimens, SEM gauge surface observations of Alloy 152(M)/52(M) specimen GBs were often obstructed by a thick layer of spinel oxides on the surface of the specimen. After 2.4 and 4.0 years, a low density of very small crack-like features with a surface length of ≤20 μm were observed during SEM examination of the specimens. Serial FIB trench cross-sectioning revealed that these features had a maximum depth of 4 μm, had a thick oxide layer along the boundary, and often had large inclusions on the boundaries. In some cases, the oxidized boundaries had no obvious connection to the surface of the specimen. These features typically had a smooth appearance, and the degree of opening varied along the length of the decohered region. These features were interpreted to be cracks produced during weld fabrication and were not present in the Alloy 690 specimens. In a few of the cross-sections of one of the examined GBs, a small number of cavities were present within the oxide. This was the only observation of GB cavities after 4.0 years.

For the 5.7-year examinations, all 24 Alloy 152(M)/52(M) specimens were subjected to SEM gauge surface observations. Five out of the 24 specimens had surface IG features appearing to be cracks ≥100 μm long. A sixth specimen had an obvious large crack. All of these features were observed on specimens that were not examined at 2.4/4.0 years. The specimens with the crack-like features were subjected to FIB trench cross-section examinations along with one 2.4/4.0-year specimen (IN128 IHI Alloy 152M).

The 2.4/4.0-year specimen examined at 5.7 years was found to have no significant change in GB appearance observed in FIB trench cross-section examinations of the previously examined GBs. However, many of the other specimens not examined at the 2.4/4.0-year timeframe had significant amounts of GB oxidation and some GB cavities along the boundaries in the FIB trench cross-section images. In some cases, these cavities extended beyond the observable depth by FIB trenching. Some of the cracks had a similar appearance to the previously mentioned short cracks, suggesting that many of the larger crack-like features observed after 5.7 years likely also weld fabrication defects. Additional proposed testing will be DCPD monitored.

The specimen with the large crack was made from Alloy 152M, and it was not instrumented for DCPD. The crack had a length of approximately 1 mm along the specimen surface and a peak depth of approximately 800 μm. There was obvious plastic strain on the surface of the specimen at both ends of the crack. The crack appearance on the surface of the specimen was IG, and x-ray tomography imaging suggested that the crack surface was IG. Because this specimen was not instrumented for DCPD, it is unknown if this crack was actively growing. Additional proposed testing will be DCPD monitored.

In comparison to Alloy 690, the Alloy 152(M)/52(M) specimens had more cracks or precursor cracks. Some of the specimens with precursor cracks had GB cavities suggesting that the

cracks were forming by the same mechanism as in Alloy 690. However, in more cases, it appeared that cracks were preexisting weld fabrication defects. It is unclear whether these cracks or crack-like features evolved with time.

6.4 Final Comments

Alloy 690/152(M)/52(M) do not undergo SCCI by GB oxidation like Alloy 600/182, but instead, SCCI occurs by stress-induced GB cavity formation which appears to require significant amounts of CW. The overall assessment is that after 5.7 years, the Alloy 690 specimens had no indications of significant GB cavity formation that could be a near-term precursor for crack formation and subsequent SCCI.

The Alloy 152(M)/52(M) specimens had significantly more crack-like features that also were much larger than observed in any of the Alloy 690 specimens. None of the specimens with larger crack-like features were instrumented for DCPD detection of initiation. Most of the crack-like features are likely to be oxidized weld fabrication defects, but a few could be due to IG creep cavity formation like what occurred for Alloy 690. The Alloy 152M specimen with the very large IG crack was unexpected, and the available information from the test and specimen examinations was insufficient to determine whether this was a preexisting weld fabrication defect or whether it formed as a result of SCCI. There also was insufficient information to determine whether it was actively undergoing SCC growth.

Further SCCI testing of this matrix of specimens is recommended to clarify the SCCI susceptibility, especially for the weld metals where a few of the specimens could have cracks of depth beyond 20 μm.

7.0 References

[1] P. Scott , M-C Meunier , F. Steltzlen , O. Calonne , M. Foucault , P. Combrade, and C. Amzallag, “Comparison of Laboratory and Field Experience of PWSCC in Alloy 182 Weld Metal”, 13th International Conference on Environmental Degradation of Materials in Nuclear Power Systems Whistler, British Columbia August 19 - 23, 2007.

[2] S.M. Bruemmer and M.B. Toloczko, "Pacific Northwest National Laboratory Investigation of Stress Corrosion Cracking in Nickel Base Alloys, Volume 1", NUREG/CR-7103, Volume 1, ML11277A230 and ML11294A228, U.S. NRC, September 2011.

[3] S.M. Bruemmer, M.B. Toloczko, M.J. Olszta, "Pacific Northwest National Laboratory Investigation of Stress Corrosion Cracking in Nickel Base Alloys, Volume 2", NUREG/CR-7103, Volume 2, ML12114A011, U.S. NRC, April 2012.

[4] M.B. Toloczko, N.R. Overman, M.J. Olszta, S.M. Bruemmer, " Pacific Northwest National Laboratory Investigation of Stress Corrosion Cracking in Nickel-Base Alloys: Stress Corrosion Cracking of Cold Worked Alloy 690", NUREG/CR-7103, Volume 3, PNNL-24647, ML16190A072, U.S. NRC, July 2016.

[5] S.M. Bruemmer, M.J. Olszta, R.J. Seffens, R.A. Bouffioux, N.R. Overman, M.B. Toloczko, "Pacific Northwest National Laboratory Investigation of Stress Corrosion Cracking in Nickel Base Alloys, Behavior of Alloy 152 and 52 Welds”, NUREG/CR-7103, Volume 4, ML19099A200, U.S. NRC, April 2019.

[6] M.B. Toloczko, et al., “Investigation of Stress Corrosion Cracking in Nickel-Base Alloys: Dissimilar Metal Interface Regions and Assessment of Program Results”, NUREG/CR-7103, Volume 5, U.S. NRC, July 2024.

[7] P. Berge et al., “Importance of Surface Preparation for Corrosion Control in Nuclear Power Stations”, *Materials Performance*, Vol. 36, November 1997, pp. 56-62.

[8] P. Scott, et al., “Comparison of Laboratory and Field Experience of PWSCC in Alloy 182 Weld Metal,” *Proc. 13th Int. Conf. Environmental Degradation of Materials in Nuclear Power Systems - Water Reactors,* Canadian Nuclear Society, 2007.

[9] S. Le Hong, et al., “Modelling of Stress Corrosion Crack Initiation on Alloy 600 in Primary Water of PWRs”, *Ninth International Symposium on Environmental Degradation of Materials in Nuclear Power Systems - Water Reactors*, TMS, 1999, pp. 115-122.

[10] C. Amzallag, J-M Boursier, C. Pages and C. Gimond, “Stress corrosion life assessment of 182 and 82 welds used in PWR components”, *Proc. 10th International Conference Environmental Degradation of Materials in Nuclear Power Systems - Water Reactors,* NACE International, 2002.

[11] J.M. Boursier, et al., “The Influence of the Strain Rate on the Stress Corrosion Cracking of Alloy 600 in High Temperature Primary Water”, *Corrosion Science*, Vol. 37, No. 3, 1995, pp. 493-508.

[12] F. Vaillant, et al., “Laboratory Stress Corrosion Cracking Propagation in a Superficial Cold Worked Layer in SG Divider Plates in Alloy 600”, *Proc. 15th Int. Conf. Environmental Degradation of Materials in Nuclear Power Systems - Water Reactors,* TMS, 2011.

[13] O. Raquet and G. Santarini, “Stress Corrosion Crack Propagation Rate of Alloy 600 in the Primary Water of PWR Influence of a Cold Worked Layer”, *Ninth International Symposium on Environmental Degradation of Materials in Nuclear Power Systems - Water Reactors*, TMS, 1999, pp. 207-213.

[14] S. Le Hong, “Influence of Surface Condition on Primary Water Stress Corrosion Cracking Initiation of Alloy 600”, *Corrosion Science*, Vol. 57, No. 4, 2001, pp. 323-333.

[15] P. L. Andresen, M. M. Morra, and Kawaljit Ahluwalia, “SCC of Alloy 152/52/52i Weld Metals in PWR Primary Water”, *Proc. 16th Int. Conf. Environmental Degradation of Materials in Nuclear Power Systems - Water Reactors,* NACE International, 2014.

[16] M. B. Toloczko, M. J. Olszta, Z. Zhai and S. M. Bruemmer, "Stress corrosion crack initiation measurements of alloy 600 in PWR primary water", in *17th International Conference on Environmental Degradation of Materials in Nuclear Power Systems - Water Reactors,* 2015, Ottawa, ON, Canada: Canadian Nuclear Society.

[17] M.B. Toloczko, “Materials Reliability Program: Stress Corrosion Crack (SCC) Initiation Testing of Ni-Base Alloys for PWR Applications - Part 1 (MRP-426)”, EPRI Product #3002010761, 2017.

[18] M.B. Toloczko, Z. Zhai, J. Wang, M.J. Olszta, R.A. Bouffioux, “PNNL PWSCC Initiation Testing of Ni-base Alloys, Report 2”, PNNL-31016, 2021.

[19] S.A. Attanasio, J.S. Fish, D.S. Morton, P.M. Rosencrans, G.S. Was, Y. Yi, “Measurement of the fundamental parameters for the film-rupture/oxidation mechanism”, KAPL Atomic Power Laboratory: Schenectady, NY, 1999 (KAPL-P-000215).

[20] H.J. Frost and M.F. Ashby, “Deformation-Mechanism Maps: The Plasticity and Creep of Metals and Ceramics”, Pergamon Press, 1982.

[21] K. Sourabh, J.B. Singh, “Creep behaviour of Alloy 690 in the temperature range 800-1000°C”, Journal of Materials Research and Technology, Vol. 17, 2022, pp. 1553-1569.

[22] J. Cadek, “Creep in Metallic Materials”, Materials Science Monographs, Vol. 48, Elsevier, 1988.

[23] Z. Zhai, et al., “FY 2023 Progress on Stress Corrosion Crack Testing of Ni-Base Alloys in PWR Primary Water”, LWRS report August 2023, PNNL-34777.

[24] Z. Zhai, et al., “Precursor Damage Evolution and Stress Corrosion Crack Initiation of Cold-Worked Alloy 690 in PWR Primary Water”, LWRS September 2016 Report, PNNL-25960.

[25] Z. Zhai, et al., “Grain Boundary Microstructure Effects on Stress Corrosion Crack Initiation Mechanisms in Alloy 600 and Alloy 690”, LWRS August 2019 report, PNNL-29086.

[26] Z. Zhai, et al., “Quantitative Analysis of Precursor Damage and Crack Evolution in Alloy 690 and Its Weld Metals after Long-Term SCC Initiation Testing in PWR Primary Water”, LWRS April 2021, PNNL-31347.

[27] Z. Zhai, M.J. Olszta, M.B. Toloczko, S.M. Bruemmer, “Crack initiation behavior of cold-worked Alloy 690 in simulated PWR primary water – role of starting microstructure, applied stress and cold work on precursor damage evolution, in Proceedings of the 19th International Conference on Environmental Degradation of Materials in Nuclear Power Systems - Water Reactors, 2019, American Nuclear Society, pp. 373-385.

[28] A. Carpentiri, “Stress intensity factors for straight-fronted edge cracks in round bars”, Engineering Fracture Mechanics, Vol. 42, 1992, pp. 1035-1040.

[29] I.S. Raju and J.C. Newman Jr., “Stress Intensity Factors for Circumferential Surface Cracks in Pipes and Rods Under Tension and Bending Loads”, NASA-TM-87594, NASA, 1985.

[30] M.A. Astiz, “An incompatible singular elastic element for two- and three-dimensional crack problems”, International Journal of Fracture, Vol. 31, 1986, pp. 105-124.

[31] Y.-S. Shih, J.-J. Chen, “The stress intensity factor study of an elliptical cracked shaft”, Nuclear Engineering and Design, Vol. 214, 2002, pp. 137-145.

[32] J. Toribio, N. Alvarez, B. Gonzalez, J.C. Matos, “A critical review of stress intensity factor solutions for surface cracks in round bars subjected to tension loading”, Engineering Failure Analysis, Vol. 16, 2009, pp. 794-809.

Pacific Northwest National Laboratory

902 Battelle Boulevard
P.O. Box 999
Richland, WA 99354
1-888-375-PNNL (7665)

www.pnnl.gov